Cell Mills: Nanofactory Manufacture of Biological Components

Robert A. Freitas Jr.
Senior Research Fellow
Institute for Molecular Manufacturing

Abstract. This paper presents a conceptual technical design and scaling study for a nanorobotic factory called a cell mill. The cell mill uses a collection of nanorobotic subsystems employing the methods of atomically precise molecular manufacturing to fabricate all biological components comprising a living cell, including completed viable biological cells. The exemplar cell mill is conceived as a desktop appliance approximately 0.1 m^3 (~100 liters) in volume – e.g., a cubical box ~46 cm on a side – with a mass of ~12.5 kg drawing ~5 kW of power in active operation. The cell mill produces finished autologous human biological cells of all types at a rate of ~1 kg/hr with an estimated start-to-finish manufacturing time of ~1.4 hours from order placement to emergence of finished product. Several small molecules are supplied in bulk as chemical feedstock for the manufacturing process. Viable autologous human tissues and organs can be fabricated from these cells at the same rate, using a tissue mill attached to the cell mill.

Cite as: Robert A. Freitas Jr., "Cell Mills: Nanofactory Manufacture of Biological Components," IMM Report No. 53, 15 June 2024; http://www.imm.org/Reports/rep053.pdf.

Table of Contents

1. Introduction

Biological cells are the fundamental units of all living things. It has recently been estimated[1] that a representative 70 kg human male body contains ~7 trillion nucleated cells (e.g., tissue and white cells) and ~29 trillion non-nucleated cells (mostly red cells), for a total of ~36 trillion native cells[2] representing a body cell mass (BCM) of ~45 kg or ~64% of total human body mass.[3] When these cells become diseased, physically injured, or succumb to serious genetic or metabolic malfunction, it would be convenient if the afflicted cells could be promptly exchanged for autologous healthy cells of identical cytotype and genotype, immediately restoring the patient to full health. The ability to quickly manufacture such cells would enable the rapid replacement of damaged tissues and organs, and would also permit whole-body rejuvenation[4] or repair thus enabling survival after even the most extreme injuries or medical circumstances.[5] This is the ultimate promise of a mature nanorobotic medical technology, aka. nanomedicine.

The cell mill is a proposed molecular manufacturing system for fabricating whole human cells of several hundred different types,[6] initially in a viable but metabolically dormant state, personalized to a specific (a) person (genetically), (b) tissue destination, and (c) metabolic state. Freitas[7] first proposed the cell mill concept in 1999. This paper is an updated and expanded version of the

---

[1] Hatton IA, Galbraith ED, Merleau NSC, Miettinen TP, Smith BM, Shander JA. The human cell count and size distribution. Proc Natl Acad Sci U S A. 2023 Sep 26;120(39):e2303077120; https://www.ncbi.nlm.nih.gov/pmc/articles/pmid/37722043/.

[2] There are also ~38 trillion non-native cells in the form of bacteria present in the human body, mostly residing in the gut.

[3] Amusingly, this tally mostly confirms the author's own published estimate back in 1999* of ~3.5 trillion tissue cells, ~2.1 trillion platelets in the blood, ~1.3 trillion white cells in the blood, lymphatics and tissues, and ~28.5 trillion red blood cells in the bloodstream and spleen storage.
* Freitas RA Jr. Nanomedicine, Volume I: Basic Capabilities, Landes Bioscience, Georgetown, TX, 1999; Section 8.5.1, "Cytometrics"; http://www.nanomedicine.com/NMI/8.5.1.htm.

[4] Freitas RA Jr. Chapter 23. Comprehensive Nanorobotic Control of Human Morbidity and Aging. In: Fahy GM, West MD, Coles LS, Harris SB, eds, The Future of Aging: Pathways to Human Life Extension, Springer, New York, 2010; http://www.nanomedicine.com/Papers/Aging.pdf.

[5] Freitas RA Jr. Cryostasis Revival: The Recovery of Cryonics Patients through Nanomedicine. Alcor Life Extension Foundation, Scottsdale AZ, 2022; https://www.alcor.org/cryostasis-revival/.

[6] Freitas RA Jr. "Appendix C. Catalog of Distinct Cell Types in the Adult Human Body", Nanomedicine, Volume I: Basic Capabilities, Landes Bioscience, Georgetown, TX, 1999, pp. 393-395; http://www.nanomedicine.com/NMI/AppendixC.htm. See also: https://en.wikipedia.org/wiki/List_of_distinct_cell_types_in_the_adult_human_body.

[7] Freitas RA Jr. Nanomedicine, Volume I: Basic Capabilities, Landes Bioscience, Georgetown, TX, 1999, p. 32; Table 1.4, "Medical Challenges of Increasing Difficulty and Possible Approaches"; http://www.nanomedicine.com/NMI/Tables/1.4.jpg.

author's earlier technical descriptions of the cell mill concept and design that were published in 2010,[8] 2016,[9] 2016,[10] and 2022.[11]

In operation, the cell mill is a desktop-style nanofactory[12] apparatus that inputs the consensus DNA sequence of a patient, then manufactures autologous[13] human tissue cells or blood cells of any type using a convergent assembly process.[14] Gross output of finished biological cells from the proposed cell mill should approach $R_{CellMill} \sim 1$ kg/hr, roughly similar to the production specifications for the mature desktop nanofactory for diamondoid products that has been described elsewhere.[15]

The current conceptual design for a cell mill principally includes three working modules:

(1) **Molecular Synthesis Module** (Section 2). All biomolecules, from the simplest organic compounds to long-chain proteins, can be produced either by atomically precise molecular manufacturing or by conventional biological or biochemical techniques. A small group of biologically relevant inorganic materials including hydroxyapatite[16] found in bone[17] and

---

[8] Freitas RA Jr. Chapter 23. Comprehensive Nanorobotic Control of Human Morbidity and Aging. In: Fahy GM, West MD, Coles LS, Harris SB, eds, The Future of Aging: Pathways to Human Life Extension, Springer, New York, 2010; Section 23.6.3.5, "Internal Injury and Nanosurgery: Tissue Printers, Cell Mills, and Organ Mills"; http://www.nanomedicine.com/Papers/Aging.pdf.

[9] Freitas RA Jr. The Whiskey Machine: Nanofactory-Based Replication of Fine Spirits and Other Alcohol-Based Beverages. IMM Report No. 47, May 2016; Section 5.3.1, "Mechanosynthesis of Ethanol and Congener Molecules"; http://www.imm.org/Reports/rep047.pdf.

[10] Freitas RA Jr. The Alzheimer Protocols: A Nanorobotic Cure for Alzheimer's Disease and Related Neurodegenerative Conditions. IMM Report No. 48, June 2016; Section 4.2.6, "Nanorobotic Cell Mills"; http://www.imm.org/Reports/rep048.pdf.

[11] Freitas RA Jr. Cryostasis Revival: The Recovery of Cryonics Patients through Nanomedicine. Alcor Life Extension Foundation, Scottsdale AZ, 2022; Appendix D, "Cell Mills"; https://www.alcor.org/cryostasis-revival/.

[12] http://www.molecularassembler.com/Nanofactory/.
[13] https://en.wikipedia.org/wiki/Autotransplantation.

[14] Merkle RC. Convergent assembly. Nanotechnology 1997;8:18-22; http://www.zyvex.com/nanotech/convergent.html. Freitas RA Jr., Merkle RC. Kinematic Self-Replicating Machines, Landes Bioscience, Georgetown, TX, 2004; Section 5.9.4, "Performance of Convergent Assembly Nanofactory Systems"; http://www.MolecularAssembler.com/KSRM/5.9.4.htm.

[15] Drexler KE. Nanosystems: Molecular Machinery, Manufacturing, and Computation, John Wiley & Sons, New York, 1992, Section 14.4, "An exemplar manufacturing system architecture," pp. 421-427; https://www.amazon.com/dp/0471575186/.

[16] https://en.wikipedia.org/wiki/Hydroxyapatite.
[17] https://en.wikipedia.org/wiki/Bone#Composition.

in the enamel,[18] dentin,[19] and cementum found in teeth, fluoroapatite[20] found in tooth enamel, and a few other calcium phosphates[21] found in dentin,[22] can also be synthesized in this Module.

(2) **Cytocomponent Assembly Module** (Section 3). Biomolecules are assembled into organelles, cytoskeleton fibers, and other cytological component structures, either using positionally controlled mechanical assembly or by using conventional biological or self-assembly techniques.

(3) **Cell Assembly Module** (Section 4). Metabolically dormant but viable whole cells are assembled from organelles and other cytocomponents, and individual molecules as required, either using positionally controlled mechanical assembly or by using conventional biological or self-assembly techniques. Purely for computational convenience, throughout this scaling study we will refer to a "typical" ~20 μm human tissue cell of approximate volume $(20\ \mu m)^3 \sim 8000\ \mu m^3$ (e.g., mass ~ 10^{-8} gm) but there is considerable variation in size between cell types and even within each cytotype, as illustrated by the chart below.[23]

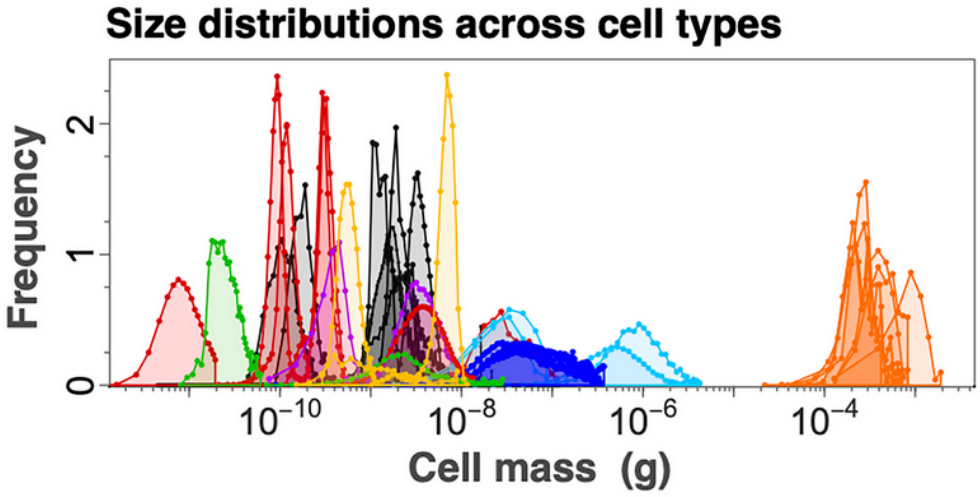

Additionally, a **Tissue Mill** (Section 5), when attached to a cell mill, can accept finished cells and other biocomponents from the cell mill and then use these components to fabricate viable autologous human tissues and whole organs.

Cell mills would be a ground-breaking biomedical technology. The development of cell mills within our lifetimes would have an immense and direct personal impact on our lives.

---

[18] https://en.wikipedia.org/wiki/Tooth_enamel#Features.
[19] https://en.wikipedia.org/wiki/Dentin.
[20] https://en.wikipedia.org/wiki/Fluorapatite.
[21] https://en.wikipedia.org/wiki/Calcium_phosphate.
[22] https://en.wikipedia.org/wiki/Dentin#Structure.

[23] Hatton IA, Galbraith ED, Merleau NSC, Miettinen TP, Smith BM, Shander JA. The human cell count and size distribution. Proc Natl Acad Sci U S A. 2023 Sep 26;120(39):e2303077120; https://www.ncbi.nlm.nih.gov/pmc/articles/pmid/37722043/.

2. Molecular Synthesis Module

All biological components to be fabricated by the cell mill are ultimately composed of biomolecules of many different kinds. All biomolecules, from the simplest organic compounds to the longest-chain proteins, may be produced either by conventional biological or biochemical techniques or by atomically precise molecular manufacturing. While the former methods are of some limited interest both for context and completeness, this paper will concentrate on molecular manufacturing approaches that can be implemented using compact "desktop" nanofactory type systems.

There are two broad classes of molecules that must be manufactured by cell mills: generic biomolecules and personalized biomolecules.

Generic Biomolecules. Many organic molecules found in the human body are generic. That is, they are found in all human bodies without regard to the unique biochemical composition of different people. These molecules are often called "highly conserved"[24] because their structures are nearly identical in all humans, reflecting their fundamental roles in basic cellular processes. Examples include glucose[25] and other simple sugars,[26] adenosine triphosphate (ATP),[27] the 20 standard amino acids used as building blocks for proteins,[28] hormonal[29] and signal[30] peptides (short amino acid chains)[31] and neuropeptides,[32] heme and hemoglobin,[33] RNA and DNA nucleotides,[34] transfer RNAs,[35] many enzymes,[36] and structural proteins such as collagens,[37] elastin,[38] and tubulins.[39] These are present in all human bodies in the same form but in somewhat differing amounts and distributions.

Section 2.1 describes the **Generic Synthesis Unit**, a means of synthesis for these generic organic molecules, using either the techniques of automated conventional organic chemical synthesis (Section 2.1.1) or the techniques of molecular manufacturing (Section 2.1.2).

Personalized Biomolecules. Other organic molecules have compositions that are unique to a single person or a limited group of people. Examples include the DNA-based chromosomes of a

---

[24] https://en.wikipedia.org/wiki/Conserved_sequence.
[25] https://en.wikipedia.org/wiki/Glucose.
[26] https://en.wikipedia.org/wiki/Monosaccharide.
[27] https://en.wikipedia.org/wiki/Adenosine_triphosphate.
[28] https://en.wikipedia.org/wiki/Amino_acid.
[29] https://en.wikipedia.org/wiki/Peptide_hormone.
[30] https://en.wikipedia.org/wiki/Signal_peptide.
[31] https://en.wikipedia.org/wiki/Peptide.
[32] https://en.wikipedia.org/wiki/Neuropeptide.
[33] https://en.wikipedia.org/wiki/Hemoglobin.
[34] https://en.wikipedia.org/wiki/Nucleotide.
[35] https://en.wikipedia.org/wiki/Transfer_RNA.
[36] https://en.wikipedia.org/wiki/Enzyme.
[37] https://en.wikipedia.org/wiki/Collagen.
[38] https://en.wikipedia.org/wiki/Elastin.
[39] https://en.wikipedia.org/wiki/Tubulin.

particular person,[40] the major histocompatibility complex (MHC)[41] proteins and glycoproteins that allow each body's immune system to distinguish self-from non-self,[42] the carbohydrate decorations of red cell surfaces that define the human ABO blood typing system,[43] antibodies (produced by B cells in response to antigens, with variable regions differing greatly among individuals),[44] T-cell receptors (specialized molecules on T-cells analogous to antibodies),[45] cell membrane proteins (which help control passage of substances in and out of cells),[46] more than 15 isoforms of laminins,[47] and other molecules that must be fabricated to match the unique biochemical structures of a particular human body.

Section 2.2 describes the production of these personalized organic molecules using the **Personalized Synthesis Unit**. The nanomanufacturing process begins with the acquisition of the patient's consensus genomic sequence (Section 2.2.1) – the patient-specific "clean" genome with all random mutations removed and corrected – which is obtained by selective genome sampling[48] (Section 2.2.1.1) followed by chromosome sequencing[49] (Section 2.2.1.2). With this data in hand, a DNA mill (Section 2.2.2) can manufacture copies of the patient's fully-corrected DNA and chromosomes, suitably methylated to match the expression pattern and activation state of the particular cytotype under construction. The same data allows a protein mill (Section 2.2.3) to fabricate proteins specific to the patient's unique biochemical signature, and related molecular mills can produce personalized carbohydrate-based (Section 2.2.4) and related organics as well.

2.1 Generic Synthesis Unit

At the most basic level, the cell mill must manufacture a large number of generic organic molecules shared by all humans. These can be produced either by the bulk methods of conventional chemical synthesis (Section 2.1.1) or by the Generic Synthesis Unit that employs the techniques of atomically precise manufacturing, using nanofactories (Section 2.1.2) and a few simple molecular feedstock chemical inputs such as CH_4, NH_3, and H_2O.

---

[40] https://en.wikipedia.org/wiki/Nucleic_acid.
[41] https://en.wikipedia.org/wiki/Major_histocompatibility_complex.

[42] The genes encoding MHC molecules are highly polymorphic, meaning there is a high degree of variability in their structure from person to person.

[43] https://en.wikipedia.org/wiki/ABO_blood_group_system.
[44] https://en.wikipedia.org/wiki/Antibody.
[45] https://en.wikipedia.org/wiki/T-cell_receptor.
[46] https://en.wikipedia.org/wiki/Membrane_protein.
[47] https://en.wikipedia.org/wiki/Laminin.

[48] Freitas RA Jr. The ideal gene delivery vector: Chromallocytes, cell repair nanorobots for chromosome replacement therapy. J Evol Technol 2007;16:1-97; Section 4.1, "Genome Sampling and Modification"; http://jetpress.org/v16/freitas.pdf.

[49] Freitas RA Jr. The ideal gene delivery vector: Chromallocytes, cell repair nanorobots for chromosome replacement therapy. J Evol Technol 2007;16:1-97; Section 4.2, "Chromosome Sequencing"; http://jetpress.org/v16/freitas.pdf.

2.1.1 Conventional Manufacturing of Generic Organics

Many of the >220,945 different chemical substances found in human cells[50] could be manufactured using conventional organic chemical synthesis techniques[51] or by automated organic chemical synthesis methods,[52] or could be purchased on the open market.[53]

Conventional manual synthetic chemistry is a very labor-intensive task, often requiring the repeated installation and removal of protecting groups to prevent solution-phase reactions from occurring in one part of the molecule, while the chemist adds a new structure to some other part of the molecule that is unprotected. For larger-size molecules, this technique becomes cumbersome because there may be exponentially more sites where unwanted reactions can occur.

Automated synthesis machines for small organic molecules have been under serious development since at least the early 1990s.[54] The synthesis of polymeric molecules using building blocks with well-defined and chemically selective interfaces got an even earlier start, first automating the production of peptides (amino acid polymers),[55] oligonucleotides (nucleic acid polymers),[56] and oligosaccharides (carbohydrate polymers).[57] Significant progress in the automated synthesis of nonpolymeric small organic molecules has awaited the development of techniques involving well-defined sets of organic building blocks with clean interfaces (image, right),[58] and several commercial manufacturers of automated chemical synthesis equipment such as Chemspeed Technologies[59] and Synple Chem[60] are available.

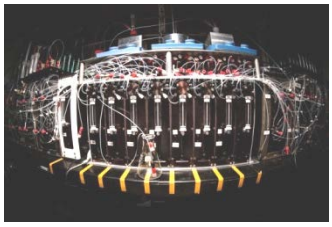

---

[50] The Human Metabolome Database, HMDB Version 5.0, as of June 2024; https://hmdb.ca/.

[51] https://en.wikipedia.org/wiki/Organic_synthesis.
[52] https://en.wikipedia.org/wiki/Automated_synthesis.

[53] For example, Fisher Scientific listed 256,205 organic chemicals available for purchase in June 2024; https://www.fishersci.com/us/en/browse/80013492/Organic-compounds.

[54] Sugawara T, Kato S, Okamoto S. Development of fully-automated synthesis systems. J Automat Chem. 1994;16(1):33-42; https://www.ncbi.nlm.nih.gov/pmc/articles/PMC2548029/pdf/JAMMC-16-033.pdf.

[55] Merrifield RB. Automated Synthesis of Peptides. Science 1965 Oct 8;150(3693):178-185; https://science.sciencemag.org/content/150/3693/178.

[56] Caruthers MH. Gene synthesis machines: DNA chemistry and its uses. Science 1985 Oct 18;230(4723):281-285; https://science.sciencemag.org/content/230/4723/281.

[57] Plante OJ, Palmacci ER, Seeberger PH. Automated Solid-Phase Synthesis of Oligosaccharides. Science 2001 Feb 23;291(5508):1523-1527; https://science.sciencemag.org/content/291/5508/1523.

[58] Li J, Ballmer SG, Gillis EP, Fujii S, Schmidt MJ, Palazzolo AM, Lehmann JW, Morehouse GF, Burke MD. Synthesis of many different types of organic small molecules using one automated process. Science 2015 Mar 13;347:1221-6; http://www.sciencemag.org/content/347/6227/1221.full.pdf. See also https://news.illinois.edu/blog/view/6367/204395, the process machine illustrated in the image above.

[59] https://www.chemspeed.com/.

More recently, a research group at SRI International announced progress in synthesis automation on the way towards a "universal synthesizer" – an automated multistep chemical synthesizer called AutoSyn that "makes milligram-to-gram-scale amounts of virtually any drug-like small molecule in a matter of hours," so far demonstrated on ten known drugs. Of the FDA-approved small-molecule drugs for which they could compute a synthetic route, "87% are predicted to be synthesizable on AutoSyn."[61] The process of "computing a synthetic route" has also greatly advanced with the development of algorithms for liquid-phase synthesis, e.g., by Synthia[62] (formerly known as Chematica),[63] a software package and database on 7 million chemicals connected by 86,000 chemical rules designed to combine long synthesis paths into shorter and more economical paths.

For a cell mill, many tens of thousands of distinct chemical species must be rapidly synthesized in order to build a living cell, and in differing amounts for each of the hundreds of possible cell types that might need to be manufactured. Despite much recent progress in miniaturizing automated chemical synthesis,[64] nanorobotic biomolecule synthesis systems[65] will be more compact, faster, and more productive than macroscale systems in achieving this objective, as illustrated in Section 2.1.2 below.

2.1.2 Molecular Manufacturing of Generic Organics

A fully automated system of atomically precise molecular manufacturing seems appropriate for the challenge of producing very small quantities of tens of thousands of specialty molecules to be used in fabricating cell structures and in populating the cytosol of manufactured human cells. As a representative example, we here provide a brief description of a hypothetical mechanosynthetic

---

[60] http://synplechem.com/.

[61] Collins N, Stout D, Lim JP, Malerich JP, White JD, Madrid PM, Latendresse M, Krieger D, Szeto J, Vu VA, Rucker K, Deleo M, Gorfu Y, Krummenacker M, Hokama LA, Karp P, Mallya S. Fully Automated Chemical Synthesis: Toward the Universal Synthesizer. Org Process Res Dev. 2020 Jun 23;24(10:2064-2077; https://pubs.acs.org/doi/abs/10.1021/acs.oprd.0c00143. See also https://www.autosyn.se/.

[62] https://www.sigmaaldrich.com/chemistry/chemical-synthesis/synthesis-software.html.
[63] https://en.wikipedia.org/wiki/Chematica.

[64] Trobe M, Burke MD. The Molecular Industrial Revolution: Automated Synthesis of Small Molecules. Angew Chem Int Ed Engl. 2018 Apr 9;57(16):4192-4214; https://www.ncbi.nlm.nih.gov/pmc/articles/pmid/29513400/. Mattes DS, Jung N, Weber LK, Bräse S, Breitling F. Miniaturized and Automated Synthesis of Biomolecules-Overview and Perspectives. Adv Mater. 2019 Jun;31(26):e1806656; https://onlinelibrary.wiley.com/doi/pdf/10.1002/adma.201806656.

[65] While we await the arrival of high-performance diamondoid molecular machine systems as envisioned elsewhere (e.g., http://www.nanomedicine.com/ and http://www.molecularassembler.com/Nanofactory/), primitive low-capacity "enzyme nanofactory" systems are being developed using DNA nanotechnology. Weinhold E, Chakraborty B. DNA modification and visualization on an origami-based enzyme nano-factory. Nanoscale. 2021 Feb 4;13(4):2465-2471; https://pubs.rsc.org/en/content/articlelanding/2021/nr/d0nr07618j/.

synthesis unit that could produce a simple organic molecule – ethyl alcohol or ethanol (C_2H_5OH) – along with tentative estimates of the mass and productivity of the nanomachinery necessary to accomplish this.[66] It is believed that a similar set of molecular tools and reaction sequences can be devised for most simple organic molecules of interest, including hydrocarbons, carbohydrates, and other important biomolecules (e.g., amino acids) containing additional key elements such as nitrogen (N), sulfur (S), and phosphorus (P), whose study is a proper subject for future research. The manufacturing subsystem is called the **Generic Synthesis Unit**, composed of 36.5 quadrillion generic organic chemical Fabrication Subunits, as described in more detail below.

2.1.2.1 Nanorobotic Fabrication Subunits

A generic organic chemical **Fabrication Subunit** builds molecules one at a time, usually on a surface via one or more tooltips that transfer reactive moieties from a source of small simple feedstock molecules (e.g., CH_4, H_2O) or surface-bound substituents (e.g., $–CH_3$, –OH, =O, –H) to the "workpiece" (i.e., the molecule that is being built). Atomically precise fabrication involves holding feedstock atoms or molecules, and a growing nanoscale workpiece, in the proper relative positions and orientations so that when they touch they will chemically bond in the desired manner. In this process, a mechanosynthetic tool is brought up to the surface of a workpiece. One or more transfer atoms are added to, or removed from, the workpiece by the tool. Then the tool is withdrawn and recharged. This process is repeated until the workpiece is completely fabricated to molecular precision with every atom in exactly the right place. Note that the transfer atoms are under positional control at all times to prevent unwanted side reactions from occurring. Side reactions are also prevented using proper reaction design so that the reaction energetics include energy barriers to avoid undesired pathological intermediate structures.[67]

The mechanosynthetic fabrication of most organic molecules containing the three elements carbon (C), hydrogen (H), and oxygen (O) will generally require the ability to build and join together just five basic types of organic building blocks made from these elements, including:

(1) hydrocarbon chains, e.g., $–CH_2–CH_2–$;

(2) linear esters with a carbon chain interrupted by an oxygen atom, e.g., $–RCO_2R'–$, where R and R′ = a hydrocarbon chain;

(3) cyclic phenyl and phenylene groups, e.g., $–C_6H_4R$ and $–C_6H_3RR'$, where R and R′ = CH_3, OH, or other organic side group;

(4) cyclic lactones, e.g., $–O(C=O)(CH_2)_2(CHR)–$ or $–O(C=O)(CH_2)(CHR)(CHR')–$; and

(5) simple terminating groups, e.g., $–CH_3$, –OH, =O, –H, and –COOH.

It is asserted that any organic CHO molecule, including ethanol, can be built, atom by atom or group by group, by the sequential application of a surprisingly short list of mechanosynthetic tools. As few as 2 primary tools and 6 intermediate tool states ("•" indicates a radical site) may suffice for manufacturing ethanol and many similar organic molecules:

---

[66] Freitas RA Jr. The Whiskey Machine: Nanofactory-Based Replication of Fine Spirits and Other Alcohol-Based Beverages. IMM Report No. 47, May 2016; Section 5.3.1, "Mechanosynthesis of Ethanol"; http://www.imm.org/Reports/rep047.pdf.

[67] Freitas RA Jr., Merkle RC. A minimal toolset for positional diamond mechanosynthesis. J Comput Theor Nanosci. 2008;5:760-861; http://www.molecularassembler.com/Papers/MinToolset.pdf.

Primary #1: H abstraction "HAbst*" tool (•CC–$C_{10}H_{15}$) to remove an H atom;
Primary #2: Ge radical "*GeRad" tool (•GeC_9H_{15}) for moiety transfer with weak bonding and for abstraction tool recharge reactions;

Intermediate #1: CH_3 transfer tool (CH_3–GeC_9H_{15}) to acquire a CH_3 group;
Intermediate #2: CH_2 donation tool (•CH_2–GeC_9H_{15}) to add a CH_2 group;
Intermediate #3: CH_3CH_2 donation tool (CH_3CH_2–GeC_9H_{15}) to add a CH_3CH_2 group;
Intermediate #4: OH donation tool (OH–GeC_9H_{15}) to add an OH group;
Intermediate #5: H donation tool (H–GeC_9H_{15}) to add an H atom; and
Intermediate #6: spent abstraction tool "HAbst-H" (H–CC–$C_{10}H_{15}$) needing recharge.

One possible minimal toolset for building linear, planar, branching, or cyclic organic molecules containing only the elements C (black), H (white), and O (red) is shown below, with the two primary tools at left (P1, P2) and six intermediate tool states at right (I1-I6). In this example, many tooltips also include Ge (yellow) atoms at the working apex or "bridgehead" position.[68]

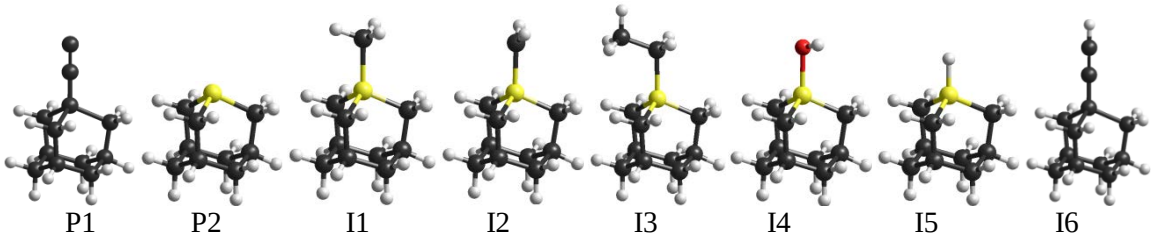

Each of these tooltips – all built on a single adamantane cage – is attached to a larger tool handle structure (not shown) that is mounted on a reagent device that is attached, in turn, to moving conveyor belt mechanisms (images, below).[69] Note the "backing surfaces" in the mechanism illustrated at center, below – these may be used to apply large crushing forces to opposing moieties in constrained volumes to overcome reaction barriers if necessary.

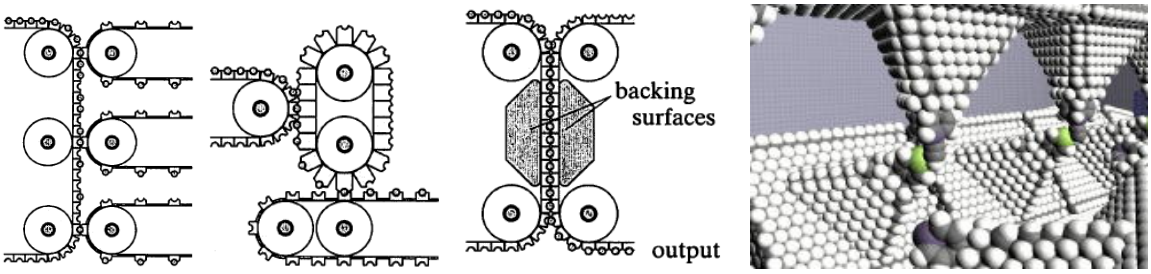

[68] Freitas RA Jr. The Whiskey Machine: Nanofactory-Based Replication of Fine Spirits and Other Alcohol-Based Beverages. IMM Report No. 47, May 2016; http://www.imm.org/Reports/rep047.pdf.

[69] Adapted from: Drexler KE. Nanosystems: Molecular Machinery, Manufacturing, and Computation, Wiley, 1992, Figs. 13.7(b), 13.7(c), 13.7(d); https://www.amazon.com/dp/0471575186/.

The following is a brief description of a hypothetical mechanosynthetic production line that could be used to build ethanol molecules in a cryogenic vacuum environment, using conveyor belts to move reactive molecules at high speed and to precisely control the location and nature of the interaction between these reactive molecules. The described chemistry is believed to be plausible but has not yet been computationally or experimentally validated. Nevertheless, even if this specific set of reaction sequences and molecular tools proves flawed upon more detailed analysis, it seems highly likely that other reaction sequences and toolsets can be found that will provide a convenient path to the same result.

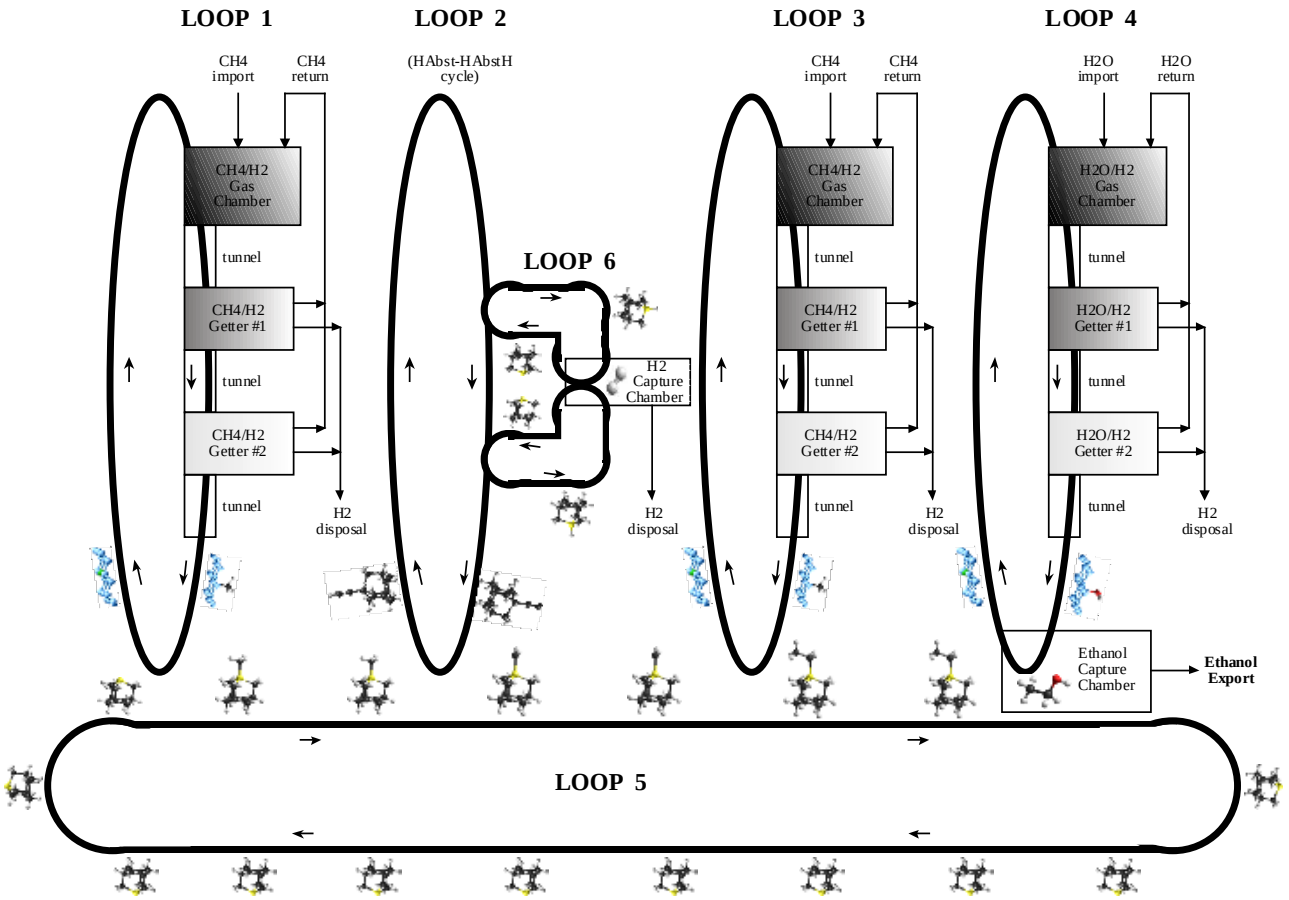

The above schematic of a hypothetical mechanosynthetic production line for ethanol molecules (black = C, white = H, yellow = Ge, red = O, blue = metal or Ge surface) has inputs of methane (CH_4) and water (H_2O) and outputs of ethanol (C_2H_5OH) and hydrogen gas (H_2). The production line consists of six interacting continuous or stepwise-moving conveyor loops as described below.

*** Loop 1: First methyl feedstock pickup.** A conveyor belt using carriers (image, right) having an outer coating of germanium (Ge)[70], platinum (Pt)[71], rhodium (Rh)[72], or iridium (Ir)[73] passes through a chamber containing methane gas molecules (CH_4). The coating surface strips one H off; the carrier is given enough residence time in the chamber to allow any H to migrate across the surface to recombine with

---

[70] A partially methylated germanium surface may provide a source of positionally controlled single-carbon feedstock. Such a surface can be prepared by thermal adsorption and reaction of CH_4 gas on Ge(100)[*] or by ion bombardment of clean Ge(111) at low substrate temperature (<470 K) using low-energy $\bullet CH_3$ ions, a strongly exoergic radical coupling reaction. After hydrocarbon CVD on Ge surfaces, absorption spectra indicate that bonding is mainly type sp^3 with CH, CH_2, and CH_3 bonds.[†] It may also be possible to prepare a CH_3-decorated Ge surface via conventional solution-phase chemical methylation,[‡] since methylated germanium is found in the natural environment.

[*] Murota J, Sakuraba M, Takehiro S. Atomically controlled processing for future Si-based devices. 2004 IEEE Workshop on Microelectronics and Electron Devices, Boise, ID, USA, 2004, pp. 31-34; https://ieeexplore.ieee.org/abstract/document/1297343.

[†] Franks J. Preparation and properties of diamondlike carbon films. J Vac Sci Technol A. 1989;7:2307; https://avs.scitation.org/doi/abs/10.1116/1.575933.

[‡] Sundermeyer W, Verbeek W. A Method for the Preparation of Methylmetal Compounds. Angew Chemie Intl Ed Engl. 1966 Jan;5(1):1-6; https://onlinelibrary.wiley.com/doi/abs/10.1002/anie.196600011; Mayer HP, Rapsomanikis S. Chemical methylation of germanium(II) in model aqueous solutions. Appl Organomet Chem. 1992 Apr;6(2):173-178; https://onlinelibrary.wiley.com/doi/abs/10.1002/aoc.590060210; Buriak JM. Organometallic chemistry on silicon and germanium surfaces. Chem Rev. 2002 May;102(5):1271-1308; http://www.gfmoorelab.com/uploads/4/2/3/1/42315775/buriak_chem_rev_2002.pdf.

[71] Methane impinging on Pt(111) causes methyl to adsorb at 120 K.[*] On Pt(111) surface, the dissociative chemisorption of methane to CH_3 and H is downhill by 6.5 kcal/mole. Breaking the second C-H bond to form CH_2 adsorbed on the surface is 1.2 kcal/mole uphill; forming CH adsorbed is then downhill by 21.7 kcal/mole.[†]

[*] Papp C, Trankenschuh B, Streber R, Fuhrmann T, Denecke R, Steinruck HP. Influence of steps on the adsorption of methane on platinum surfaces. J Phys Chem C. 2007 Jan 18;111(5):2177-2184; https://pubs.acs.org/doi/abs/10.1021/jp066268f.

[†] Kua J, Goddard WA III. Chemisorption of Organics on Platinum. 2. Chemisorption of C_2H_x and CH_x on Pt(111). J Phys Chem B 1998 Nov 3;102(47):9492-9500; http://www.wag.caltech.edu/publications/sup/pdf/394.pdf.

[72] Methane adsorbs dissociatively to the Rh(111) surface.[*]

[*] Mavrikakis M, Rempel J, Greeley J, Hansen LB, Norskov JK. Atomic and molecular adsorption on Rh(111). J Chem Phys. 2002 Oct 8;117(14):6737-6744; https://core.ac.uk/download/pdf/13727515.pdf.

[73] Methane dissociatively adsorbs on Ir(111) surface.[*] It may be possible to start with ethylene which deposits on Ir surface as ethylidyne (C-CH_3) at 300 K. Abstraction of the CH_3 by GeRad may be possible because the C-C bond is apparently weak – the hydrocarbon decomposes at 500 K leaving only a C layer on the surface.[†]

[*] e.g., Henkelman G, Jónsson H. Theoretical Calculations of Dissociative Adsorption of CH_4 on an Ir(111) Surface. Phys Rev Lett. 2001 Jan 22;86(4):664-7; http://www.henkelmanlab.org/pubs/henkelman01_664.pdf.

[†] Kostov KL, Marinova TS. Ethylene adsorption on a clear iridium surface. Reaction Kinetics Catalysis Lett. 1986 Mar;32:141-146; https://link.springer.com/article/10.1007/BF02063463.

another H on the surface, then to leave the surface as H_2 gas while remaining trapped in the chamber. This leaves a CH_3 bound to the Loop 1 carrier surface. The Loop 1 carriers then traverse a series of tunnels tight enough to prevent most stray CH_4 or H_2 molecules from following the carriers through the tunnel. At intervals the tunnels open up into small getter chambers equipped with sorting rotors[74] having binding sites for CH_4 and H_2 to collect and remove any of these molecules that happen to slip through.

Cleared of any bound molecules other than the desired CH_3, the conveyor belt finally emerges into a vacuum where each carrier is brought into firm contact with carriers from another conveyor belt (Loop 5) whose carriers protrude a •GeRad tool. The CH_3 group hops from the Loop 1 carrier onto the •GeRad tool because this transfer is favored energetically, making a CH_3-GeRad intermediate on the Loop 5 carriers. The empty Ge-, Pt-, Rh- or Ir-coated carriers are returned to the starting point, re-entering the methane chamber ready for the next cycle without further processing.

*** Loop 2: Hydrogen abstraction from first methyl.** Each carrier that is attached to the Loop 2 conveyor belt protrudes an HAbst• tool and operates entirely in vacuum. The Loop 2 carriers are brought into firm contact with a CH_3 bound to a CH_3-GeRad intermediate in Loop 5, abstracting one of the H atoms from the bound CH_3 and leaving a •CH_2-GeRad intermediate bound to the carrier of System 5. The spent (hydrogenated) HAbst-H intermediates on the carriers of Loop 2 are brought into contact with a recharge subsystem (Loop 6) whereupon the excess H is removed and disposed of, after which the reclaimed and reactivated HAbst• tools resume the next cycle of Loop 2 operation without further processing.

*** Loop 3: Second methyl feedstock pickup.** This conveyor belt system is exactly the same as Loop 1, and runs parallel to and in synchrony with it. Once the second -CH_3 group has been transferred (see Loop 5), the empty carriers are returned to the starting point, ready for the next cycle without further processing.

*** Loop 4: Hydroxyl feedstock pickup.** The Loop 4 conveyor belt system is almost the same as Loop 1, except that the feedstock attached to the carriers is an -OH group rather than a -CH_3 group (image, right). The bulk input is a chamber containing water (H_2O), which, like the methane, has had one H dissociatively removed, yielding in this case a migrating H and an –OH group bound to the carrier.[75] Once the -OH group has been transferred, the empty carriers are returned to the starting point ready for the next cycle without further processing.

---

[74] Drexler KE. Nanosystems: Molecular Machinery, Manufacturing, and Computation, John Wiley & Sons, New York, 1992, Section 13.2.1(a) “Modulated receptors for selective transport: Basic concepts”; https://www.amazon.com/dp/0471575186/. Freitas RA Jr. Nanomedicine, Volume I: Basic Capabilities, Landes Bioscience, Georgetown, TX, 1999; Section 3.4.2, “Sorting Rotors”; http://www.nanomedicine.com/NMI/3.4.2.htm.

[75] A Cu(110) surface catalyzes water dissociation into H and OH under ambient conditions, and autocatalytic water dissociation is believed to be a general phenomenon on metal surfaces.* An $(IrO_2)_n$ (n=1-5) cluster when exposed to one H_2O molecule with 15.1 kcal/mole energy added can be driven uphill to form $IrO_2.H_2O$, which then exoergically transforms to $IrO(OH)_2$ which is downhill by -17.9 kcal/mole.† Oxygen-assisted water dissociation reaction (OWD: $H_2O + O \rightarrow 2OH$), based on a tunnel mechanism of H

*** Loop 5: Build ethanol from two methyl groups and one hydroxyl group, then release.** Note that this is the previously-mentioned vacuum-residing conveyor belt system whose carriers initially protrude a •GeRad tool. A molecule of ethanol is assembled on each carrier as the Loop 5 belt encounters, in sequence, carriers from Loop 1, Loop 2, Loop 3, and Loop 4.

Encounter with Loop 1: When brought into contact with a Loop 1 carrier, a CH_3 group transfers from that carrier onto the Loop 5 •GeRad tool, making a CH_3-GeRad intermediate on the Loop 5 carrier. The empty Loop 1 carrier is returned to the starting point, ready for the next cycle without further processing.

Encounter with Loop 2: The CH_3-GeRad intermediate on the Loop 5 carrier is next brought into contact with an HAbst• tool on a Loop 2 carrier, which abstracts one of the H atoms from the bound CH_3 group, leaving a •CH_2-GeRad intermediate on the Loop 5 carrier.

Encounter with Loop 3: The •CH_2-GeRad intermediate on the Loop 5 carrier is next brought into contact with a Loop 3 carrier, whereupon a snap-on reaction occurs because there is an energetic preference for the CH_3 group on the Loop 3 carrier to be bonded to the C atom of the •CH_2-GeRad intermediate on the Loop 5 carrier rather than to the Ge or metal atom holding the CH_3 group onto the Loop 3 carrier. This leaves a CH_3CH_2-GeRad intermediate on the Loop 5 carrier. The empty Loop 3 carrier is returned to the starting point, ready for the next cycle without further processing.

Encounter with Loop 4: The CH_3CH_2–GeRad intermediate on the Loop 5 carrier is then pressed into contact with the OH-metal intermediate on the Loop 4 carrier inside an ethanol collection chamber. The hydroxyl group should have some energetic preference to be bonded to the Ge-bonded C atom of the CH_3CH_2–GeRad intermediate rather than to the metal atom holding the OH- group on the Loop 4 carrier,[76] so a metal-Ge bond may form as the -OH group inserts

---

transfer, has activation energies much lower than those of water dissociation on clean metal (Pt, Cu, Ni, Rh) surfaces.[‡] OH groups rest stably on the Rh(111) surface with the H pointing away from the surface.[**]

[*] Andersson K, Ketteler G, Bluhm H, Yamamoto S, Ogasawara H, Pettersson LGM, Salmeron M, Nilsson A. Autocatalytic water dissociation on Cu(110) at near ambient conditions. J Am Chem Soc. 2008 Mar 5;130(9):2793-2797; https://escholarship.org/content/qt0zc1q9rv/qt0zc1q9rv.pdf.

[†] Zhou X, Yang J, Li C. Theoretical study of structure, stability, and the hydrolysis reactions of small iridium oxide nanoclusters. J Phys Chem A. 2012 Oct 11;116(40):9985-9995; https://pubmed.ncbi.nlm.nih.gov/22985267/.

[‡] German ED, Sheintuch M. Oxygen-Assisted Water Dissociation on Metal Surfaces: Kinetics and Quantum Effects. J Phys Chem C. 2011 Apr 29;115(20):10063-10072; https://pubs.acs.org/doi/abs/10.1021/jp200457h.

[**] Mavrikakis M, Rempel J, Greeley J, Hansen LB, Norskov JK. Atomic and molecular adsorption on Rh(111). J Chem Phys. 2002 Oct 8;117(14):6737-6744; https://core.ac.uk/download/pdf/13727515.pdf.

[76] Since metal-oxygen and metal-germanium bond energy data were not readily available, we assumed for the purposes of this calculation that the OH group on Loop 4 is bonded to a GeRad. In this case, the reaction could be plausibly estimated to be exoergic because we are breaking one C-Ge bond (2.47 eV) and one (Loop 4) Ge-O bond (2.81 eV), total +5.28 eV, while creating one (Loop 4-Loop 5) Ge-Ge bond (1.95 eV) and one C-O bond (3.71 eV), total -5.66 eV, therefore the reaction appears energetically favored by **-0.38 eV**. However, this reaction has not been validated using quantum chemistry simulations. Sources:

into the Ge-C bond on the CH_3CH_2–GeRad intermediate on the Loop 5 carrier, creating a CH_3-CH_2-OH molecule of ethanol that is released into the ethanol collection chamber. The Loop 4 and Loop 5 carriers are then pulled apart, breaking the temporary bond between them. This leaves an empty carrier on Loop 4 and a •GeRad tool on Loop 5, both of which are returned to the starting point in their respective loops, ready for the next cycle without further processing.

*** Loop 6: HAbst-H tool recharge.** The recharge subsystem required for Loop 2 may involve two identical tracks and two pairs of specially configured •GeRad tools. In each pair, the first •GeRad tool alternately bonds and unbonds to the distal C atom of the ethynyl C_2 group on an HAbst-H intermediary on Loop 2, a process that can cycle endlessly. The second •GeRad tool of the pair approaches the excess H atom on the HAbst-H intermediary and abstracts it, making an H-GeRad intermediary on a Loop 6 carrier and restoring the active HAbst• tool on a Loop 2 carrier. The second pair of •GeRad tools performs the same operations on a second HAbst-H intermediary on Loop 2. The two H-GeRad intermediaries are then brought into forcible contact while parked inside a separate hydrogen capture chamber, creating a Ge-Ge bond between the two tools and releasing an H_2 gas molecule into the chamber which can be safely exhausted from the system. The two Loop 6 tools are then pulled apart, removed from the H_2 capture chamber, and returned to the starting point ready for the next recharge cycle without further processing. Alternatively, the H-GeRad intermediaries could be re-routed to a reaction sequence for building some molecule other than ethanol in which a hydrogen donation was required.

A similar process may be applied to build any CHO molecule of known structure and elemental composition. Many reaction sequences can be determined in advance and can be hard-coded. Production lines could use switchyards (image, left) to route carriers from one Loop to another Loop on the fly, essentially creating a reprogrammable production network. But in order to be able to handle any known molecule that is composed only of C, H, and O atoms and one or more of the five basic types of organic building blocks mentioned earlier, we will also need automated mechanosynthetic sequence generation to minimize or eliminate the human labor requirement. This seems achievable with future research, given the relative structural simplicity of the molecular targets and the relatively small number of primary tools and core reactions that are likely to be needed (i.e., a relatively small "chemical alphabet" is required) to build organic molecules mechanosynthetically, functional group by functional group. Adding a few more elements such as nitrogen, sulfur, and phosphorus would raise the complexity level and increase the tooltype count – but probably tolerably so, while greatly extending the scope of manufacturable molecules to the full range of biologicals including amino acids, peptides, nucleotides, proteins and DNA.

---

http://www.wiredchemist.com/chemistry/data/bond_energies_lengths.html and Jan Felix Binder, *Electronic and Structural Properties of the Ge/GeO2 Interface through Hybrid Functionals*, PhD Thesis, École Polytechnique Fédérale de Lausanne, 2012, p.30 and Fig. 3.9/p.37 (for estimate of Ge-O bond strength); http://infoscience.epfl.ch/record/176949/files/EPFL_TH5363.pdf.

2.1.2.2 Quantitative Productivity of Generic Synthesis Unit

The 6-loop schema described above appears to fabricate individual molecules of ethanol fairly efficiently using only methane and water as the bulk inputs and generating hydrogen gas as the only waste product. Assuming that each conveyor belt/roller mechanism requires ~1 million carbon atoms,[77] then six of these, along with infrastructure support including ~1 million atoms for the sorting rotor "getters" plus 5 million atoms for each of 11 chamber/getter boxes with tunnels and equipment housings, sums to 62 million carbon atoms. Adding in motors, controllers, and other hardware, each mechanosynthetic **Fabrication Subunit** incorporates perhaps $n_{C\text{-}FS} \sim 100$ million carbon atoms of total mass $M_{FS} = m_C\ n_{C\text{-}FS} = 2 \times 10^{-18}$ kg (taking $m_C = 2 \times 10^{-26}$ kg/C atom). Each Fabrication Subunit may occupy a $(100\ nm)^3$ cube having a volume $V_{FS} \sim 0.001$ micron^3, with about half of this volume occupied by machinery and the rest by empty space (vacuum).

While mechanosynthetic production lines are thought to be operable at MHz frequencies,[78] to keep power consumption low we assume in the present example that each Fabrication Subunit will be operated at a frequency of only $\nu_{FS} = 0.1$ MHz. This produces $r_{organics} = 10^5$ molecules/sec of organic (ethanol) molecules, representing a production rate of $R_{FS} = r_{organics}\ MW_{organics} / N_A = 7.6 \times 10^{-21}$ kg/sec of ethanol per Fabrication Subunit, taking molecular weight as $MW_{organics} \sim MW_{ethanol} = 0.046$ kg/mole, with Avogadro's number $N_A = 6.023 \times 10^{23}$ molecules/mole. Similar production rates should be achievable for other organic molecules of reasonable size, perhaps averaging ~0.090 kg/mole (~100 daltons), simply by adding a few more fabrication loops to Fabrication Subunit production lines.

For scaling purposes, we assume that the generic organic Fabrication Subunits comprising the **Generic Synthesis Unit** must produce near-absolute purity organic molecules similar to ethanol at a target production rate of $R_{FSB} = N_{FS}\ R_{FS} = 0.278$ gm/sec (~**1 kg/hr** ~ $R_{CellMill}$). This requires $N_{FS} = 36{,}500$ trillion Fabrication Subunits having a volume of $V_{FSB} = N_{FS}\ V_{FS} =$ **36.5 cm^3** and a mass of $M_{FSB} = N_{FS}\ M_{FS} =$ **73 gm**.

To estimate the power consumption for performing mechanosynthesis, we note that the standard enthalpy of formation for liquid ethanol is 470 zJ/molecule.[79] With an efficient design, we should be able to closely approach this figure, but conservatively assuming ~50% energy efficiency implies a net energy dissipation of $E_{diss} = 940$ zJ/molecule.[80] Adopting this estimate, the

---

[77] Drexler KE. Nanosystems: Molecular Machinery, Manufacturing, and Computation, John Wiley & Sons, New York, 1992, Section 13.3.5; https://www.amazon.com/dp/0471575186/.

[78] Drexler KE. Nanosystems: Molecular Machinery, Manufacturing, and Computation, John Wiley & Sons, New York, 1992, Table 14.4; https://www.amazon.com/dp/0471575186/.

[79] http://en.wikipedia.org/wiki/Standard_enthalpy_change_of_formation_(data_table).

[80] Even if we pessimistically assumed that all mechanosynthetic bond-breaking and bond-making events were completely dissipative, the energy cost would only be about 5.7-fold higher, around 5350 zJ/molecule for ethanol. This includes breaking a C-H bond (671 zJ) and making a C-Ge bond (391 zJ) at Loop 1, breaking a C-H bond (671 zJ) at Loop 2, breaking a C-H bond (671 zJ) and making a C-C bond (556 zJ) at

Fabrication Subunits would produce generic organic molecules similar in size to ethanol at an energy cost of $E_{ethanol} = E_{diss}\ N_A / MW_{ethanol}$ = 12.3 MJ/kg and the entire Fabrication Subunit block would have a power draw of $P_{FSB} = R_{FSB}\ E_{diss}\ N_A / MW_{ethanol}$ = **3400 W** when operated at the R_{FSB} = 0.278 gm/sec ethanol production rate, with each Fabrication Subunit drawing $P_{FS} = P_{FSB}/N_{FS}$ = 0.094 pW. Power density for the Fabrication Subunits would then be $P_{d\text{-}FSB} = P_{FSB} / V_{FSB}$ ~10^8 W/m^3, well below the ~10^{10} W/m^3 power density estimated for molecular transport[81] and significantly lower than the ~10^{11} W/m^3 power density estimated for the Lab Module Block of the Molecular Assay System described elsewhere.[82]

2.2 Personalized Synthesis Unit

Perhaps the most important task of the Molecular Synthesis Module in the cell mill is to synthesize copies of the patient's own genetically autologous proteins and other relevant personalized biomolecules, working from analysis of the patient's genome, possibly supplemented with samples of the patient's tissues. These synthetic activities are accomplished by the **Personalized Synthesis Unit**, comprising DNA Mills, Protein Mills, and Carbohydrate Mills (see below), which, together with the Generic Synthesis Unit (Section 2.1), comprises the Molecular Synthesis Module (Section 2) of the cell mill.

To perform these synthesis functions for a patient who does not already possess a complete personal genomic sequence, a small representative set of microscopic physical samples of the patient's genome are obtained from noncritical tissues, allowing computational reconstruction of the individual's consensus genomic sequence (Section 2.2.1). Using this computed sequence, **DNA Mills** (Section 2.2.2) can then assemble patient-specific complete genome-length DNA strands for use in assembling manufactured cell nuclei.

After computationally translating the codons contained in the consensus genomic sequence, **Protein Mills** (Section 2.2.3) can assemble patient-specific proteins of all kinds found in the human body. Similar nanorobotic systems comprising **Carbohydrate Mills** (Section 2.2.4) will be able to assemble carbohydrate-containing polymers (polysaccharides),[83] glycoproteins,[84] glycolipids,[85] lipoproteins,[86] nucleoproteins[87] and the like with similar productivity.

Loop 3, breaking an O-H bond (753 zJ) and making a C-O bond (575 zJ) at Loop 4, breaking a C-Ge bond (391 zJ) at Loop 5, and breaking a C-H bond (671 zJ) at Loop 6.

[81] Freitas RA Jr. Nanomedicine, Volume I: Basic Capabilities, Landes Bioscience, Georgetown TX, 1999, Section 6.5.6(A), "Power Analysis in Design: Molecular Transport"; http://www.nanomedicine.com/NMI/6.5.6.htm#p2.

[82] Freitas RA Jr. Cryostasis Revival: The Recovery of Cryonics Patients through Nanomedicine. Alcor Life Extension Foundation, Scottsdale AZ, 2022; Section F.2, "Molecular Assay System Scaling"; https://www.alcor.org/cryostasis-revival/.

[83] https://en.wikipedia.org/wiki/Polysaccharide.
[84] https://en.wikipedia.org/wiki/Glycoprotein.
[85] https://en.wikipedia.org/wiki/Glycolipid.
[86] https://en.wikipedia.org/wiki/Lipoprotein.
[87] https://en.wikipedia.org/wiki/Nucleoprotein.

2.2.1 Consensus Genomic Sequence

It is necessary to obtain the patient's consensus DNA sequence in order to manufacture biomolecules personalized to that patient. A consensus DNA sequence[88] is the ordered list of nucleotide base pairs comprising a "clean" or "original" genome that results from sampling the entire set of chromosomes from at least 100 of the patient's cells and then compiling the most likely representative DNA sequence on which the majority of chromosomal samples agree, screening out all randomly occurring point mutations, viral insertions accumulated over a lifetime, read errors, and various other local genetic defects, and incorporating all tissue- or organ-specific molecular decorations such as methylation patterns.

The patient's existing cellular chromosome set must be sampled and sequenced using a fast *ex vivo* DNA reading facility, first by securing representative physical samples of the patient's DNA (Section 2.2.1.1) and then by rapidly sequencing the DNA samples in order to compile the consensus sequence (Section 2.2.1.2).

2.2.1.1 Genome Sampling

The first step in obtaining a patient's consensus genomic sequence is to secure samples of the patient's existing DNA.[89] In the future nanomedical treatment environment in which cell mill technology has been developed, templates for the standard human DNA sequences in each organ and for each cytotype (including tissue-, organ-, and age-specific[90] epigenetic information such as methylation patterns) will be readily available. The task of the medical team is to ascertain how the patient's personal DNA – including the >1 million known single nucleotide polymorphisms (SNPs)[91] and other structural and epigenetic variations – differs from standard sequences by directly sampling the patient's genome.

Genome acquisition would begin with the collection of at least 100 whole-cell samples taken from the patient's body. Future research should determine if these samples should be randomly collected throughout the body, or should be clustered in specific locations or organs where DNA

---

[88] Freitas RA Jr. The Ideal Gene Delivery Vector: Chromallocytes, Cell Repair Nanorobots for Chromosome Replacement Therapy. J. Evol. Technol. 2007 Jun;16:1-97; http://jetpress.org/v16/freitas.pdf.

[89] adapted from: Freitas RA Jr. The Ideal Gene Delivery Vector: Chromallocytes, Cell Repair Nanorobots for Chromosome Replacement Therapy. J. Evol. Technol. 2007 Jun;16:1-97; Section 4.1, "Genome Sampling and Modification"; http://jetpress.org/v16/freitas.pdf.

[90] Horvath S. DNA methylation age of human tissues and cell types. Genome Biol. 2013;14(10):R115; https://www.ncbi.nlm.nih.gov/pmc/articles/PMC4015143/. Erratum: https://www.ncbi.nlm.nih.gov/pmc/articles/PMC4427927/.

[91] Sachidanandam R, *et al*. International SNP Map Working Group. A map of human genome sequence variation containing 1.42 million single nucleotide polymorphisms. Nature 2001 Feb 15;409:928-933; http://repository.cshl.edu/id/eprint/29293/.

damage is believed to be minimized. The removal of ~0.000001% of randomly-placed sampling cells should not disturb overall tissue or organ function in any way.

After the sampled cells are collected, their DNA is extracted nondestructively and intact. The DNA collected from each set of 100 cell nuclei is sequenced (Section 2.2.1.2) and compared. This yields a consensus sequence that should be identical to the original pristine pre-adult or adult DNA such that all sequence information errors due to DNA damage accumulated during the patient's lifetime (e.g., due to aging or viral corruption) have been averaged out and eliminated. The statistical probability that a majority of 100 independent DNA samples of each cytotype will possess identical random single base pair errors at the exact same positions in the sequence is vanishingly small. Note that the consensus sequence for each chromosome will include one maternal- and one paternal-contributed set.

Systematic base pair errors and variations are more problematic. For example, all descendents of a reproducing cell that bears a retrovirus-modified sequence will retain the same sequence modifications, but this will be a known effect of the retrovirus and hence recognizable and correctable. Additional mixing may occur with recombination or transposons,[92] but not identically in all or a majority of cells, hence is excludable. Some regions of the genome (e.g., hypervariable minisatellite DNA repeats at recombination hotspots,[93] hotspots at microRNA genes,[94] and the hypermutating immunoglobulin variable region[95] and proto-oncogenes[96]) may be more susceptible to recombination or mutation[97] than other regions and hence might accumulate similar types of errors preferentially in those locations.

To deal with such systematic errors, the consensus sequence should be compared to earlier genome sequencing scans that may be recorded in the patient's medical records, perhaps even

---

[92] https://en.wikipedia.org/wiki/Transposable_element.

[93] Wahls WP, Moore PD. Recombination hotspot activity of hypervariable minisatellite DNA requires minisatellite DNA binding proteins. Somat Cell Mol Genet. 1998 Jan;24(1):41-51; https://www.ncbi.nlm.nih.gov/pmc/articles/PMC3151739/. Myers S, Bottolo L, Freeman C, McVean G, Donnelly P. A fine-scale map of recombination rates and hotspots across the human genome. Science. 2005 Oct 14;310(5746):321-324; https://pubmed.ncbi.nlm.nih.gov/16224025/.

[94] Calin GA, Croce CM. MicroRNAs and chromosomal abnormalities in cancer cells. Oncogene. 2006 Oct 9;25(46):6202-6210; https://www.nature.com/articles/1209910.pdf?origin=ppub.

[95] Woo CJ, Martin A, Scharff MD. Induction of somatic hypermutation is associated with modifications in immunoglobulin variable region chromatin. Immunity. 2003 Oct;19(4):479-489; https://core.ac.uk/download/pdf/82119720.pdf.

[96] Pasqualucci L, Neumeister P, Goossens T, *et al*. Hypermutation of multiple proto-oncogenes in B-cell diffuse large-cell lymphomas. Nature. 2001 Jul 19;412(6844):341-346; https://pubmed.ncbi.nlm.nih.gov/11460166/.

[97] Yauk C. Monitoring for induced heritable mutations in natural populations: application of minisatellite DNA screening. Mutat Res. 1998 Aug;411(1):1-10; https://macsphere.mcmaster.ca/bitstream/11375/6616/1/fulltext.pdf#page=52.

from infancy, and these may be augmented by further sampling, either from the patient's quiescent stem cells[98] (very low-activity cells likely to retain the most pristine copies of the "original" genome) or from the patient's undifferentiated white blood cell (WBC),[99] hepatic,[100] muscle,[101] neural[102] or other progenitor cells which have presumably undergone relatively fewer mutations and may be more abundant than stem cells. Comparing even a few of these should allow all errors other than those present in the original fertilized egg cell to be detected and eliminated. Additionally, the unequal recombination of numerous (noncoding) minisatellite DNA regions (tandemly repeated 10-100 bp units typically representing <10% of mammalian genomes)[103] can slightly adjust region lengths, making every individual genome distinct,[104] but these systematic variations should be easily recognizable in the sequence data. Comparison to a few representative sample genomes from other organs of the patient might be warranted to detect any possible epigenetic organ-specific asymmetric distribution patterns of post-mitotic old/new sister chromatid copies, as has been proposed by Armakolas and Klar.[105]

Another complication is the discovery[106] that in addition to single nucleotide polymorphisms, the genome of each person also has natural genetic "structural variations," including most importantly deletions, duplications and large-scale copy-number variants – collectively termed

---

[98] Young HE. Existence of reserve quiescent stem cells in adults, from amphibians to humans. Curr Top Microbiol Immunol. 2004;280:71-109; https://pubmed.ncbi.nlm.nih.gov/14594208/.

[99] Pelayo R, Miyazaki K, Huang J, Garrett KP, Osmond DG, Kincade PW. Cell cycle quiescence of early lymphoid progenitors in adult bone marrow. Stem Cells. 2006 Dec;24(12):2703-2713; https://www.ncbi.nlm.nih.gov/pmc/articles/PMC1849950/.

[100] Santoni-Rugiu E, Jelnes P, Thorgeirsson SS, Bisgaard HC. Progenitor cells in liver regeneration: molecular responses controlling their activation and expansion. APMIS 2005 Nov-Dec;113:876-902; https://onlinelibrary.wiley.com/doi/pdf/10.1111/j.1600-0463.2005.apm_386.x.

[101] Relaix F. Skeletal muscle progenitor cells: from embryo to adult. Cell Mol Life Sci. 2006 Jun;63(11):1221-1225; https://search.proquest.com/openview/85523a50f0dcf5839e699ed12a52f27d/1?pq-origsite=gscholar&cbl=54068.

[102] Klassen HJ, Imfeld KL, Kirov II, Tai L, Gage FH, Young MJ, Berman MA. Expression of cytokines by multipotent neural progenitor cells. Cytokine. 2003 May;22(3-4):101-106; https://pubmed.ncbi.nlm.nih.gov/12849709/.

[103] Lewin B. Genes V, Oxford University Press, New York NY, 1995; https://www.amazon.com/dp/0198542879/.

[104] Lewin B. Genes V, Oxford University Press, New York NY, 1995; https://www.amazon.com/dp/0198542879/.

[105] Armakolas A, Klar AJ. Cell type regulates selective segregation of mouse chromosome 7 DNA strands in mitosis. Science. 2006 Feb 24;311(5764):1146-1149; https://pubmed.ncbi.nlm.nih.gov/16497932/.

[106] Tuzun E, Sharp AJ, Bailey JA, Kaul R, Morrison VA, Pertz LM, Haugen E, Hayden H, Albertson D, Pinkel D, Olson MV, Eichler EE. Fine-scale structural variation of the human genome. Nat Genet. 2005 Jul;37(7):727-32; http://eichlerlab.gs.washington.edu/eichler/pdfs/Eray2005natureGenetics.pdf.

copy-number variants or copy-number polymorphisms[107] – as well as insertions, inversions and translocations.[108] There are 1,447 copy number variable regions (CNVRs) in the human genome,[109] ranging in size from 960 bp to 3.4 Mb,[110] with ~12% of the genome variable in copy number.[111] These structural variants can comprise millions of nucleotides of heterogeneity within every genome, and possibly may contribute to human diversity and disease susceptibility.[112] One initial mapping[113] located 415,436 unique human insertion and deletion (INDEL) polymorphisms up to 9989 bp in length and split almost equally between insertions and deletions. The map identified five major classes of INDELs: (1) insertions and deletions of single-base pairs, (2) monomeric base pair expansions, (3) multi-base pair expansions of 2-15 bp repeat units, (4) transposon insertions, and (5) INDELs containing random DNA sequences. These INDELs are distributed throughout the human genome with an average density of one INDEL per 7.2 kb of DNA.[114] Since all cells in a target organ of a given patient should share the same structural variants, the patient's uniquely variant genomic structure should be reconstructable during sequencing based on information provided by the genomic sampling procedure previously described.

Additional complications involve cell differences due to epigenetic gene regulation, most notably methylation (e.g., only ~10% of genes are activated at any given time). The eukaryotic genome is normally demethylated, then is re-methylated early in embryonic development via epigenetic

---

[107] Sebat J, Lakshmi B, Troge J, *et al*. Large-scale copy number polymorphism in the human genome. Science. 2004 Jul 23;305(5683):525-528; http://gene-quantification.org/sebat-cnv-2004.pdf.

[108] Feuk L, Carson AR, Scherer SW. Structural variation in the human genome. Nat Rev Genet. 2006 Feb;7(2):85-97; http://psych.colorado.edu/~carey/pdffiles/cnv_feuk.pdf.

[109] Redon R, *et al*. Global variation in copy number in the human genome. Nature. 2006 Nov 23;444(7118):444-54; https://www.ncbi.nlm.nih.gov/pmc/articles/PMC2669898/.

[110] Komura D, Shen F, Ishikawa S, *et al*. Genome-wide detection of human copy number variations using high-density DNA oligonucleotide arrays. Genome Res. 2006 Dec;16(12):1575-1584; https://www.ncbi.nlm.nih.gov/pmc/articles/PMC1665641/.

[111] Redon R, *et al*. Global variation in copy number in the human genome. Nature. 2006 Nov 23;444(7118):444-54; https://www.ncbi.nlm.nih.gov/pmc/articles/PMC2669898/.

[112] Feuk L, Carson AR, Scherer SW. Structural variation in the human genome. Nat Rev Genet. 2006 Feb;7(2):85-97; https://intranet.lcg.unam.mx/frontiers/files/frontiers/Structural%20variation.pdf.

[113] Mills RE, Luttig CT, Larkins CE, Beauchamp A, Tsui C, Pittard WS, Devine SE. An initial map of insertion and deletion (INDEL) variation in the human genome. Genome Res. 2006 Sep;16(9):1182-90; https://www.ncbi.nlm.nih.gov/pmc/articles/pmc1557762/.

[114] Mills RE, Luttig CT, Larkins CE, Beauchamp A, Tsui C, Pittard WS, Devine SE. An initial map of insertion and deletion (INDEL) variation in the human genome. Genome Res. 2006 Sep;16(9):1182-90; https://www.ncbi.nlm.nih.gov/pmc/articles/pmc1557762/.

reprogramming.[115] After birth, differences in maternal care can induce differential methylation patterns in some promoter regions, influencing gene expression.[116] It is now known that methylation correlates predictably with age in almost all organs, with methylation decreasing with age in about half of DNA sites and increasing with age in the other half.[117] Genome-wide hypomethylation[118] and hypermethylation[119] may be implicated in cancer. An important special case is X-chromosome inactivation (XCI)[120] in which the X-chromosome contributed from either maternal or paternal parent is silenced (becoming Barr bodies[121]), leaving the other one active, in female mammalian cells. XCI for each cell is chosen randomly[122] during embryogenesis and is presumed to be a permanent selection for all descendants of a cell. While X-linked transmembrane proteins such as the teneurins[123] reside on the plasma membrane and thus may be antigenically visible, even in rare cases of extremely skewed XCI (e.g., 80% of cells favoring one parent,[124] rather than the usual ~50%), the immune system recognizes both isoforms so a different assignment to any particular cell during molecular reconstruction should elicit no immune

---

[115] Haaf T. Methylation dynamics in the early mammalian embryo: implications of genome reprogramming defects for development. Curr Top Microbiol Immunol. 2006;310:13-22; https://pubmed.ncbi.nlm.nih.gov/16909904/.

[116] Weaver IC, Cervoni N, Champagne FA, D'Alessio AC, Sharma S, Seckl JR, Dymov S, Szyf M, Meaney MJ. Epigenetic programming by maternal behavior. Nat Neurosci. 2004 Aug;7(8):847-854; https://pubmed.ncbi.nlm.nih.gov/15220929/.

[117] Horvath S. DNA methylation age of human tissues and cell types. Genome Biol. 2013;14(10):R115; https://www.ncbi.nlm.nih.gov/pmc/articles/PMC4015143/. Erratum: https://www.ncbi.nlm.nih.gov/pmc/articles/PMC4427927/.

[118] Chen RZ, Pettersson U, Beard C, Jackson-Grusby L, Jaenisch R. DNA hypomethylation leads to elevated mutation rates. Nature. 1998 Sep 3;395(6697):89-93; https://pubmed.ncbi.nlm.nih.gov/9738504/.

[119] Nakayama M, Gonzalgo ML, Yegnasubramanian S, Lin X, De Marzo AM, Nelson WG. GSTP1 CpG island hypermethylation as a molecular biomarker for prostate cancer. J Cell Biochem. 2004 Feb 15;91(3):540-552; https://pubmed.ncbi.nlm.nih.gov/14755684/.

[120] Chow JC, Yen Z, Ziesche SM, Brown CJ. Silencing of the mammalian X chromosome. Annu Rev Genomics Hum Genet. 2005;6:69-92; https://pubmed.ncbi.nlm.nih.gov/16124854/.

[121] Anoop UR, Ramesh V, Balamurali PD, Nirima O, Premalatha B, Karthikshree VP. Role of Barr bodies obtained from oral smears in the determination of sex. Indian J Dent Res. 2004 Jan-Mar;15(1):5-7; https://pubmed.ncbi.nlm.nih.gov/15682788/.

[122] Haig D. Self-imposed silence: parental antagonism and the evolution of X-chromosome inactivation. Evolution. 2006 Mar;60(3):440-447; https://haiggroup.oeb.harvard.edu/files/haig/files/haig-2006-evolution.pdf.

[123] Tucker RP, Kenzelmann D, Trzebiatowska A, Chiquet-Ehrismann R. Teneurins: transmembrane proteins with fundamental roles in development. Int J Biochem Cell Biol. 2007;39(2):292-297; https://pubmed.ncbi.nlm.nih.gov/17095284/.

[124] Ørstavik KH. Skewed X inactivation in healthy individuals and in different diseases. Acta Paediatr Suppl. 2006 Apr;95(451):24-29; https://pubmed.ncbi.nlm.nih.gov/16720461/.

response. Nevertheless, a conservative protocol would ensure that any replacement genome will encode the parentally-correct XCI for each cell that is reconstructed. The XCI information may be acquired for each cell during initial whole-organ mapping by using chemical sensors to examine appropriate plasma membrane proteins such as teneurin and then to record whether the maternal or paternal variants are expressed in that cell.

The patient's genome can be repaired or modified during the replacement process, as described at length elsewhere,[125] but this topic is beyond the scope of the present discussion.

2.2.1.2 Chromosome Sequencing

A nanorobotic DNA sequencing facility[126] could be extremely small, fast, and cheap. As early as 2002, J. Craig Venter had announced he was explicitly pursuing the goal of $1000/copy human whole-genome sequencing by 2012. In 2003 the J. Craig Venter Science Foundation offered a $500,000 prize for achieving this milestone, then announced in 2005 that it was seeking to raise the prize to $10 million.[127] The NIH also solicited proposals for research leading to the $1000 genome.[128] Noted Venter: "Once this threshold has been reached, it will be feasible for the majority of individuals to have their genome sequenced and encoded as part of their medical record."

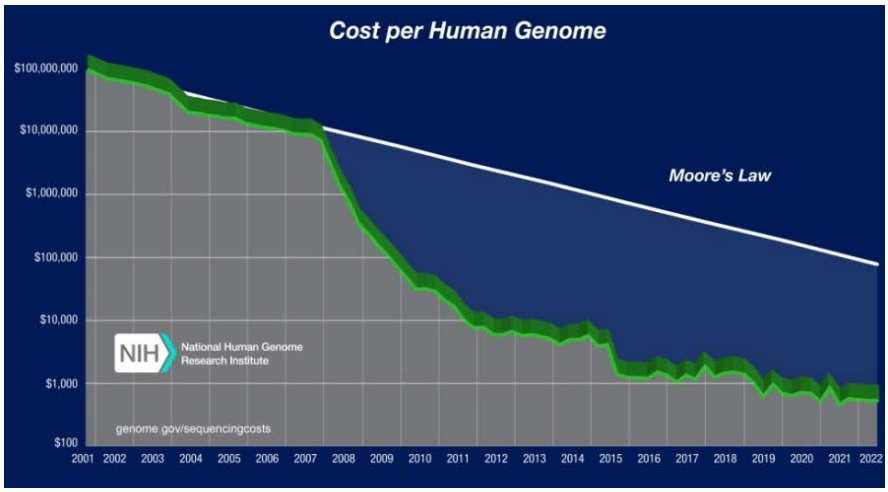

As shown in the chart at right,[129] by 2015-8

---

[125] Freitas RA Jr. The Ideal Gene Delivery Vector: Chromallocytes, Cell Repair Nanorobots for Chromosome Replacement Therapy. J. Evol. Technol. 2007 Jun;16:1-97; Section 4.1, "Genome Sampling and Modification"; http://jetpress.org/v16/freitas.pdf.

[126] adapted from: Freitas RA Jr. The Ideal Gene Delivery Vector: Chromallocytes, Cell Repair Nanorobots for Chromosome Replacement Therapy. J. Evol. Technol. 2007 Jun;16:1-97; Section 4.2, "Chromosome Sequencing"; http://jetpress.org/v16/freitas.pdf.

[127] K. Davies, "Venter Raises Stakes for $1,000 Genome Prize," Bio-IT World, 19 October 2005; http://www.bio-itworld.com/newsitems/2005/oct2005/10-19-05-news-genome-prize.

[128] M. Anderson, "NIH offers $1000 genome grant," The Scientist 5(2004):20040223-05; http://www.the-scientist.com/news/20040223/05/.

[129] National Human Genome Research Institute (NHGRI). The Cost of Sequencing a Human Genome (2024). https://www.genome.gov/about-genomics/fact-sheets/Sequencing-Human-Genome-cost.

the goal of a research-quality $1000 human genome was reached, with raw sequencing costs falling to ~$10/gigabase of DNA.

One of the foremost companies in automated genome sequencing is Illumina,[130] whose industry-leading NovaSeq 6000 machine[131] generated 20 billion base-pair reads in a single run and can read ~6 trillion base-pairs per day[132] ($R_{NovaSeq}$ = 6.93 x 10^7 bp/sec) with ~99.9% accuracy.[133] According to the technical specifications,[134] this amazingly compact machine (image, right) measured 165.6 cm x 80.0 cm x 94.5 cm ($V_{NovaSeq}$ = 1.25 m^3) with a mass of m_{NovSeq} = 481 kg and a peak power consumption of $P_{NovaSeq}$ = 2500 watts, yielding the following figures of merit for performance: ψ_V = 5.56 x 10^7 bp/m^3-sec, ψ_m = 1.44 x 10^5 bp/kg-sec, and ψ_P = 2.78 x 10^4 bp/watt-sec.

A competing DNA sequencing technology in 2020 was offered by Oxford Nanopore Technologies,[135] in which electrophoresis is used to transport individual polynucleotide molecules through a nanopore measuring ~1 nm in diameter, bathed in an electrolyte solution, across which an electric field is applied. Passage of the molecule through the pore causes minute changes in the current passing through the pore that observably differ depending on which nucleotide base (A,G, C or T) is passing through the pore at the time. Oxford Nanopore sequencing[136] systems are generally small in size. For example, Oxford offered the MinION system (image, left)[137] incorporating 512 parallel nanopore channels that allowed sequencing at 20 billion base-pairs in 48 hours

---

[130] http://www.illumina.com/.
[131] https://www.illumina.com/systems/sequencing-platforms/novaseq.html.
[132] https://www.illumina.com/systems/sequencing-platforms.html.
[133] https://en.wikipedia.org/wiki/Illumina,_Inc.#DNA_sequencing.

[134] https://support.illumina.com/content/dam/illumina-support/documents/documentation/system_documentation/novaseq/novaseq-site-prep-guide-1000000019360-06.pdf.

[135] http://nanoporetech.com/.
[136] https://en.wikipedia.org/wiki/Nanopore_sequencing.
[137] https://nanoporetech.com/products/minion.

(R_{MinION} = 1.16 x 10^5 bp/sec) with a mass of 450 gm, dimensions 14 cm x 8 cm x 3 cm (336 cm^3), and power supplied through a 2.5 watt USB cable, yielding the following figures of merit for performance: ψ_V = 3.44 x 10^8 bp/m^3-sec, ψ_m = 2.57 x 10^5 bp/kg-sec, and ψ_P = 4.63 x 10^4 bp/watt-sec.

Mature nanomechanical sequencing systems should allow the raw speed of DNA reading to be improved by another 1-2 orders of magnitude beyond these diffusion-based methods, as illustrated by the following simple scaling analysis. We start by placing a whole-chromosome sample from a single cell in a small fluid-filled sorting chamber which is perhaps a few microns wide. Histones, other proteins, and attached mRNA strands are enzymatically removed and discarded, then the chromosomes are biochemically and mechanically separated into 46 haploid strands of dsDNA having a total duplex-DNA contour length of ~2 meters. A length measurement and a few other simple tests determine the chromosome number of every double strand. Each dsDNA duplex strand, ranging in length from 15.7-82.1 mm in contour length and suspended in an appropriate carrier fluid, is then transferred into a separate long narrow channel. The positionally-controlled end-effectors[138] of two nanorobotic manipulator arms[139] attach to either end of the dsDNA to establish orientation. The strand is cleaved in half at the center of the strand using a nuclease-like enzymatic end-effector mounted on a third positionally-controlled manipulator arm or sharp scanning probe tip,[140] and the two cleaved ends are attached[141] to another pair of manipulator arms to maintain the two strands in a known orientation. (Cleavage of individual chromosomes via femtolaser nanosurgery was first demonstrated experimentally in 1999.[142]) Each half is transported under full positional control to a second pair of manipulator arms where the cleaving process is repeated. After 10 such cleavings, there would be a total of

---

[138] Freitas RA Jr. Nanomedicine, Volume I: Basic Capabilities, Landes Bioscience, Georgetown, TX, 1999; Section 9.3.2, "Nanoscale End-Effectors and Tool Tips"; http://www.nanomedicine.com/NMI/9.3.2.htm.

[139] Freitas RA Jr. Nanomedicine, Volume I: Basic Capabilities, Landes Bioscience, Georgetown, TX, 1999; Section 9.3.1, "Nanoscale Manipulators"; http://www.nanomedicine.com/NMI/9.3.1.htm.

[140] e.g., Iwabuchii S, Mori T, Ogawa K, Sato K, Saito M, Morita Y, Ushiki T, Tamiyaet E. Atomic force microscope-based dissection of human metaphase chromosomes and high resolutional imaging by carbon nanotube tip. Arch Histol Cytol. 2002 Dec;65(5):473-479; https://www.jstage.jst.go.jp/article/aohc/65/5/65_5_473/_pdf. Oberringer M, Englisch A, Heinz B, Gao H, Martin T, Hartmann U. Atomic force microscopy and scanning near-field optical microscopy studies on the characterization of human metaphase chromosomes. Eur Biophys J. 2003 Nov;32(7):620-627; https://pubmed.ncbi.nlm.nih.gov/14586520/. An HJ, Guo YC, Zhang XD, Zhang Y, Hu J. Nanodissection of single- and double-stranded DNA by atomic force microscopy. J Nanosci Nanotechnol. 2005 Oct;5(10):1656-1659; https://pubmed.ncbi.nlm.nih.gov/16245523/. Hoshi O, Shigeno M, Ushiki T. Atomic force microscopy of native human metaphase chromosomes in a liquid. Arch Histol Cytol. 2006 Mar;69(1):73-78; https://www.jstage.jst.go.jp/article/aohc/69/1/69_1_73/_pdf.

[141] Thalhammer S, Stark RW, Müller S, Wienberg J, Heckl WM. The atomic force microscope as a new microdissecting tool for the generation of genetic probes. J Struct Biol. 1997 Jul;119(2):232-237; http://citeseerx.ist.psu.edu/viewdoc/download?doi=10.1.1.12.6581&rep=rep1&type=pdf.

[142] König K, Riemann I, Fischer P, Halbhuber KJ. Intracellular nanosurgery with near infrared femtosecond laser pulses. Cell Mol Biol (Noisy-le-grand). 1999 Mar;45(2):195-201; https://pubmed.ncbi.nlm.nih.gov/10230728/.

1000 strand segments each of length 15.7-82.1 micron (47,000-245,000 bp) rigidly held by ~2000 manipulator arms. Each strand segment would then be mechanically scanned using an AFM-mounted tooltip that can chemotactically sense the size and orientation of the exposed nucleotide bases comprising each base pair, along with their methylation,[143] thus fully sequencing the segment.[144] Alternatively, dsDNA strands can be mechanically unzipped by applying as little as ~15 pN of force[145] and it may be possible to partially infer single base-pair sequence by this means because the force is base-pair dependent.[146] (Contemporary scanning probe techniques are more commonly used to produce 3D ultrastructure images of chromatin strands with a minimum feature resolution of some tens of nanometers.[147])

---

[143] Zhu R, Howorka S, Pröll J, Kienberger F, Preiner J, Hesse J, Ebner A, Pastushenko VP, Gruber HJ, Hinterdorfer P. Nanomechanical recognition measurements of individual DNA molecules reveal epigenetic methylation patterns. Nat Nanotechnol. 2010 Nov;5(11):788-91; https://www.ncbi.nlm.nih.gov/pmc/articles/pmid/21037576/. Marszalek PE. DNA sequencing: detecting methylation with force. Nat Nanotechnol. 2010 Nov;5(11):765-6; https://pubmed.ncbi.nlm.nih.gov/21048791/.

[144] e.g., Kelson I, Nussinov S. A scheme for sequencing large DNA molecules by identifying local nuclear-induced effects. Proc Natl Acad Sci U S A. 1994 Jul 19;91(15):6963-6; https://www.ncbi.nlm.nih.gov/pmc/articles/PMC44318/. Seong GH, Niimi T, Yanagida Y, Kobatake E, Aizawa M. Single-molecular AFM probing of specific DNA sequencing using RecA-promoted homologous pairing and strand exchange. Anal Chem. 2000 Mar 15;72(6):1288-1293; https://pubmed.ncbi.nlm.nih.gov/10740872/. Voulgarakis NK, Redondo A, Bishop AR, Rasmussen KO. Sequencing DNA by dynamic force spectroscopy: limitations and prospects. Nano Lett. 2006 Jul;6(7):1483-1486; http://cnls.lanl.gov/External/voulgarakis_nano.pdf.

[145] Cocco S, Monasson R, Marko JF. Unzipping dynamics of long DNAs. Phys Rev E Stat Nonlin Soft Matter Phys. 2002 Nov;66(5 Pt 1):051914; http://www.phys.ens.fr/~cocco/Art/21unzlongdna.pdf.

[146] e.g., Sattin BD, Pelling AE, Goh MC. DNA base pair resolution by single molecule force spectroscopy. Nucleic Acids Res. 2004 Sep 14;32(16):4876-4883; https://www.ncbi.nlm.nih.gov/pmc/articles/pmid/15367697/. Singh N, Singh Y. Effect of genome sequence on the force-induced unzipping of a DNA molecule. Eur Phys J E Soft Matter. 2006 Feb;19(2):233-238; https://pubmed.ncbi.nlm.nih.gov/16505948/. Lee CH, Danilowicz C, Coljee VW, Prentiss M. Comparison of the measured phase diagrams in the force-temperature plane for the unzipping of two different natural DNA sequences. Eur Phys J E Soft Matter. 2006 Mar;19(3):339-344; https://pubmed.ncbi.nlm.nih.gov/16541209/. Baldazzi V, Cocco S, Marinari E, Monasson R. Inference of DNA sequences from mechanical unzipping: an ideal-case study. Phys Rev Lett. 2006 Mar 31;96(12):128102; http://www.phys.ens.fr/~cocco/Art/dnaseqprl.pdf.

[147] e.g., Oberringer M, Englisch A, Heinz B, Gao H, Martin T, Hartmann U. Atomic force microscopy and scanning near-field optical microscopy studies on the characterization of human metaphase chromosomes. Eur Biophys J. 2003 Nov;32(7):620-627; https://pubmed.ncbi.nlm.nih.gov/14586520/. Fukushi D, Ushiki T. The structure of C-banded human metaphase chromosomes as observed by atomic force microscopy. Arch Histol Cytol. 2005;68(1):81-87; https://pubmed.ncbi.nlm.nih.gov/15827381/. An HJ, Guo YC, Zhang XD, Zhang Y, Hu J. Nanodissection of single- and double-stranded DNA by atomic force microscopy. J Nanosci Nanotechnol. 2005 Oct;5(10):1656-1659; https://pubmed.ncbi.nlm.nih.gov/16245523/. Hoshi O, Shigeno M, Ushiki T. Atomic force microscopy of native human metaphase chromosomes in a liquid. Arch Histol Cytol. 2006 Mar;69(1):73-78; https://www.jstage.jst.go.jp/article/aohc/69/1/69_1_73/_pdf.

If: (1) initial sample preparation in the sorting chamber requires 10 seconds, (2) fluid transfer into the first channel occurs at ~10 mm/sec over a maximum 82.1 mm distance, (3) each subsequent positionally-controlled cleaving, attachment and transfer operation takes ~5 seconds, given that a manipulator end effector requires only 0.1 sec to be transported 100 microns at a conservative arm velocity of 1 mm/sec, and (4) the linear nucleotide sequencing of the final segment occurs at a conservative net scan rate of 1 micron/sec, then the total throughput time to mechanically sequence the longest chromosome would be ~**150 sec** (R_{nano} = 2.67 x 10^7 bp/sec). A contemporaneous scanning process could measure the methylation pattern of the dsDNA sample segments, matching these to the (by then) well-known human methylome[148] for this cytotype and organ.

If: (1) the volume of each channel is ~1000 times the volume of the dsDNA segment placed within it, giving ~100,000 micron^3 of total channel volume for each haploid strand sequenced, and (2) each of the 2000 manipulator arms including all appurtenant structures averages ~1000 micron^3 in volume, giving ~2,000,000 micron^3 of total manipulator volume for each haploid strand sequenced, then the volume of channels and manipulators to process all 46 haploid chromosomes from a single cell sample, in parallel, is ~**0.1 mm^3**, weighing ~**0.0002 gm** assuming a net density about half that of diamond. The power demand for operating 2000 x 46 manipulator arms, assuming ~10 pW per micron-length manipulator, is **0.92 x 10^{-6} watts**, yielding the following figures of merit for performance: ψ_V = 2.67 x 10^{17} bp/m^3-sec, ψ_m = 1.33 x 10^{14} bp/kg-sec, and ψ_P = 2.90 x 10^{13} bp/watt-sec.

Comparison of the relative performance of the three systems in **Table 1** shows that the nanorobotic DNA sequencing system described above should provide **productivity gains of about one billion-fold** over the best present-day high-throughput gene sequencing technologies.

Table 1. Figures of merit for DNA sequencing system productivity for three sequencing technologies

DNA Sequencing System	Raw System Seq. Rate R_{nano} (bp/sec)	Volumetric Productivity ψ_V (bp/m^3-sec)	Productivity Per Unit Mass Ψ_m (bp/kg-sec)	Productivity per Unit Power Consumption Ψ_P (bp/watt-sec)
NovaSeq 6000	6.93 x 10^7	5.56 x 10^7	1.44 x 10^5	2.78 x 10^4
MinION	1.16 x 10^5	3.44 x 10^8	2.57 x 10^5	4.63 x 10^4
Nano Sequencer	2.67 x 10^7	2.67 x 10^{17}	1.33 x 10^{14}	2.90 x 10^{13}

[148] e.g., Wilson IM, Davies JJ, Weber M, Brown CJ, Alvarez CE, MacAulay C, Schubeler D, Lam WL. Epigenomics: mapping the methylome. Cell Cycle. 2006 Jan;5(2):155-158; https://pubmed.ncbi.nlm.nih.gov/16397413/. Jeltsch A, Walter J, Reinhardt R, Platzer M. German human methylome project started. Cancer Res. 2006 Jul 15;66(14):7378; https://cancerres.aacrjournals.org/content/canres/66/14/7378.full.pdf. Schöb H, Grossniklaus U. The first high-resolution DNA "methylome". Cell. 2006 Sep 22;126(6):1025-1028; https://www.sciencedirect.com/science/article/pii/S0092867406011494.

2.2.2 DNA Mill

One of the most important biomolecules that a cell mill must produce is DNA for constructing chromosomes to be inserted into the nucleus of the manufactured cell. Each cell would require at least one duplicate copy[149] of the patient's own DNA, suitably methylated to match the expression pattern (e.g., the methylome, transcriptome,[150] etc.) and activation state of the particular cytotype under construction.

A large number of methods for artificial gene synthesis[151] have been employed in molecular biology, generally involving a two step process in which short-chain polymers consisting of ~200 nucleotides called oligonucleotides are synthesized using the techniques of solid-phase DNA synthesis,[152] after which these oligonucleotides are connected to each other in the proper sequence using various DNA assembly methods.[153] Solid-phase oligonucleotide synthesis has been highly automated[154] but remains expensive when product is ordered from a service. For example, a 100-base ("100-mer") sequence of unmodified double-stranded DNA cost $9,300/gm from Integrated DNA Technologies in 2024.[155]

---

[149] In humans, long cylindrical skeletal muscle cells called **myocytes** contain multiple nuclei due to their large size and the fusion of multiple precursor cells (myoblasts) during development (https://en.wikipedia.org/wiki/Muscle_cell). **Osteoclasts** (https://en.wikipedia.org/wiki/Osteoclast) are large multinucleate bone-resorbing cells formed from the fusion of multiple monocyte or macrophage precursor cells. A significant number of **hepatocytes** (https://en.wikipedia.org/wiki/Hepatocyte) are binucleate due to the liver's high regenerative capacity where some cells do not complete cytokinesis after DNA replication. A few pathological **skin cell** types are also multinucleate, including Langhans giant cells (https://en.wikipedia.org/wiki/Langhans_giant_cell) and foreign body giant cells (https://en.wikipedia.org/wiki/Foreign-body_giant_cell). All such multinucleate cells require more than one chromosomal copy per cell.

[150] https://en.wikipedia.org/wiki/Transcriptome.
[151] https://en.wikipedia.org/wiki/Artificial_gene_synthesis.

[152] "The occurrence of side reactions sets practical limits for the length of synthetic oligonucleotides (up to about 200 nucleotide residues) because the number of errors accumulates with the length of the oligonucleotide being synthesized." (https://en.wikipedia.org/wiki/Oligonucleotide_synthesis)

[153] https://en.wikipedia.org/wiki/Artificial_gene_synthesis#DNA_assembly.

[154] Anderson NG, Anderson NL, Taylor J, Goodman J. Large-scale oligonucleotide synthesizers. I. Basic principles and system design. Appl Biochem Biotechnol. 1995 Jul-Sep;54(1-3):19-42; https://pubmed.ncbi.nlm.nih.gov/7486979/. Lönnberg H. Synthesis of oligonucleotides on a soluble support. Beilstein J Org Chem. 2017 Jul 12;13:1368-1387; https://www.ncbi.nlm.nih.gov/pmc/articles/pmid/28781703/. Molina AG, Sanghvi YS. Liquid-Phase Oligonucleotide Synthesis: Past, Present, and Future Predictions. Curr Protoc Nucleic Acid Chem. 2019 Jun;77(1):e82; https://pubmed.ncbi.nlm.nih.gov/30920171/.

[155] https://www.idtdna.com/pages/products/custom-dna-rna/dna-oligos/custom-dna-oligos.

Several existing vendors provide the equipment needed to perform high-throughput automated oligonucleotide synthesis. For example, in 2020 the ÄKTA oligopilot plus lab scale oligonucleotide synthesizer (ÄKTA oligopilot plus 10; image, right)[156] measured 0.48 m x 0.45 m x 0.61 m ($V_{ÄKTA}$ = 0.132 m^3) in size with mass $m_{ÄKTA}$ = 63 kg and power draw $P_{ÄKTA}$ = 600 watts. It could reportly[157] process 3 millimole batches of 25-mer oligonucleotides in 30 minutes, or $R_{ÄKTA}$ = 1 x 10^{18} oligos/sec ~ 25 x 10^{18} bp/sec (although with "some assembly required"), yielding the following figures of merit for performance: ψ_V = 1.90 x 10^{20} bp/m^3-sec, ψ_m = 3.98 x 10^{17} bp/kg-sec, and ψ_P = 4.18 x 10^{16} bp/watt-sec.

However, these simplistic figures of merit ignore the hardest and most time-consuming part of the synthesis problem – the rather substantial additional effort that would be required to string together millions of 25-mer oligos into a precisely-specified sequence to make ~200,000,000-mer human chromosomes using the rather cumbersome current techniques of DNA assembly.[158] To calibrate the limitations of present-day technology, we note that the first complete genome of a simple microbial life form (*Mycoplasma genitalium*) with 485 protein-coding genes, containing a total of **582,970 base pairs**, was assembled by Venter's group in 2008 from ~10,000 synthetic oligonucleotides each ~50 nucleotides in length in a laboratory experiment that was described as "a formidable technical challenge"[159] and required "several years of work perfecting chemical assembly".[160] Venter's group next created a synthetic *Mycoplasma mycoides* genome with **1,079,000 base pairs** in 2010,[161] and by 2019 a British team had "recoded" and synthesized an entire *E. coli* genome comprising ~**4 million base pairs**[162] – apparently the world record length for assembling a single molecule of DNA from synthetic oligos as of 2024. A 15-year ongoing

---

[156] This particular product was discontinued by the manufacturer in 2021; https://web.archive.org/web/20201021165225/https://www.cytivalifesciences.com/en/us/shop/molecular-biology/oligonucleotide-synthesis/instruments/akta-oligopilot-plus-oligonucleotide-synthesizer-p-05544.

[157] Sarah Goforth, "The Core of DNA Synthesis," The Scientist, 9 June 2002; https://www.the-scientist.com/technology-profile/the-core-of-dna-synthesis-53217.

[158] https://en.wikipedia.org/wiki/Artificial_gene_synthesis#DNA_assembly.

[159] Gibson DG, Benders GA, Andrews-Pfannkoch C, *et al*. Complete chemical synthesis, assembly, and cloning of a *Mycoplasma genitalium* genome. Science. 2008 Feb 29;319(5867):1215-1220; http://biol.wwu.edu/young/470/papers_2009/artificialchrompaper.pdf.

[160] https://www.sciencedaily.com/releases/2008/01/080124175924.htm.

[161] Hutchison CA 3rd, Chuang RY, Noskov VN, *et al*. Design and synthesis of a minimal bacterial genome. Science. 2016 Mar 25;351(6280):aad6253; http://www.cba.mit.edu/docs/papers/16.04.minimal.pdf.

[162] Fredens J, Wang K, de la Torre D, Funke LFH, Robertson WE, Christova Y, Chia T, Schmied WH, Dunkelmann DL, Beránek V, Uttamapinant C, Llamazares AG, Elliott TS, Chin JW. Total synthesis of *Escherichia coli* with a recoded genome. Nature. 2019 May;569(7757):514-518; https://www.ncbi.nlm.nih.gov/pmc/articles/PMC7039709/.

international effort called the Synthetic Yeast Genome Project aims to synthesize all 16 chromosomes found in the nucleus of a yeast cell by 2025, which will make it the world's first complete eukaryotic[163] cell (i.e., having a nucleus) genome.[164] The entire yeast genome is **12.2 million base pairs** with 6275 genes, and 14 of the 16 chromosomes had been synthesized by year-end 2023.[165] Conventional modern-day genome-length DNA assembly operations remain a herculean task that involves many months and multiple personnel in well-equipped experimental laboratories, and are commonly referred to as "moonshot demonstrations."[166] The assembly of a ~200,000,000 base-pair human-chromosome-length single strand of DNA from synthesized oligonucleotide fragments has not yet been accomplished and appears unlikely to be achieved by conventional chemosynthetic means for at least 5-10 more years, given the current pace of improvements.

In sharp contrast, positionally-controlled molecular manufacturing of long-strand DNA would represent a fundamentally different and far more advanced process compared to present-day oligonucleotide hybridization and DNA assembly techniques, likely avoiding many current limitations such as high cost, low speed, and high error rate[167] that produce unplanned process mutagenicity.

How fast could chromatin be manufactured in a nanorobotic-based DNA synthesizer using the techniques of positionally-controlled molecular manufacturing? Published scaling analyses for convergent-assembly-based desktop-sized nanofactories[168] for manufacturing molecularly precise diamondoid products using positionally-controlled mechanosynthesis predict a start-to-finish

---

[163] i.e., cells having a membrane-bound nucleus containing the genome; https://en.wikipedia.org/wiki/Eukaryote.

[164] https://syntheticyeast.github.io/.
[165] https://syntheticyeast.github.io/sc2-0/data/.

[166] Hughes RA, Ellington AD. Synthetic DNA Synthesis and Assembly: Putting the Synthetic in Synthetic Biology. Cold Spring Harb Perspect Biol. 2017 Jan 3;9(1):a023812; https://www.ncbi.nlm.nih.gov/pmc/articles/PMC5204324/.

[167] Carr PA, Park JS, Lee YJ, Yu T, Zhang S, Jacobson JM. Protein-mediated error correction for *de novo* DNA synthesis. Nucleic Acids Res. 2004 Nov 23;32(20):e162; https://www.ncbi.nlm.nih.gov/pmc/articles/pmid/15561997/. Binkowski BF, Richmond KE, Kaysen J, Sussman MR, Belshaw PJ. Correcting errors in synthetic DNA through consensus shuffling. Nucleic Acids Res. 2005 Mar 30;33(6):e55; https://www.ncbi.nlm.nih.gov/pmc/articles/pmid/15800206/. Fuhrmann M, Oertel W, Berthold P, Hegemann P. Removal of mismatched bases from synthetic genes by enzymatic mismatch cleavage. Nucleic Acids Res. 2005 Mar 30;33(6):e58; https://www.ncbi.nlm.nih.gov/pmc/articles/pmid/15800209/.

[168] Drexler KE. Nanosystems: Molecular Machinery, Manufacturing, and Computation, John Wiley & Sons, New York, 1992, Section 14.4, "An exemplar manufacturing system architecture," pp. 421-427; https://www.amazon.com/dp/0471575186/. Merkle RC. Convergent assembly. Nanotechnology 1997;8:18-22; http://www.zyvex.com/nanotech/convergent.html. Freitas RA Jr., Merkle RC. Kinematic Self-Replicating Machines, Landes Bioscience, Georgetown, TX, 2004; Section 5.9.4, "Performance of Convergent Assembly Nanofactory Systems"; http://www.MolecularAssembler.com/KSRM/5.9.4.htm.

throughput time of ~100 sec with productivity ratios of ~1 kg/hour of product per kg of nanofactory for a mature nanotechnology system.

Some biological comparisons are instructive. **Ribosomes** assemble proteins according to digitally encoded instructions using mechanochemically-driven positionally-controlled placement of amino acids *in vivo*.[169] Analogously to the hypothesized nanofactory, ~1 kg of proteins can be assembled by ~1 kg of bacterial ribosomes in 270-710 sec,[170] a productivity rate of **5-13 kg/hr of proteins per kg of ribosome**. Similarly, nonprocessive **DNA polymerase enzymes** can add $n_{polymerase}$ ~ 1 nucleotide/sec to the growing DNA chain,[171] which implies a DNA polymer production rate of $R_{polymerase} \sim 0.5\ m_{bp}\ n_{polymerase} \sim 5.45 \times 10^{-25}$ kg/sec = 1.96×10^{-21} kg/hour of DNA for each active polymerase molecule of mass $m_{polymerase} \sim 1.82 \times 10^{-22}$ kg,[172] assuming ~650 daltons/base-pair for typical DNA[173] or $m_{bp} \sim 1.09 \times 10^{-24}$ kg/bp. This gives a net enzyme productivity of **~11 kg/hr of DNA per kg of polymerase**, very similar to ribosome productivity for protein synthesis.

Biological mechanochemistry is found in DNA-related systems[174] and the mechanochemistry of organic polymers using positionally-controlled scanning probe microscope tips has been demonstrated experimentally in a liquid solvent environment.[175] Alternatively, DNA could be assembled as a rigid polymer structure at low temperature (e.g., 20-80 K) and in vacuum using

---

[169] Nierhaus KH, Wilson DN, eds. Protein Synthesis and Ribosome Structure: Translating the Genome, John Wiley & Sons NY, 2004; https://www.amazon.com/dp/3527306382/.

[170] Freitas RA Jr., Merkle RC. Kinematic Self-Replicating Machines, Landes Bioscience, Georgetown, TX, 2004; Section 4.2, "Ribosomes: Molecular Positional Assembly for Self-Replication"; http://www.MolecularAssembler.com/KSRM/4.2.htm.

[171] Losick R, Watson JD, Baker TA, Bell S, Gann A, Levine MW. Molecular Biology of the Gene, 6th edition, Pearson/Benjamin Cummings, San Francisco CA, 2008; https://www.amazon.com/dp/B01JQ5RU9I/. However, much faster enzymatic rates have been reported. For example, processive DNA polymerase enzyme has been measured adding $n_{polymerase}$ = 749 nucleotides/sec in phage T4-infected *E. coli* cells during the period of exponential DNA increase at 37 °C; McCarthy D, Minner C, Bernstein H, Bernstein C. DNA elongation rates and growing point distributions of wild-type phage T4 and a DNA-delay amber mutant. *J Mol Biol*. 1976 Oct 5;106(4):963-981; https://pubmed.ncbi.nlm.nih.gov/789903/.

[172] The polymerase I enzyme found in *E. coli* has a molecular weight of ~109,000 daltons ~ 1.82×10^{-22} kg at ~1.67×10^{-27} kg/dalton; http://www.worthington-biochem.com/DNAECI/default.html.

[173] http://cels.uri.edu/gsc/cndna.html.

[174] Lionnet T, Dawid A, Bigot S, F.X. Barre FX, Saleh OA, Heslot F, Allemand JF, Bensimon D, Croquette V. DNA mechanics as a tool to probe helicase and translocase activity. Nucleic Acids Res. 2006;34(15):4232-4244; https://academic.oup.com/nar/article/34/15/4232/3111868.

[175] Duwez AS, Cuenot S, Jérôme C, Gabriel S, Jerome R, Rapino S, Zerbetto F. Mechanochemistry: targeted delivery of single molecules. Nat Nanotechnol. 2006 Nov;1(2):122-125; http://citeseerx.ist.psu.edu/viewdoc/download?doi=10.1.1.188.9873&rep=rep1&type=pdf.

mechanosynthetic tooltips similar to those envisioned for the fabrication of diamondoid structures under similar conditions.[176]

Rather than creating a detailed design for a nanorobotic DNA long-strand fabrication system (which is beyond the scope of this paper but would be a suitable task for future research), we shall assume that DNA and protein assembly times in mature nanofactories specialized for this purpose may be comparable to the assembly times required to manufacture diamondoid products, given that the making and breaking of predominantly C-C, C-H, C-N and related covalent bonds are involved in both cases.

Table 2. Estimated gross molecular contents of a "typical" 20 µm human cell[177]

Molecule Type	Molecular Weight *(daltons)*	Number of Molecules	Fraction of all Molecules	Fraction of all Molecule Mass
Water	18	1.74×10^{14}	98.73 %	65 %
Other Inorganics	55	1.31×10^{12}	0.74 %	1.5 %
Lipids	700	8.4×10^{11}	0.475 %	12 %
Other Organics	250	7.7×10^{10}	0.044 %	0.4 %
Proteins	50,000	1.9×10^{10}	0.011 %	20 %
RNA	1×10^{6}	5×10^{7}	3×10^{-5} %	1.0 %
DNA	1×10^{11}	46	3×10^{-11} %	0.1 %
Totals	---	***1.76×10^{14}***	***100 %***	***100 %***

Note that DNA represents $f_{CellDNA}$ ~ 0.1% of cell mass (**Table 2**), so a cell mill manufacturing $R_{CellMill}$ ~ 1 kg/hr of cells must produce $R_{DNAMill} \sim f_{CellDNA}\ R_{CellMill}$ ~ 0.001 kg/hr of DNA to sustain the overall cell production rate, requiring a ~0.001 kg "DNA mill" if we assume that a ~1 kg mature nanofactory can produce ~1 kg/hr of atomically-precise molecular product. The required DNA production rate is $R_{DNAMillbp} \sim R_{DNAMill} / m_{bp} \sim 2.55 \times 10^{17}$ bp/sec for a DNA mill having a volume of $V_{DNAmill} = f_{CellDNA}\ V_{mNF} \sim$ **50 cm^3**, mass $M_{DNAmill} = f_{CellDNA}\ M_{mNF} \sim$ **1 gm**, and power draw $P_{DNAmill} = f_{CellDNA}\ P_{mNF} \sim$ **1.3 watt**, extrapolated from published estimates[178] that a mature nanofactory with a production rate of $R_{CellMill}$ ~ 1 kg/hr would have a mass of M_{mNF} ~ 1 kg, volume $V_{mNF} \sim 0.05$ m^3, and power draw P_{mNF} ~ 1300 watts. This yields the following

---

[176] Freitas RA Jr., Merkle RC. A minimal toolset for positional diamond mechanosynthesis. J Comput Theor Nanosci. 2008;5:760-861; http://www.molecularassembler.com/Papers/MinToolset.pdf.

[177] Freitas RA Jr. Nanomedicine, Volume I: Basic Capabilities, Landes Bioscience, Georgetown, TX, 1999; Table 3.2; http://www.nanomedicine.com/NMI/Tables/3.2.jpg.

[178] Drexler KE. Nanosystems: Molecular Machinery, Manufacturing, and Computation, John Wiley & Sons, New York, 1992, Section 14.4.4, "Mass and volume"; https://www.amazon.com/dp/0471575186/.

figures of merit for DNA mill performance: ψ_V = 5.10 x 10^{21} bp/m^3-sec, ψ_m = 2.55 x 10^{20} bp/kg-sec, and ψ_P = 1.96 x 10^{17} bp/watt-sec. These figures exceed those of the ÄKTA system by only 25-fold, 641-fold, and 5-fold, respectively. However, our nanorobotic DNA mill will be producing genome-length DNA strands ready for methylation, histone-wrapping, and installation in cell nuclei – not just beakers full of unconnected 25-mer oligos as is the case with the ÄKTA system.

2.2.3 Protein Mill

The second most important biomolecules that a cell mill must produce are proteins that comprise most of the functional molecules and structural elements of the manufactured cell. Proteins can be made from amino acids prepared earlier in the Generic Synthesis Unit (Section 2.1.2) that are polymerized into a chain by enzymatically removing an H from the $–NH_2$ group at one end of an amino acid (the N-terminus), creating a radical site, and then joining it to a radical site at the other end of an amino acid that is created by removing the –OH from a –COOH group at the other end of another amino acid (the C-terminus) using the vacuum-phase nanofactory-based mechanochemical processes described earlier. Peptides are short chains of 2-50 amino acids, with "oligopeptides" running 2-15 residues in length, "polypeptides" running up to 15-50 residues, and "proteins" generally having >50 residues.[179]

Solid-phase peptide synthesis (SPPS) is the classical method for preparing peptides in the lab,[180] involving the rapid assembly of a peptide chain through successive reactions of amino acid derivatives on an insoluble porous support.[181] SPPS is limited by reaction yields to peptides and proteins in the range of 70 amino acids; synthetic difficulty is again sequence dependent, with aggregation-prone sequences such as amyloids being especially difficult to make.[182]

Longer lengths can be accessed by using ligation approaches such as native chemical ligation,[183] where two shorter fully deprotected synthetic peptides can be joined together in solution – this method has prepared the 166-residue synthetic erythropoietin[184] and the 203-residue HIV-1

---

[179] https://en.wikipedia.org/wiki/Peptide.

[180] Merrifield RB. Solid Phase Peptide Synthesis. I. The Synthesis of a Tetrapeptide. J Am Chem Soc. 1963;85(14):2149-2154; https://pubs.acs.org/doi/pdf/10.1021/ja00897a025. Chan WC, White PD. Fmoc Solid Phase Peptide Synthesis: A Practical Approach. Oxford University Press, Oxford UK, 2000; https://www.amazon.com/Fmoc-Solid-Phase-Peptide-Synthesis/dp/0199637253/.

[181] https://en.wikipedia.org/wiki/Peptide_synthesis#Solid-phase_synthesis.

[182] Tickler AK, Clippingdale AB, Wade JD. Amyloid-beta as a "difficult sequence" in solid phase peptide synthesis. Protein Pept Lett. 2004 Aug;11(4):377-384; https://pubmed.ncbi.nlm.nih.gov/15327371/.

[183] https://en.wikipedia.org/wiki/Native_chemical_ligation.

[184] Wang P, Dong S, Shieh JH, Peguero E, Hendrickson R, Moore MAS, Danishefsky SJ. Erythropoietin derived by chemical synthesis. Science. 2013 Dec 13;342(6164):1357-1360; https://www.ncbi.nlm.nih.gov/pmc/articles/PMC4080428/.

protease proteins.[185] An automated flow-based SPPS laboratory system[186] has synthesized the single-domain 164-residue sortase[187] protein in 6.5 hours, achieving a production rate of R_{SPPS} ~ 0.007 residues/sec, typically in milligram quantities.

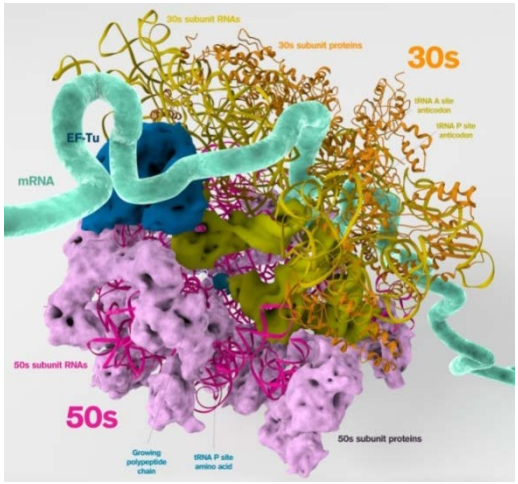

In biological systems, bacterial ribosomes (image, right)[188] can assemble their own weight in protein in 270-710 sec,[189] a production rate of ~0.001 kg/sec per kg of ribosomes or $\psi_m = 5 \times 10^{21}$ residues/kg-sec, given the $m_{residue}$ ~ 110 dalton average molecular weight of protein residues[190] (amino acids having one water molecule removed). The volumetric production figure of merit for a bacterial ribosome[191] with a volume of $V_{Ribosome}$ ~ $(20\ nm)^3 = 8000\ nm^3$ and a mass of $m_{Ribosome} \sim 4.2 \times 10^{-21}$ kg per ribosome is $\psi_V = (m_{Ribosome} / V_{Ribosome})\ \psi_m = 2.6 \times 10^{24}$ residues/m^3-sec.

Each cell requires ~19 billion protein molecules comprising ~20% of total cell mass (**Table 2**), so a cell mill manufacturing $R_{CellMill}$ ~ 1 kg/hr of cells must produce $R_{ProteinMill}$ ~ 0.2 kg/hr (~3×10^{20} residues/sec) of protein mass to sustain the needed overall cell production rate. Conservatively adopting the ribosome productivity of only $\psi_m = 5 \times 10^{21}$ residues/kg-sec for the likely much

---

[185] Torbeev VY, Kent SB. Convergent chemical synthesis and crystal structure of a 203 amino acid "covalent dimer" HIV-1 protease enzyme molecule. Angew Chem Int Ed Engl. 2007;46(10):1667-70; https://onlinelibrary.wiley.com/doi/full/10.1002/anie.200604087.

[186] Hartrampf N, Saebi A, Poskus M, Gates ZP, Callahan AJ, Cowfer AE, Hanna S, Antilla S, Schissel CK, Quartararo AJ, Ye X, Mijalis AJ, Simon MD, Loas A, Liu S, Jessen C, Nielsen TE, Pentelute BL. Synthesis of proteins by automated flow chemistry. Science 2020 May 29;368(6494):980-987; https://science.sciencemag.org/content/368/6494/980/tab-pdf.

[187] https://en.wikipedia.org/wiki/Sortase.

[188] https://3dciencia.com/blog/2011/02/bacterial-ribosome-internal-structure/.

[189] Freitas RA Jr., Merkle RC. Kinematic Self-Replicating Machines, Landes Bioscience, Georgetown, TX, 2004; Section 4.2, "Ribosomes: Molecular Positional Assembly for Self-Replication"; http://www.MolecularAssembler.com/KSRM/4.2.htm.

[190] The average molecular weight of amino acid residues was determined using a weighted mean approach that takes into account the relative proportion of each of the twenty amino acids present in proteins; https://www.promega.com/~/media/files/resources/technical%20references/amino%20acid%20abbreviations%20and%20molecular%20weights.pdf.

[191] Freitas RA Jr., Merkle RC. Kinematic Self-Replicating Machines, Landes Bioscience, Georgetown, TX, 2004; Section 4.2, "Ribosomes: Molecular Positional Assembly for Self-Replication"; http://www.MolecularAssembler.com/KSRM/4.2.htm.

more productive nanorobotic protein synthesis system to be designed in future research,[192] the resulting protein mill component would have a mass of $m_{ProteinMill} = R_{ProteinMill} / \psi_m$ ~ **60 gm** and a volume of $V_{ProteinMill} = m_{ProteinMill} / \rho_{ProteinMill}$ ~ **3000 cm^3** assuming the protein mill has a device density of $\rho_{ProteinMill}$ ~ 20 kg/m^3 (equivalent to ~3% solid diamond and ~97% vacuum by volume inside the device), the same as the DNA mill. Taking the operating power density of the protein mill as similar to that of the DNA mill (~26,000 W/m^3; Section 2.2.2), the protein mill power draw is $P_{ProteinMill}$ ~ **78 watts**.

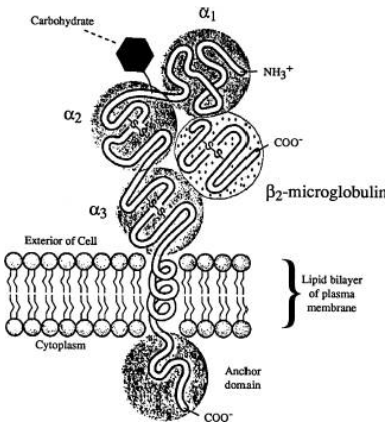

Besides providing the ability to replicate chromosomes in the cell mill, the genome DNA consensus sequence (Section 2.2.1.1) makes it possible to build proteins, carbohydrates, glycoproteins, and other molecules that are customized to the particular biology of the patient. For example, glycoprotein molecules known as the major histocompatibility complex (MHC)[193] are embedded in the plasma membranes of all human cells and allow the immune system to distinguish self from non-self. MHC-I molecules (image, left) comprise up to ~1% of the protein content of the plasma membrane;[194]

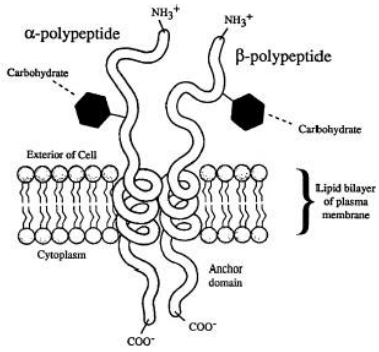

MHC-II molecules (image, right) are less widely distributed, being found on glial cells in the brain and elsewhere; and MHC-III genes encode the 20 proteins that comprise the complement system. The residue sequences of MHC molecules are encoded in a 3.8 million base section of the human genome and together create ~2 x 10^{14} fourteen-allele combinations, making the MHC protein set of every person essentially unique. Red cells contain no MHC molecules but instead include a set of 22 different blood group systems, 7 antigen collections, and 47 additional antigens not associated with any collection, which together allow ~10^{19} different combinations to be expressed.[195] In addition, the plasma membranes of cells appear to be marked with protein antigens that identify the type of cell – for instance, platelets employ 5 separate alloantigen systems, and white cells and tissue cells

---

[192] Ribosomes typically add 2-15 residues/sec to a growing protein chain. It is plausible to expect that an efficient nanorobotic system could operate at ~MHz frequencies instead of the ~10 Hz frequency found in biology, possibly offering up to several orders of magnitude of productivity improvement over the performance of biological systems.

[193] Freitas RA Jr. Nanomedicine, Volume I: Basic Capabilities, Landes Bioscience, Georgetown TX, 1999, Section 8.5.2.1, "Identification of Self"; http://www.nanomedicine.com/NMI/8.5.2.1.htm.

[194] Becker WM, Deamer DW. The World of the Cell, Second Edition, Benjamin/Cummings Publishing Company, Redwood City CA, 1991; https://www.amazon.com/dp/0805308709/.

[195] Freitas RA Jr. Nanomedicine, Volume I: Basic Capabilities, Landes Bioscience, Georgetown TX, 1999, Section 8.5.2.1, "Identification of Self"; http://www.nanomedicine.com/NMI/8.5.2.1.htm.

bear other specific sets of markers that are genetically determined.[196] Knowledge of the patient's personal gene sequences allows the protein mill to build cells with autologous proteins that the patient's immune system will recognize as self and that properly identify the variants of each cytotype that are the patient's own.

Multi-subunit proteins can be assembled under full positional control or may be allowed to self-assemble if future research deems this appropriate. More than 2 decades ago, functional copies of the human red cell **band 3 anion exchanger 1** (AE1, aka. Band 3, solute carrier family 4 member 1 (SLC4A1), or Band 3 anion transport protein), a proteinaceous transmembrane pump, were self-assembled from sets of 3, 4, or 5 complementary molecular fragment "subunits" that were separately cloned in *Xenopus* oocytes.[197]

More recently, custom protein factories have been created using cell-free microfabricated bioreactors (which eliminates the maintenance of living systems inside the devices) and are now being used to facilitate the on-demand production of therapeutic proteins for medicines and biopharmaceuticals.[198] As reviewed by Tinafar *et al.* (image, right),[199] the methods of cell-free synthesis[200] have been used to produce increasingly intricate cytoprotein complexes including the hepatitis B core antigen HBc VLP,[201] the *E. coli* RNA polymerase,[202] the human T-cell receptor,[203] an ATP synthase,[204] and finally the T4[205] and T7[206] phages (~1500 "nanoparts").

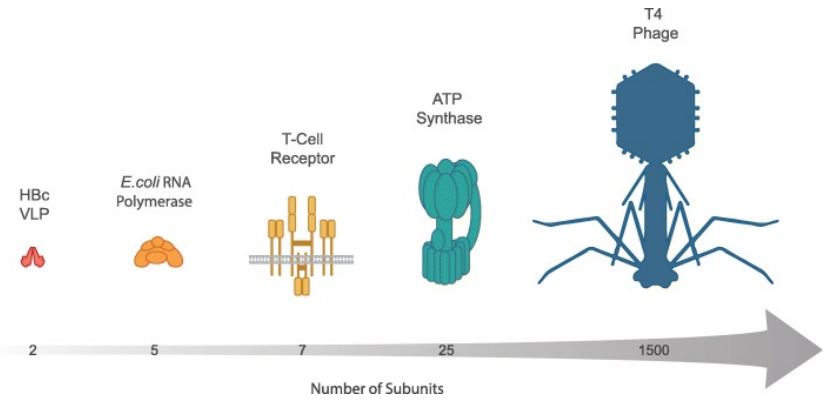

---

[196] Freitas RA Jr. Nanomedicine, Volume I: Basic Capabilities, Landes Bioscience, Georgetown TX, 1999, Section 8.5.2.2, "Identification of Cell Type"; http://www.nanomedicine.com/NMI/8.5.2.2.htm.

[197] Groves JD, Wang L, Tanner MJ. Functional reassembly of the anion transport domain of human red cell band 3 (AE1) from multiple and non-complementary fragments. FEBS Lett. 1998 Aug 21;433(3):223-7; http://www.sciencedirect.com/science/article/pii/S0014579398009090/pdf?md5=5a6fd338036616de263d878735192af6&pid=1-s2.0-S0014579398009090-main.pdf.

[198] Ron Walli, "ORNL cell-free protein synthesis is potential lifesaver," Oak Ridge National Laboratory, 29 Dec 2015; https://www.ornl.gov/news/ornl-cell-free-protein-synthesis-potential-lifesaver.

[199] Tinafar A, Jaenes K, Pardee K. Synthetic Biology Goes Cell-Free. BMC Biol. 2019 Aug 8;17(1):64; https://www.ncbi.nlm.nih.gov/pmc/articles/PMC6688370/.

[200] https://en.wikipedia.org/wiki/Cell-free_protein_synthesis.

[201] Bundy BC, Franciszkowicz MJ, Swartz JR. *Escherichia coli*-based cell-free synthesis of virus-like particles. Biotechnol Bioeng. 2008;100(1):28-37; https://pubmed.ncbi.nlm.nih.gov/18023052/.

2.2.4 Carbohydrate Mill

Automated systems using conventional chemical techniques to produce carbohydrate polymers, or oligosaccharides, while lagging well behind the technologies for synthesizing oligonucleotides (Section 2.2.2) and oligopeptides (see above), also continue to progress.[207] Nanorobot-based carbohydrate mills analogous to the previously-described DNA and protein mills should be able to produce both generic and personalized carbohydrate-based polymers much more quickly and efficiently than conventional synthetic techniques.

---

[202] Asahara H, Chong S. *In vitro* genetic reconstruction of bacterial transcription initiation by coupled synthesis and detection of RNA polymerase holoenzyme. Nucleic Acids Res. 2010 Jul;38(13):e141; https://www.ncbi.nlm.nih.gov/pmc/articles/PMC2910072/..

[203] Huppa JB, Ploegh HL. *In vitro* translation and assembly of a complete T cell receptor-CD3 complex. J Exp Med. 1997;186(3):393-403; https://www.ncbi.nlm.nih.gov/pmc/articles/pmid/9236191/.

[204] Matthies D, Haberstock S, Joos F, Dötsch V, Vonck J, Bernhard F, *et al*. Cell-free expression and assembly of ATP synthase. J Mol Biol. 2011;413(3):593–603; https://www.ncbi.nlm.nih.gov/pubmed/21925509.

[205] Rustad M, Eastlund A, Jardine P, Noireaux V. Cell-free TXTL synthesis of infectious bacteriophage T4 in a single test tube reaction. Synth Biol. 2018;3(1):1-7; http://noireauxlab.com/html%20pages/docs%20website/publications/Rustad%20et%20al%20-%202018.pdf.

[206] Shin J, Jardine P, Noireaux V. Genome replication, synthesis, and assembly of the bacteriophage T7 in a single cell-free reaction. ACS Synth Biol. 2012 Sep 21;1(9):408-413; http://noireauxlab.com/html%20pages/docs%20website/publications/Shin%20et%20al%20-%202012.pdf. Rustad M, Eastlund A, Marshall R, Jardine P, Noireaux V. Synthesis of Infectious Bacteriophages in an *E. coli*-based Cell-free Expression System. J Vis Exp. 2017 Aug 17;(126):56144; https://www.ncbi.nlm.nih.gov/pmc/articles/PMC5614349/.

[207] e.g., Plante OJ, Palmacci ER, Seeberger PH. Automated solid-phase synthesis of oligosaccharides. Science. 2001 Feb 23;291(5508):1523-1527; http://citeseerx.ist.psu.edu/viewdoc/download?doi=10.1.1.985.5831&rep=rep1&type=pdf. Seeberger PH. Automated oligosaccharide synthesis. Chem Soc Rev. 2008 Jan;37(1):19-28; https://pubs.rsc.org/en/content/articlehtml/2008/cs/b511197h. Panza M, Pistorio SG, Stine KJ, Demchenko AV. Automated Chemical Oligosaccharide Synthesis: Novel Approach to Traditional Challenges. Chem Rev. 2018 Sep 12;118(17):8105-8150; https://www.ncbi.nlm.nih.gov/pmc/articles/pmid/29953217/. Wen L, Edmunds G, Gibbons C, *et al*. Toward Automated Enzymatic Synthesis of Oligosaccharides. Chem Rev. 2018 Sep 12;118(17):8151-8187; https://pubmed.ncbi.nlm.nih.gov/30011195/. Zhang J, Chen C, Gadi MR, *et al*. Machine-Driven Enzymatic Oligosaccharide Synthesis by Using a Peptide Synthesizer. Angew Chem Int Ed Engl. 2018 Dec 17;57(51):16638-16642; https://www.ncbi.nlm.nih.gov/pmc/articles/pmid/30375138/. Joseph AA, Pardo-Vargas A, Seeberger PH. Total Synthesis of Polysaccharides by Automated Glycan Assembly. J Am Chem Soc. 2020 May 13;142(19):8561-8564; https://www.ncbi.nlm.nih.gov/pmc/articles/pmid/32338884/. Tian J, Li Y, Ma B, Tan Z, Shang S. Automated Peptide Synthesizers and Glycoprotein Synthesis. Front Chem. 2022 May 5;10:896098; https://www.ncbi.nlm.nih.gov/pmc/articles/pmid/35601548/.

3. Cytocomponent Assembly Module

The cell mill concept relies on the assumption that the components of a cell are essentially modular, hence can be manufactured separately and later assembled into a complete working biological cell.[208] The same assumption applies to the assembly of individual organelles and other basic components of cells, which can also be viewed as collections of modular components and thus can presumably be put together from basic subunits or nanoparts.

Table 3 lists the 14 most important intracellular organelles. The "typical" ~8000 μm^3 cell has ~3500 μm^3 of organelles (~44% of total cell volume). There are ~26 million organelles in each individual cell, mostly accounted for by 20 million ribosomes and 5.7 million proteasomes.

Table 3. Approximate number of non-nucleus intracellular organelles in a human body[209]

Organelle	Volume of Organelle (μm^3)	Avg Volume per Cell (μm^3)	Total Number in 70 kg Human	Total Volume in 70 kg Human (cm^3)
Rough ER	1120	1120	3.5×10^{12}	3900
Mitochondria	1	1000	3.5×10^{15}	3500
Golgi apparatus	410-520	450	3.5×10^{12}	1600
Smooth ER	420	420	3.5×10^{12}	1500
Secretory vesicles	4×10^{-3}	210	1.8×10^{17}	740
Lysosomes	0.31	90	1×10^{15}	320
Peroxisomes	0.31	90	1×10^{15}	320
Ribosomes	4×10^{-6}	80	7×10^{19}	280
Proteasomes	3.4×10^{-6}	20	2×10^{19}	70
Golgi vesicles	6.5×10^{-5}	13	7×10^{17}	50
Lipid droplets	0.1	10	3.5×10^{14}	35
Glycogen granules	1×10^{-5}	1	3.5×10^{17}	4
Vaults	5×10^{-5}	0.16	1.1×10^{16}	0.6
Centrioles	0.007	0.014	7×10^{12}	0.05
TOTALS		***3500***	***9.1×10^{19}***	***12,300***

[208] Jeon KW, Lorch IJ, Danielli JF. Reassembly of living cells from dissociated components. Science. 1970 Mar 20;167(3925):1626-7; http://science.sciencemag.org/content/sci/167/3925/1626.full.pdf. Deamer D. A giant step towards artificial life? Trends Biotechnol. 2005 Jul;23(7):336-8; https://citeseerx.ist.psu.edu/document?repid=rep1&type=pdf&doi=adf5e4e794ecf5c7498921cc977fc03d9792a923.

[209] Assumes 3.5×10^{12} cells in a 70-kg human body; organelle data from: Freitas RA Jr., Nanomedicine, Volume I: Basic Capabilities, Landes Bioscience, Georgetown, TX, 1999, Table 8.17, "Approximate Quantification of the Components of a Typical 20-μm Human Tissue Cell"; http://www.nanomedicine.com/NMI/Tables/8.17.jpg.

This Section briefly describes the nanorobotic manufacture all major cell components (cytocomponents) including cell membranes (Section 3.1), six types of macromolecular organelles (Section 3.2), five types of vesicular organelles (Section 3.3), two types of membraneous organelles (Section 3.4), and the cell nucleus (Section 3.5).

3.1 Cell Membranes

The most prominent feature that all cells have in common, and which is also shared by many subcellular organelles, is the lipid cell membrane. For example, the plasma membrane which forms the boundary between the cell and its exterior environment consists of a bilayer[210] of phospholipid molecules, each comprising a water-soluble (hydrophilic) phosphate head and a water-insoluble (hydrophobic) tail consisting of two fatty acid chains (e.g., long-chain hydrocarbon molecules). The phospholipid molecules readily self-assemble[211] into solid micelles (with almost no interior space), hollow unilamellar liposomes,[212] or large bilayer sheets (images, right),[213] averaging ~8 nm thick.[214] In the case of cells, the lipid bilayer sheet folds into a large spherical shell (image, left) that provides a persistent barrier between a water-soluble interior space and the water-soluble exterior spaces, thus enabling both containment and separation.[215]

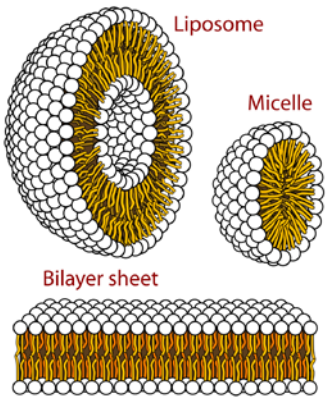

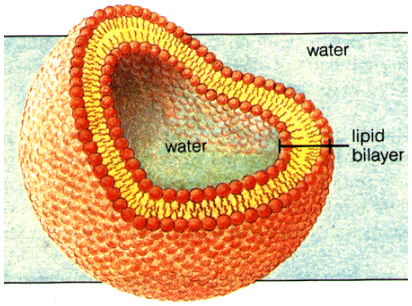

The several varieties of phospholipid molecules[216] can be manufactured from (a) phosphate ions, (b) small nitrogen-

---

[210] https://en.wikipedia.org/wiki/Lipid_bilayer.

[211] Marrink SJ, Lindahl E, Edholm O, Mark AE. Simulation of the spontaneous aggregation of phospholipids into bilayers. J Am Chem Soc. 2001 Sep 5;123(35):8638-9; http://compbio.chemistry.uq.edu.au/mediawiki/upload/5/5b/AM_01_07.pdf.

[212] "A unilamellar liposome is a spherical chamber/vesicle, bounded by a single bilayer of an amphiphilic lipid or a mixture of such lipids, containing aqueous solution inside the chamber." https://en.wikipedia.org/wiki/Unilamellar_liposome.

[213] Mariana Ruiz Villarreal: "Cross section of the different structures that phospholipids can take in a aqueous solution. The circles are the hydrophilic heads and the wavy lines are the fatty acyl side chains." https://en.wikipedia.org/wiki/Lipid_bilayer#/media/File:Phospholipids_aqueous_solution_structures.svg.

[214] Freitas RA Jr., Nanomedicine, Volume I: Basic Capabilities, Landes Bioscience, Georgetown, TX, 1999, Table 8.17, "Approximate Quantification of the Components of a Typical 20-μm Human Tissue Cell"; http://www.nanomedicine.com/NMI/Tables/8.17.jpg.

[215] https://en.wikipedia.org/wiki/Lipid_bilayer#Containment_and_separation.

[216] https://en.wikipedia.org/wiki/Phospholipid#Main_phospholipids.

containing molecules, and (c) hydrocarbon chains, all prepared earlier in the Generic Synthesis Unit (Section 2.1). With these phospholipids in hand, the automated self-assembly of uniform 5-20 μm diameter spherical liposomes with lipid bilayers has been demonstrated experimentally in a controlled, robust, efficient and simple way using chip-based microfluidics.[217] Biological-based phospholipids are commonplace components of self-assembled conventional liposomes[218] employed in a variety of medical therapeutics.[219]

In a cell mill that employs positional assembly,[220] the conceptual process of building a spherical plasma membrane of a precise and uniform size[221] might begin with a hemispherical mould (image, right) with a 20 μm diameter half-sphere indented into the surface. The concave surface of the mould is coated with embedded presentation semaphores[222] providing a staggered array of chemically inert alternating hydrophilic and hydrophobic ligands (images below, left).[223] When the computer-controlled

---

[217] Deshpande S, Caspi Y, Meijering AE, Dekker C. Octanol-assisted liposome assembly on chip. Nat Commun. 2016 Jan 22;7:10447; http://www.ncbi.nlm.nih.gov/pmc/articles/PMC4735860/. Deshpande S, Birnie A, Dekker C. On-chip density-based purification of liposomes. Biomicrofluidics. 2017 May 8;11(3):034106; https://www.ncbi.nlm.nih.gov/pmc/articles/pmid/28529672/. Deshpande S, Dekker C. On-chip microfluidic production of cell-sized liposomes. Nat Protoc. 2018 May;13(5):856-874; https://pubmed.ncbi.nlm.nih.gov/29599442/.

[218] https://en.wikipedia.org/wiki/Liposome.

[219] e.g., Riaz MK, Riaz MA, Zhang X, Lin C, Wong KH, Chen X, Zhang G, Lu A, Yang Z. Surface Functionalization and Targeting Strategies of Liposomes in Solid Tumor Therapy: A Review. Int J Mol Sci. 2018 Jan 9;19(1):195; https://www.ncbi.nlm.nih.gov/pmc/articles/PMC5796144/. Wang S, Chen Y, Guo J, Huang Q. Liposomes for Tumor Targeted Therapy: A Review. Int J Mol Sci. 2023 Jan 31;24(3):2643; https://www.ncbi.nlm.nih.gov/pmc/articles/PMC9916501/. Fulton MD, Najahi-Missaoui W. Liposomes in Cancer Therapy: How Did We Start and Where Are We Now. Int J Mol Sci. 2023 Apr 1;24(7):6615; https://www.ncbi.nlm.nih.gov/pmc/articles/pmid/37047585/.

[220] Tavares GD, de Oliveira MC, Vilela JMC, Andrade MS. Deposition of Lipid Bilayers with Atomic Force Microscopy. Microscopy and Microanalysis 2005 Dec;11(S03):44-47; https://search.proquest.com/openview/3ac85cd0fec1f75152e73ff9c4af01e4/1?pq-origsite=gscholar&cbl=33692.

[221] Cells of nonspherical shapes will require nonspherical moulds; reconfigurable moulds also may be designed using structures similar to the pincushion sensor described elsewhere; Freitas RA Jr. Nanomedicine, Vol. I: Basic Capabilities, 1999; Sec. 3.5.7.4, “Pin Cushion Model”; http://www.nanomedicine.com/NMI/3.5.7.4.htm.

[222] Freitas RA Jr. Nanomedicine, Volume I: Basic Capabilities, Landes Bioscience, Georgetown, TX, 1999; Section 5.3.6, “Presentation Semaphores”; http://www.nanomedicine.com/NMI/5.3.6.htm.

[223] Freitas RA Jr. Nanomedicine, Volume I: Basic Capabilities, Landes Bioscience, Georgetown, TX, 1999; Figure 5.18; http://www.nanomedicine.com/NMI/Figures/5.18.jpg.

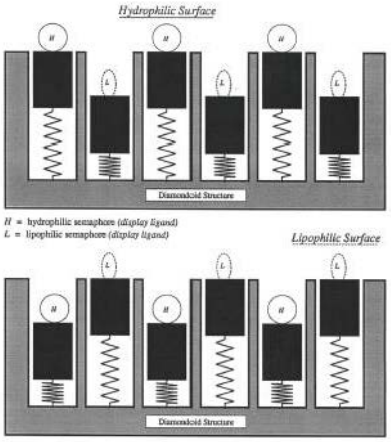

pistons extend the hydrophilic ligands and retract the hydrophobic ones (drive motors not shown), the surface will attract hydrophilic moieties such as the phosphate heads of phospholipid molecules. When offered to the surface one by one, these molecules will coat the interior surface of the cavity in a monolayer with their hydrophobic tails pointing outward towards the center of the sphere. Molecule-by-molecule placement of another monolayer of phospholipid molecules will bond to the first monolayer, hydrophobic tails to tails, with the hydrophilic heads now pointing toward the center, forming a hemispherical bilayer sheet following the shape of the mould.

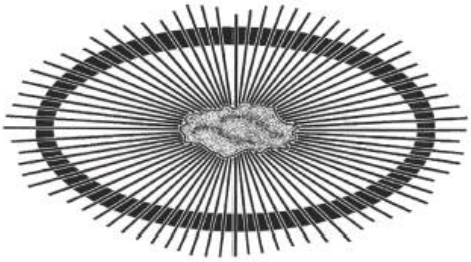

If needed for additional flexibility, the aforementioned fixed-configuration hemispherical moulds could be replaced by variable-configuration moulds modeled after the "pin cushion receptor" concept that has been described elsewhere[224] in the context of a universal molecular binding site (image, right).[225] Such variable moulds could consist of a flat plate or curved sheet through which a number of rods protrude, each of which may be moved in or out in graduated steps through holes in the plate (image, left). When inserted through the plate to varying depths, the endpoints of the rods define a negative image surface which may be made to mirror the topography of a cavity of arbitrary size and shape, and can be rapidly reconfigured to assume whichever size and shape is needed for the particular cell being fabricated. Variable-configuration moulds will generally be larger and mechanically more complex than the fixed variety, but their use may reduce the total volume of moulds required and should greatly increase operational flexibility.

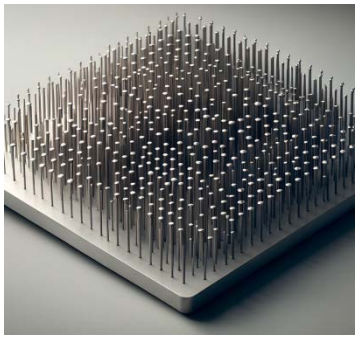

Additional work can now be done on this nascent plasma membrane, such as embedding integral proteins one by one or linking cytoskeletal elements to transmembrane proteins. The addition of membrane proteins, glycocalyx, and related decorations to completed bilayer membranes is briefly discussed later as part of final cell assembly (Section 4.1).

When all interior work is completed, the first membrane hemisphere can be pressed mouth-to-mouth onto a second finished membrane hemisphere of equal size, causing the two miscible halves to join seamlessly into a sealed sphere. The presentation semaphores embedded in the surface of the mould are then switched from hydrophilic to hydrophobic as the two moulds are

---

[224] Freitas RA Jr. Nanomedicine, Volume I: Basic Capabilities, Landes Bioscience, Georgetown TX, 1999; Section 3.5.7.4, "Pin Cushion Model; http://www.nanomedicine.com/NMI/3.5.7.4.htm.

[225] Freitas RA Jr. Nanomedicine, Volume I: Basic Capabilities, Landes Bioscience, Georgetown TX, 1999, Fig. 3.14; http://www.nanomedicine.com/NMI/Figures/3.14.jpg.

pulled apart, repelling the phosphate heads in contact with the departing mould surface and freeing the completed spherical lipid bilayer plasma membrane. The entire process may be conducted either in an aqueous environment or under a humid inert gas such as argon or nitrogen.

Table 4. Mass % biochemical composition of organelle and cell membranes[226]

Type of Component Membrane Molecule	Mitochon-drion Inner / Outer Membranes	Endo-plasmic Reticulum Membrane	Myelin Sheath	Liver Cell Plasma Membrane	Red Cell Plasma Membrane
Lipid	~24% / ~48%	---	~81%	---	40%
Protein	~76% / ~52%	~50%	~19%	~50%	52%
Carbohydrate	---	---	---	---	8%
Lipid Class:					
Cholesterol	3%	6%	22%	17%	23%
Phospholipids:					
Phosphatidylethanolamine	35%	17%	15%	7%	18%
Phosphatidylserine	2%	5%	9%	4%	7%
Phosphatidylcholine	39%	40%	10%	24%	17%
Sphingomyelin	0%	5%	8%	19%	18%
Glycolipids	trace	trace	28%	7%	3%
Other lipids	21%	27%	8%	22%	13%

Each biological cell or constituent membraneous organelle requires a slightly different combination of component protein, carbohydrate, and lipid molecules for its construction, as illustrated in **Table 4** above. All required component molecules can be manufactured in the Generic Synthesis Unit (Section 2.1). (Artificial self-assembling bilayer membranes such as polymersomes[227] that can serve as the foundation for building synthetic living cells are also the subject of much recent research interest.)

---

[226] Freitas RA Jr. Nanomedicine, Volume I: Basic Capabilities, Landes Bioscience, Georgetown, TX, 1999; Table 8.18; http://www.nanomedicine.com/NMI/Tables/8.18.jpg.

[227] Martino C, Kim SH, Horsfall L, Abbaspourrad A, Rosser SJ, Cooper J, Weitz DA. Protein expression, aggregation, and triggered release from polymersomes as artificial cell-like structures. Angew Chem Int Ed Engl. 2012 Jun 25;51(26):6416-6420; https://weitzlab.seas.harvard.edu/files/weitzlab/files/2012_angewchem_martino.pdf. Spoelstra WK, Deshpande S, Dekker C. Tailoring the appearance: what will synthetic cells look like? Curr Opin Biotechnol. 2018 Jun;51:47-56.; https://ceesdekkerlab.nl/wp-content/uploads/1-s2.0-S0958166917301349-main.pdf. Lo CH, Zeng J. Application of polymersomes in membrane protein study and drug discovery: Progress, strategies, and perspectives. Bioeng Transl Med. 2022 Jun 28;8(1):e10350; https://www.ncbi.nlm.nih.gov/pmc/articles/pmid/36684106/. Zhu Y, Cao S, Huo M, van Hest JCM, Che H. Recent advances in permeable polymersomes: fabrication, responsiveness, and applications. Chem Sci.

Erythrocytes, or red blood cells (RBCs),[228] deserve special mention as they constitute ~81% or ~29 trillion of the ~36 trillion cells in the human body (Section 1). Red cells are fairly small biconcave disks (image, left), averaging ~7.8 μm in diameter, ~2 μm thick, and only ~94 μm^3 in volume compared to the much larger ~8000 μm^3 of a representative tissue cell.

RBCs have no nucleus, no organelles, no mitochondrial energy sources, no DNA, and no protein biosynthesis, though they do contain a few enzymes such as nitric oxide synthase that produces NO, several enzymes (CSE, CBS, and 3-MST)[229] that produce hydrogen sulfide, and several others. But for the most part, red cells are simply membrane bags full of hemoglobin,[230] the iron-rich pigment responsible for oxygen transport in the blood. The red cell membrane itself has three components: a carbohydrate-rich glycocalyx on the exterior, a single lipid bilayer containing various transmembrane proteins, and the membrane skeleton (images, below) which is

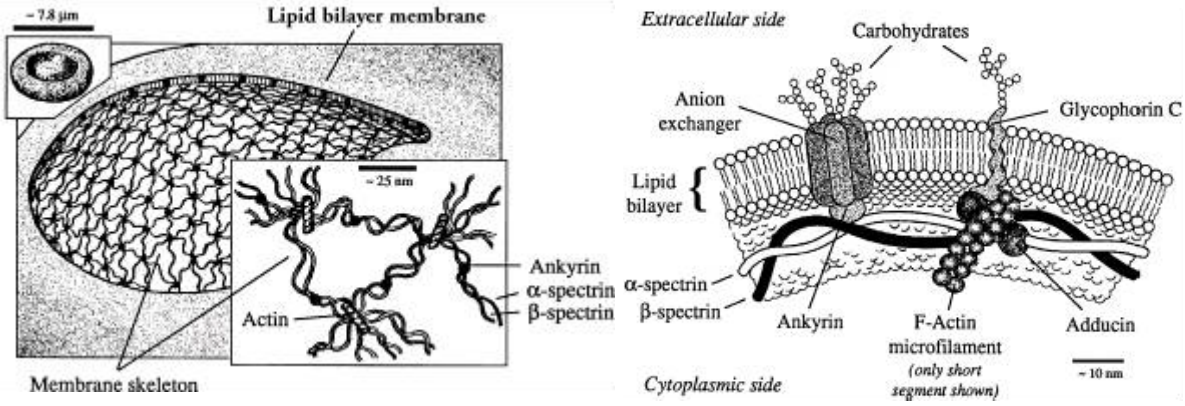

a highly organized two-dimensional triangulated network of actin oligomers tethered to spectrin tetramer filaments interconnecting ~70,000 nodes[231] or microfilament junctional complexes

---

2023 Jun 21;14(27):7411-7437; https://www.ncbi.nlm.nih.gov/pmc/articles/pmid/37449076/. Sun Q, Shi J, Sun H, Zhu Y, Du J. Membrane and Lumen-Compartmentalized Polymersomes for Biocatalysis and Cell Mimics. Biomacromolecules. 2023 Nov 13;24(11):4587-4604; https://pubmed.ncbi.nlm.nih.gov/37842883/.

[228] https://en.wikipedia.org/wiki/Red_blood_cell.

[229] Wang G, Huang Y, Zhang N, Liu W, Wang C, Zhu X, Ni X. Hydrogen Sulfide Is a Regulator of Hemoglobin Oxygen-Carrying Capacity via Controlling 2,3-BPG Production in Erythrocytes. Oxid Med Cell Longev. 2021 Feb 13;2021:8877691; https://www.ncbi.nlm.nih.gov/pmc/articles/pmid/33628390/.

[230] https://en.wikipedia.org/wiki/Hemoglobin.

[231] C.W.M. Haest, "Interactions Between Membrane Skeleton Proteins and the Intrinsic Domain of the Erythrocyte Membrane," Biochim. Biophys. Acta 694(1982):331-352.

comprising an equal number of triangular ~50 nm-wide meshes[232] (mean mesh size 3000-4800 nm^2).[233] RBCs should be manufacturable using the methods described for vesicular organelles in Section 3.3.

3.2 Macromolecular Organelles

Six well-known macromolecular organelles found in human cells must be manufactured in the cell mill, including:

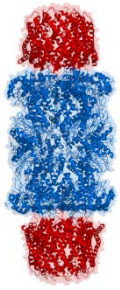

(1) **Proteasomes**[234] are "protein complexes which degrade unneeded or damaged proteins by proteolysis." Proteasomes normally self-assemble with the assistance of four chaperone molecules.[235] Proteasomes are ~11 nm in diameter with a typical volume of $V_{proteasome} \sim 3.4 \times 10^{-24}$ m^3 (**Table 3**) and mass of $m_{proteasome} = 4.18 \times 10^{-21}$ kg (~2.5 MDa),[236] composed of $n_{ResidueProt} = m_{proteasome} / m_{residue} \sim 22{,}700$ amino acid residues, assuming $m_{residue} \sim 110$ dalton/residue (Section 2.2.3). There are $n_{proteasome} \sim 10^7$ proteasomes per "typical" $V_{cell} \sim 8000$ μm^3 tissue cell, representing $f_{proteasome} \sim n_{proteasome} V_{proteasome} / V_{cell} \sim 0.425$ % of cell volume, so a cell mill manufacturing $R_{CellMill} \sim 1$ kg/hr of cells must assemble $R_{ProtMill} \sim f_{proteasome} R_{CellMill} \sim 0.00425$ kg/hr ($R_{ProtMillRes} \sim 6.4 \times 10^{18}$ residues/sec) of proteasome mass to sustain the overall cell production rate.

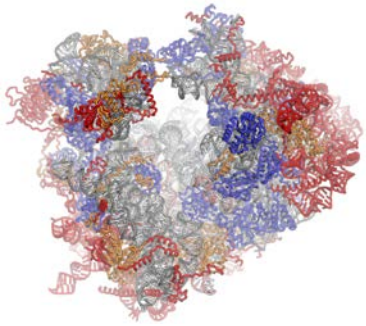

(2) **Ribosomes**[237] are "macromolecular machines that perform biological protein synthesis (mRNA translation), and consist of two major components – the small and large ribosomal subunits – with each subunit including one or more ribosomal RNA (rRNA) molecules and many ribosomal proteins." For example, the 80S eukaryotic ribosome (image, right) has a 40S subunit with 1753 nucleotides and 33 r-proteins and a large 60S

---

[232] Christoph F. Schmidt, Karel Svoboda, Ning Lei, Irena B. Petsche, Lonny E. Berman, Cyrus R. Safinya, Gary S. Grest, "Existence of a Flat Phase in Red Cell Membrane Skeletons," Science 259(12 February 1993):952-955.

[233] M. Takeuchi, H. Miyamoto, Y. Sako, H. Komizu, A. Kusumi, "Structure of the erythrocyte membrane skeleton as observed by atomic force microscopy," Biophys. J. 74(May 1998):2171-2183.

[234] https://en.wikipedia.org/wiki/Proteasome.

[235] Murata S, Yashiroda H, Tanaka K. Molecular mechanisms of proteasome assembly. Nat Rev Mol Cell Biol. 2009 Feb;10(2):104-115; https://pubmed.ncbi.nlm.nih.gov/19165213/. See also: https://en.wikipedia.org/wiki/Proteasome#Assembly.

[236] Tanaka K. The proteasome: overview of structure and functions. Proc Jpn Acad Ser B Phys Biol Sci. 2009 Jan;85(1):12-36; https://www.ncbi.nlm.nih.gov/pmc/articles/PMC3524306/.

[237] https://en.wikipedia.org/wiki/Ribosome.

subunit with 3628 nucleotides and 46 r-proteins.[238] Ribosomes use positionally-controlled solution-phase mechanochemistry to fabricate proteins from amino acid building blocks,[239] a process that should be readily automated in a nanomechanical cell mill, although a small number of autologous proteins fabricated in this manner could then self-assemble into complete ribosomes, a simple way to make lots of copies of this organelle. The conventional reconstitution of ribosomes *in vitro* is well established,[240] and the first steps toward artificial ribosomes have also been reported.[241]

Ribosomes are ~25 nm in diameter with a typical volume of $V_{ribosome}$ ~4 x 10^{-24} m^3 (**Table 3**) and mass of $m_{ribosome}$ = 5.34 x 10^{-21} kg (~3.2 MDa). There are $n_{ribosome}$ ~ 10^7 ribosomes per "typical" V_{cell} ~ 8000 μm^3 tissue cell, representing $f_{ribosome}$ ~ $n_{ribosome}$ $V_{ribosome}$ / V_{cell} ~ 0.5 % of cell volume, so a cell mill manufacturing $R_{CellMill}$ ~ 1 kg/hr of cells must assemble $R_{RiboMill}$ ~ $f_{ribosome}$ $R_{CellMill}$ ~ 0.005 kg/hr of ribosome mass to sustain the overall cell production rate.

(3) **Glycogen granules**[242] are a multibranched polysaccharide of glucose that serves as a form of energy storage in animals, and is the main storage form of glucose in the body. Granules self-assemble with the assistance of several enzymes in a process called glycogenesis.[243] Glycogen granules or "glycosomes" are 10-40 nm in diameter with a typical volume of $V_{glycosome}$ ~1 x 10^{-23} m^3 (**Table 3**) and mass of $m_{glycosome}$ = 1.6 x 10^{-20} kg.[244] There are $n_{glycosome}$ ~ 10^5 glycosomes per "typical" V_{cell} ~ 8000 μm^3 tissue cell, representing $f_{glycosome}$ ~ $n_{glycosome}$ $V_{glycosome}$ / V_{cell} ~ 0.0125 % of cell volume, so a cell mill manufacturing

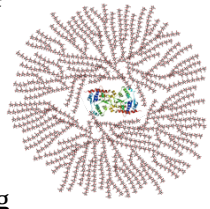

---

[238] https://en.wikipedia.org/wiki/Eukaryotic_ribosome_(80S).

[239] Freitas RA Jr., Merkle RC. Kinematic Self-Replicating Machines. Landes Bioscience, Georgetown, TX, 2004, Section 4.2, "Ribosomes: Molecular Positional Assembly for Self-Replication," pp. 96-101; http://www.MolecularAssembler.com/KSRM/4.2.htm.

[240] Nierhaus KH, Dohme F. Total reconstitution of functionally active 50S ribosomal subunits from *Escherichia coli*. Proc Natl Acad Sci U S A. 1974 Dec;71(12):4713-7; https://www.pnas.org/content/pnas/71/12/4713.full.pdf. Nierhaus KH. Reconstitution of ribosomes, in: Ribosomes and Protein Synthesis, A Practical Approach, Oxford University Press, 1990. Jewett MC, Fritz BR, Timmerman LE, Church GM: *In vitro* integration of ribosomal RNA synthesis, ribosome assembly, and translation. Mol Syst Biol 2013, 9:678; https://www.embopress.org/doi/pdf/10.1038/msb.2013.31.

[241] Orelle C, Carlson ED, Szal T, Florin T, Jewett MC, Mankin AS. Protein synthesis by ribosomes with tethered subunits. Nature. 2015 Aug 6;524(7563):119-24; http://www.ncbi.nlm.nih.gov/pubmed/26222032. Carlson ED, d'Aquino AE, Kim DS, Fulk EM, Hoang K, Szal T, Mankin AS, Jewett MC. Engineered ribosomes with tethered subunits for expanding biological function. Nat Commun. 2019 Sep 2;10(1):3920 ; https://www.ncbi.nlm.nih.gov/pmc/articles/pmid/31477696/. Kofman C, Lee J, Jewett MC. Engineering molecular translation systems. Cell Syst. 2021 Jun 16;12(6):593-607; https://www.cell.com/cell-systems/pdf/S2405-4712(21)00110-1.pdf.

[242] https://en.wikipedia.org/wiki/Glycogen.
[243] https://en.wikipedia.org/wiki/Glycogenesis.

[244] Prats C, Graham TE, Shearer J. The dynamic life of the glycogen granule. J Biol Chem. 2018 May 11;293(19):7089-7098; https://www.jbc.org/content/293/19/7089.full.pdf.

$R_{CellMill}$ ~ 1 kg/hr of cells must assemble $R_{GlycoMill} \sim f_{glycosome}\ R_{CellMill}$ ~ 0.000125 kg/hr of glycosome mass to sustain the overall cell production rate.

(4) **Vaults**[245] are "large ribonucleoprotein particles consisting primarily of proteins that have been implicated in a broad range of cellular functions including nuclear-cytoplasmic transport, mRNA localization, drug resistance, cell signaling, nuclear pore assembly, and innate immunity." Vaults self-assemble by linking and folding multiple joined copies of the major vault protein.[246] Vaults are ~55 nm in diameter with a typical volume of V_{vault} ~5 x 10^{-23} m^3 (**Table 3**) and mass of m_{vault} = 2.2 x 10^{-20} kg (~13 MDa). There are n_{vault} ~ 3000 vaults per "typical" V_{cell} ~ 8000 μm^3 tissue cell, representing $f_{vault} \sim n_{vault}\ V_{vault} / V_{cell}$ ~ 1.9 x 10^{-5} of cell volume, so a cell mill manufacturing $R_{CellMill}$ ~ 1 kg/hr of cells must assemble $R_{VaultMill} \sim f_{vault}\ R_{CellMill}$ ~ 1.9 x 10^{-5} kg/hr of vault mass to sustain the overall cell production rate.

(5) **Centrioles**[247] are "cylindrical organelles (composed mainly of a protein called tubulin) whose main function as a bound pair is to produce the aster and mitotic spindle during cell division." Centrioles normally arise in association with an existing centriole, but under certain circumstances centrioles can self-assemble free of an existing centriole (*de novo* assembly).[248] Two centrioles bound at nearly right angles form the core of the centrosome,[249] the main microtubulin organizing center during cell division. Centrioles are ~400 nm in diameter with a typical volume of $V_{centriole}$ ~7 x 10^{-21} m^3 (**Table 3**) and mass of $m_{centriole}$ = 9.5 x 10^{-18} kg (assuming mean protein density ~1350 kg/m^3). There are $n_{centriole}$ ~ 2 centrioles per "typical" V_{cell} ~ 8000 μm^3 tissue cell, representing $f_{centriole} \sim n_{centriole}\ V_{centriole} / V_{cell}$ ~ 1.75 x 10^{-6} of cell volume, so a cell mill manufacturing $R_{CellMill}$ ~ 1 kg/hr of cells must assemble $R_{CentMill} \sim f_{centriole}\ R_{CellMill}$ ~ 1.75 x 10^{-6} kg/hr of centriole mass to sustain the overall cell production rate.

---

[245] https://en.wikipedia.org/wiki/Vault_(organelle).

[246] Muñoz-Juan A, Carreño A, Mendoza R, Corchero JL. Latest Advances in the Development of Eukaryotic Vaults as Targeted Drug Delivery Systems. Pharmaceutics. 2019 Jun 28;11(7):300; https://www.ncbi.nlm.nih.gov/pmc/articles/PMC6680493/.

[247] https://en.wikipedia.org/wiki/Centriole.

[248] Song MH, Miliaras NB, Peel N, O'Connell KF. Centrioles: some self-assembly required. Curr Opin Cell Biol. 2008 Dec;20(6):688-693; https://www.ncbi.nlm.nih.gov/pmc/articles/pmid/18840522/.

[249] https://en.wikipedia.org/wiki/Centrosome.

(6) **Chromosomes**[250] are "a DNA molecule that includes packaging proteins which, aided by chaperone proteins, bind to and condense the DNA molecule to prevent it from becoming an unmanageable tangle." The fabrication of a genome-length strand of pure DNA with a specified base-pair sequence has previously been described (Section 2.2.2). Chromosomes are DNA strands wrapped around spool-shaped histone octamer[251] molecules (image, right)[252] that bind to DNA and serve as anchors around which the strands are wound, forming a DNA/protein complex called chromatin[253] that when quadruply-folded (compacted) is 40,000 times shorter than an unpacked molecule (image, below).[254] Each histone octamer wrapped with its 147-bp of spooled DNA is called a nucleosome.[255]

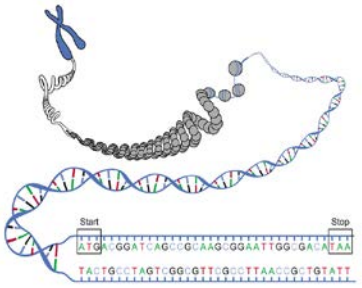

The manufactured genetic material destined for each manufactured cell will consist first of duplex dsDNA (ds = double-strand) which is assembled[256] from two complementary strands of ssDNA (ss = single strand) that have been positionally fabricated base by base in a DNA mill (Section 2.2.2). Using positionally controlled functionalized tooltips analogous to DNA methyltransferase enzymes,[257] the dsDNA haploid

---

[250] https://en.wikipedia.org/wiki/Chromosome.
[251] https://en.wikipedia.org/wiki/Histone_octamer.

[252] Image created by David O. Morgan from The Cell Cycle; https://en.wikipedia.org/wiki/File:Basic_units_of_chromatin_structure.svg.

[253] https://en.wikipedia.org/wiki/Chromatin.

[254] Boston University School of Public Health, "Chromosomes Contain Our Genetic Code"; https://sphweb.bumc.bu.edu/otlt/MPH-Modules/PH/DNA-Genetics/DNA-Genetics2.html.

[255] https://en.wikipedia.org/wiki/Nucleosome.

[256] Cserpan I, Kalman M, Tjörnhammar ML, Simoncsits A. Conversion of single-stranded oligonucleotides into cloned duplexes and its consecutive application to short artificial genes. Acta Chem Scand. 1991 Mar;45(3):265-272; https://pubmed.ncbi.nlm.nih.gov/1645560/.

[257] Pljevaljcic G, Schmidt F, Peschlow A, Weinhold E. Sequence-specific DNA labeling using methyltransferases. Methods Mol Biol. 2004;283:145-161; https://pubmed.ncbi.nlm.nih.gov/15197308/.

strand is next partially methylated for the particular cell type, thus allowing the DNA, once installed in the manufactured nucleus (Section 3.5), to express only the appropriate exons (at non-methylated sites) that are active in the cell type under construction. (Methylation involves the addition of methyl groups to deactivate expression of a given section of DNA.) The partially methylated strand is then wrapped around properly modified[258] (possibly acetylated,[259] methylated,[260] phosphorylated,[261] monoubiquitylated,[262] or sumoylated[263]) histones – normally incorporating post-translational modifications perhaps constituting a "histone code" that may be used by the cell to encrypt various chromatin conformations and gene expression states[264] – after being joined with its homologue strand to make a diploid chromosome that is joined at the waist by a centromere.[265] (Future research should determine if alternative processes involving partial self-assembly of histones[266] and other chromatin-associated proteins[267] or "architectural

---

Dalhoff C, Lukinavicius G, Klimasăuskas S, Weinhold E. Direct transfer of extended groups from synthetic cofactors by DNA methyltransferases. Nat Chem Biol. 2006 Jan;2(1):31-32; https://pure.mpg.de/rest/items/item_2630060_3/component/file_2630063/content. Bheemanaik S, Reddy YV, Rao DN. Structure, function and mechanism of exocyclic DNA methyltransferases. Biochem J. 2006 Oct 15;399(2):177-90; https://www.ncbi.nlm.nih.gov/pmc/articles/PMC1609917/.

[258] LaVoie HA. Epigenetic control of ovarian function: the emerging role of histone modifications. Mol Cell Endocrinol. 2005 Nov 24;243(1-2):12-18; https://pubmed.ncbi.nlm.nih.gov/16219412/.

[259] Clayton AL, Hazzalin CA, Mahadevan LC. Enhanced histone acetylation and transcription: a dynamic perspective. Mol Cell. 2006 Aug 4;23(3):289-296; https://www.cell.com/molecular-cell/pdf/S1097-2765(06)00432-1.pdf.

[260] Torok MS, Grant PA. The generation and recognition of histone methylation. Results Probl Cell Differ. 2006;41:25-46; https://pubmed.ncbi.nlm.nih.gov/16909889/.

[261] Wang Y, Fischle W, Cheung W, Jacobs S, Khorasanizadeh S, Allis CD. Beyond the double helix: writing and reading the histone code. Novartis Found Symp. 2004;259:3-17; https://pubmed.ncbi.nlm.nih.gov/15171244/.

[262] Osley MA. H2B ubiquitylation: the end is in sight. Biochim Biophys Acta. 2004 Mar 15;1677(1-3):74-78; https://pubmed.ncbi.nlm.nih.gov/15020048/.

[263] Nathan D, Ingvarsdottir K, Sterner DE, Bylebyl GR, Dokmanovic M, Dorsey JA, Whelan KA, Krsmanovic M, Lane WS, Meluh PB, Johnson ES, Berger SL. Histone sumoylation is a negative regulator in *Saccharomyces cerevisiae* and shows dynamic interplay with positive-acting histone modifications. Genes Dev. 2006 Apr 15;20(8):966-76; https://www.ncbi.nlm.nih.gov/pmc/articles/PMC1472304/.

[264] Villar-Garea A, Imhof A. The analysis of histone modifications. Biochim Biophys Acta. 2006 Dec;1764(12):1932-1939; https://pubmed.ncbi.nlm.nih.gov/17015046/.

[265] https://en.wikipedia.org/wiki/Centromere.

[266] Fyodorov DV, Kadonaga JT. Dynamics of ATP-dependent chromatin assembly by ACF. Nature. 2002 Aug 22;418(6900):897-900; https://pubmed.ncbi.nlm.nih.gov/12192415/.

[267] Hakimi MA, Bochar DA, Schmiesing JA, Dong Y, Barak OG, Speicher DW, Yokomori K, Shiekhattar R. A chromatin remodelling complex that loads cohesin onto human chromosomes. Nature. 2002 Aug 29;418(6901):994-998; https://pubmed.ncbi.nlm.nih.gov/12198550/.

proteins"[268] onto positionally synthesized DNA can be equally reliable but more efficient.) The centromere is coded by a conserved relatively short repeating heterochromatin sequence and includes a small complex of associated proteins.[269] Each completed 23-diploid-chromatid set of chromatin fibers would be fully condensed (e.g., by nondisruptive methods functionally similar to chemically-induced premature chromosome condensation)[270] into compact supercoiled form,[271] then stored for later use during the assembly of a manufactured nucleus (Section 3.5).

The histone octamer is a squat cylinder ~11 nm in diameter and ~5.5 nm tall,[272] giving a volume of $V_{histone} \sim 5.3 \times 10^{-25}$ m^3 with a typical mass of $m_{histone} = 1.81 \times 10^{-22}$ kg (~108,000 daltons) or $n_{ResidueHist} = 990$ amino acid residues.[273] There are $n_{histone} \sim 25 \times 10^6$ histone octamers per "typical" $V_{cell} \sim 8000$ μm^3 tissue cell, representing $f_{histone} \sim n_{histone} V_{histone} / V_{cell} \sim 0.166$ % of cell volume, so a cell mill manufacturing $R_{CellMill} \sim 1$ kg/hr of cells must assemble $R_{HistMill} \sim f_{histone} R_{CellMill} \sim 0.00166$ kg/hr ($R_{HistMillRes} \sim 2.5 \times 10^{18}$ residues/sec) of histone octamer mass to sustain the overall cell production rate.

For all six macromolecular organelles, the total manufacturing requirement is $R_{MacromolOrgs} = R_{ProtMill} + R_{RiboMill} + R_{GlycoMill} + R_{VaultMill} + R_{CentMill} + R_{HistMill} \sim 0.0111$ kg/hr (or $R_{MacromolOrgsRes} \sim 1.67 \times 10^{19}$ residues/sec) to sustain the overall cell production rate of $R_{CellMill} \sim 1$ kg/hr. Again conservatively adopting the ribosome productivity of only $\psi_m = 5 \times 10^{21}$ residues/kg-sec for the nanorobotic protein synthesis system (Section 2.2.3), the additional protein mill component would have a mass of $m_{ProteinMillMO} = R_{MacromolOrgsRes} / \psi_m \sim$ **3 gm** and a volume of $V_{ProteinMillMO} = m_{ProteinMill} / \rho_{ProteinMill} \sim$ **170 cm^3** assuming the protein mill has a device density of $\rho_{ProteinMill} \sim 20$ kg/m^3 (equivalent to ~3% solid diamond and ~97% vacuum by volume inside the device), the same as the DNA mill. Taking the operating power density of the protein mill as similar to that

---

[268] https://en.wikipedia.org/wiki/Nuclear_organization#Architectural_proteins.

[269] Foltz DR, Jansen LE, Black BE, Bailey AO, Yates JR 3rd, Cleveland DW. The human CENP-A centromeric nucleosome-associated complex. Nat Cell Biol. 2006 May;8(5):458-469; http://www.jansenlab.org/files/2006foltz.pdf.

[270] Prasanna PG, Blakely WF. Premature chromosome condensation in human resting peripheral blood lymphocytes for chromosome aberration analysis using specific whole-chromosome DNA hybridization probes. Methods Mol Biol. 2005;291:49-57; https://pubmed.ncbi.nlm.nih.gov/15502211/.

[271] Grigoryev SA, Bednar J, Woodcock CL. MENT, a heterochromatin protein that mediates higher order chromatin folding, is a new serpin family member. J Biol Chem. 1999 Feb 26;274(9):5626-5636; https://www.jbc.org/content/274/9/5626.full.pdf. Kimura K, Rybenkov VV, Crisona NJ, Hirano T, Cozzarelli NR. 13S condensin actively reconfigures DNA by introducing global positive writhe: implications for chromosome condensation. Cell. 1999 Jul 23;98(2):239-248; https://core.ac.uk/download/pdf/82504740.pdf.

[272] Richmond TJ, Finch JT, Rushton B, Rhodes D, Klug A. Structure of the nucleosome core particle at 7 A resolution. Nature. 1984 Oct 11-17;311(5986):532-537; https://pubmed.ncbi.nlm.nih.gov/6482966/. Cutter AR, Hayes JJ. A brief review of nucleosome structure. FEBS Lett. 2015 Oct 7;589(20 Pt A):2914-22; https://www.ncbi.nlm.nih.gov/pmc/articles/PMC4598263/.

[273] https://www.activemotif.com/catalog/details/31472/recombinant-histone-octamer-h3-3.

of the DNA mill (~26,000 W/m^3; Section 2.2.2), the additional protein mill power draw is $P_{ProteinMillMO}$ ~ **4 watts**.

3.3 Vesicular Organelles

Five other organelles found in human cells consist of a vesicle or membrane that encloses metabolically active materials of various kinds. Each of these organelles consists of a phospholipid monolayer or bilayer membrane enclosing a roughly spherical or cylindrical space filled with lipids, digestive enzymes, material being transported, or, in the case of the mitochondrion, a system of internal membranes, ribosomes, granules, and DNA almost as complex as a complete living cell but much smaller, reflecting its ancient bacterial evolutionary origin.[274] These vesicular organelles must be manufactured in the cell mill, and include:

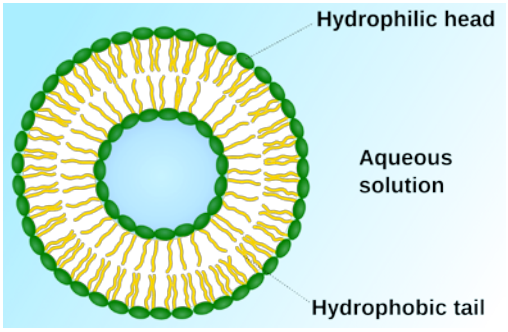

(1) **Transport vesicles**[275] or **endosomes** are phospholipid membranes (**Table 4**) that form containers for protein transport that extrude from the endoplasmic reticulum and "are transported to the *cis* face of the Golgi apparatus, where they fuse with the Golgi membrane and empty their contents into the lumen," or which contain proteins destined for other organelles within the cell (e.g., lysosomes) or for extracellular release. A "typical" V_{cell} ~ 8000 μm^3 tissue cell might contain ~200,000 Golgi vesicles ~50 nm in diameter (each ~6.5 x 10^{-23} m^3 and ~7.3 x 10^{-20} kg, with shell volume ~4 x 10^{-23} m^3) and ~50,000 secretory vesicles ~0.1 μm in diameter (each ~4 x 10^{-21} m^3 and ~4.5 x 10^{-18} kg, with shell volume ~2 x 10^{-22} m^3).[276] This gives a total vesicle volume of $V_{vesicle}$ = 2.2 x 10^{-16} m^3 and $M_{vesicle}$ = 2.5 x 10^{-13} kg per cell, representing $f_{vesicle}$ ~ $V_{vesicle}$ / V_{cell} ~ 2.75 % of cell volume, so a cell mill manufacturing $R_{CellMill}$ ~ 1 kg/hr of cells must assemble $R_{VesiMill}$ ~ $f_{vesicle}$ $R_{CellMill}$ ~ 0.0275 kg/hr of vesicle mass (roughly half protein, half lipid) to sustain the overall cell production rate.

Endosomes (membrane-bound intracellular compartments originating from the Golgi *trans* face containing molecules or ligands internalized from the plasma membrane that may be targeted to lysosomes for degradation) have been reconstituted *in vitro* from purified components.[277]

---

[274] Sagan L. On the origin of mitosing cells. J Theor Biol. 1967 Mar;14(3):255-74; http://web.gps.caltech.edu/classes/ge246/endosymbiotictheory_marguli.pdf.

[275] https://en.wikipedia.org/wiki/Golgi_apparatus#Vesicular_transport.

[276] Freitas RA Jr., Nanomedicine, Volume I: Basic Capabilities, Landes Bioscience, Georgetown, TX, 1999, Table 8.17, "Approximate Quantification of the Components of a Typical 20-μm Human Tissue Cell"; http://www.nanomedicine.com/NMI/Tables/8.17.jpg.

[277] Wollert T. Reconstituting multivesicular body biogenesis with purified components. Methods Cell Biol. 2012;108:73-92; http://www.ncbi.nlm.nih.gov/pubmed/22325598.

(2) **Lipid droplets**[278] (aka. lipid bodies, oil bodies, or adiposomes) are "lipid-rich cellular organelles found largely in the adipose tissue that regulate the storage and hydrolysis of neutral lipids, and also serve as a reservoir for cholesterol and acyl-glycerols for membrane formation and maintenance." Lipid droplets have a neutral lipid core (triacylglycerols and cholesteryl esters) surrounded by a phospholipid monolayer 0.2-5 μm in diameter with a typical volume of $V_{droplet} \sim 10^{-19}$ m^3 and mass of $m_{droplet} = 8.5 \times 10^{-17}$ kg.[279] If there are $n_{droplet} \sim 100$ lipid droplets per "typical" $V_{cell} \sim 8000$ μm^3 tissue cell, representing $f_{droplet} \sim n_{droplet} V_{droplet} / V_{cell} \sim 0.125$ % of cell volume, then a cell mill manufacturing $R_{CellMill} \sim 1$ kg/hr of cells must assemble $R_{DropMill} \sim f_{droplet} R_{CellMill} \sim 0.00125$ kg/hr of lipid droplet mass to sustain the overall cell production rate.

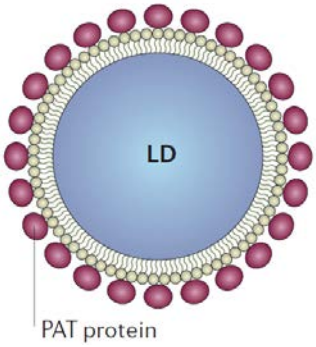

(3) **Lysosomes**[280] are roughly spherical vesicles containing ~50 hydrolytic enzymes that can degrade extracellular material internalized by endocytosis/phagocytosis, and can degrade and recycle intracellular components that are delivered via autophagy.[281] Lysosomes[282] have a lipid bilayer membrane in which is embedded special transmembrane transport proteins that use ATP to pump H^+ into the organelle lumen to maintain internal pH at 5, along with special docking marker acceptor proteins that mark a lysosome as a target for fusion with specific transport vesicles in the cell.[283] Lysosomes are ~0.5-1 μm in diameter with a

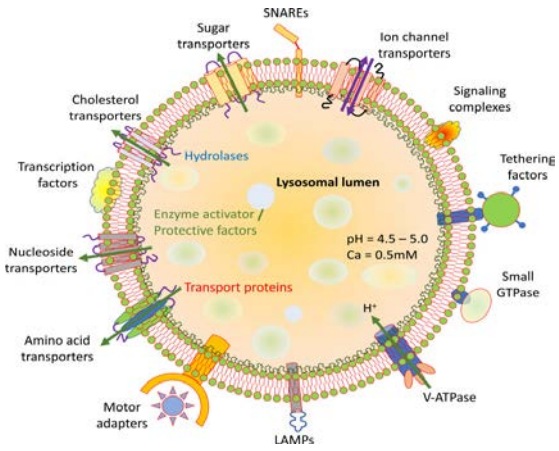

---

[278] Image from: Martin S, Parton RG. Lipid droplets: a unified view of a dynamic organelle. Nat Rev Mol Cell Biol. 2006 May;7(5):373-378; https://pubmed.ncbi.nlm.nih.gov/16550215/. See also https://en.wikipedia.org/wiki/Lipid_droplet.

[279] Freitas RA Jr., Nanomedicine, Volume I: Basic Capabilities, Landes Bioscience, Georgetown, TX, 1999, Table 8.17, "Approximate Quantification of the Components of a Typical 20-μm Human Tissue Cell"; http://www.nanomedicine.com/NMI/Tables/8.17.jpg.

[280] https://en.wikipedia.org/wiki/Lysosome.

[281] Wang F, Gómez-Sintes R, Boya P. Lysosomal membrane permeabilization and cell death. Traffic. 2018 Dec;19(12):918-931; https://onlinelibrary.wiley.com/doi/full/10.1111/tra.12613.

[282] Image from: Allemailem KS, Almatroudi A, Alrumaihi F, Almatroodi SA, Alkurbi MO, Basfar GT, Rahmani AH, Khan AA. Novel Approaches of Dysregulating Lysosome Functions in Cancer Cells by Specific Drugs and Its Nanoformulations: A Smart Approach of Modern Therapeutics. Int J Nanomedicine. 2021 Jul 26;16:5065-5098; https://www.ncbi.nlm.nih.gov/pmc/articles/pmc8324981/.

[283] Freitas RA Jr. Nanomedicine, Volume I: Basic Capabilities, Landes Bioscience, Georgetown, TX, 1999; Section 8.5.3.8, "Lysosomes and Proteasomes"; http://www.nanomedicine.com/NMI/5.3.6.htm.

typical volume of $V_{lysosome}$ ~ 3.1 x 10^{-19} m^3 and mass $m_{lysosome}$ = 3.5 x 10^{-16} kg.[284] If there are $n_{lysosome}$ ~ 300 lysosomes per "typical" V_{cell} ~ 8000 μm^3 tissue cell, representing $f_{lysosome}$ ~ $n_{lysosome}$ $V_{lysosome}$ / V_{cell} ~ 1.16 % of cell volume, then a cell mill manufacturing $R_{CellMill}$ ~ 1 kg/hr of cells must assemble $R_{LysoMill}$ ~ $f_{lysosome}$ $R_{CellMill}$ ~ 0.0116 kg/hr of lysosome mass to sustain the overall cell production rate.

One of the first artificial lysosome "models" was reported in 1969.[285] Lysosomal ion channel molecules have been successfully inserted into artificial membranes by conventional means.[286]

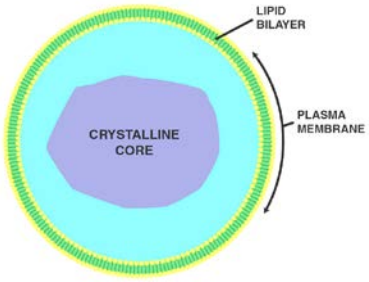

(4) **Peroxisomes**[287] are cytoplasmic membrane-bound oxidative organelles that "perform key roles in lipid metabolism and the conversion of reactive oxygen species." They "contain a variety of enzymes, which primarily function together to rid the cell of toxic substances, and in particular, hydrogen peroxide."[288] Much like lysosomes, peroxisomes are ~0.5-1 μm in diameter with a typical volume of $V_{peroxisome}$ ~ 3.1 x 10^{-19} m^3 and mass $m_{peroxisome}$ = 3.9 x 10^{-16} kg.[289] If there are $n_{peroxisome}$ ~ 300 peroxisomes per "typical" V_{cell} ~ 8000 μm^3 tissue cell, representing $f_{peroxisome}$ ~ $n_{peroxisome}$ $V_{peroxisome}$ / V_{cell} ~ 1.16 % of cell volume, then a cell mill manufacturing $R_{CellMill}$ ~ 1 kg/hr of cells must assemble $R_{PeroxMill}$ ~ $f_{peroxisome}$ $R_{CellMill}$ ~ 0.0116 kg/hr of peroxisome mass to sustain the overall cell production rate. "Peroxisomes can be derived from the endoplasmic reticulum under certain experimental conditions and replicate by membrane growth and division out of pre-existing organelles."[290]

---

[284] Freitas RA Jr., Nanomedicine, Volume I: Basic Capabilities, Landes Bioscience, Georgetown, TX, 1999, Table 8.17, "Approximate Quantification of the Components of a Typical 20-μm Human Tissue Cell"; http://www.nanomedicine.com/NMI/Tables/8.17.jpg.

[285] Sessa G, Weissman GJ. Formation of artificial lysosome *in vitro*. J Clin Invest. 1969 Jan 1;48(6):A76-A77. Sessa G, Weissmann G. Incorporation of lysozyme into liposomes. A model for structure-linked latency. J Biol Chem. 1970 Jul 10;245(13):3295-301; http://www.jbc.org/content/245/13/3295.long.

[286] Venturi E, Sitsapesan R. Reconstitution of lysosomal ion channels into artificial membranes. Methods Cell Biol. 2015;126:217-36; http://www.ncbi.nlm.nih.gov/pubmed/25665448.

[287] https://en.wikipedia.org/wiki/Peroxisome.
[288] https://upload.wikimedia.org/wikipedia/commons/8/82/Peroxisome.jpg.

[289] Freitas RA Jr., Nanomedicine, Volume I: Basic Capabilities, Landes Bioscience, Georgetown, TX, 1999, Table 8.17, "Approximate Quantification of the Components of a Typical 20-μm Human Tissue Cell"; http://www.nanomedicine.com/NMI/Tables/8.17.jpg.

[290] Schrader M, Costello JL, Godinho LF, Azadi AS, Islinger M. Proliferation and fission of peroxisomes - An update. Biochim Biophys Acta. 2016 May;1863(5):971-983; https://www.sciencedirect.com/science/article/pii/S0167488915003365.

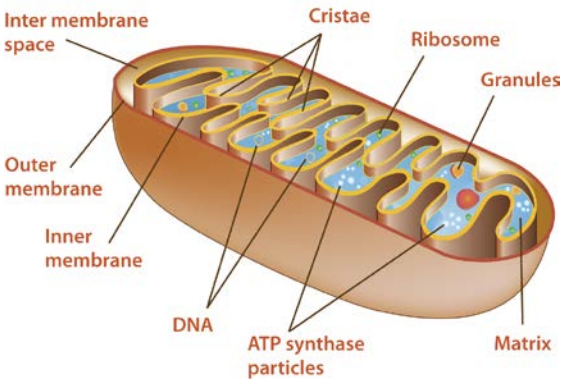

(5) **Mitochondria**[291] are double-membrane-bound organelles whose main function is to provide energy for the cell, most importantly by the production of the energy molecule ATP. Mitochondria are 0.5-1 μm wide and 2-3 μm long, with a typical volume of $V_{mitochondrion} \sim 1 \times 10^{-18}$ m^3 and mass of $m_{mitochondrion} = 1.2 \times 10^{-15}$ kg.[292] There are $n_{mitochondrion} \sim 1000$ mitochondria per "typical" $V_{cell} \sim 8000$ μm^3 tissue cell, representing $f_{mitochondrion} \sim n_{mitochondrion} V_{mitochondrion} / V_{cell} \sim 12.5$ % of cell volume, so a cell mill manufacturing $R_{CellMill} \sim 1$ kg/hr of cells must assemble $R_{MitoMill} \sim f_{mitochondrion} R_{CellMill} \sim 0.125$ kg/hr of mitochondrial mass to sustain the overall cell production rate. A significant fraction of mitochondrial mass will consist of manufactured proteins such as enzymes (Section 2.2.3), macromolecular organelles such as ribosomes and granules (Section 3.2), and mitochondrial DNA in the form of a single 16 kilobase circular chromosome with 37 genes,[293] requiring some special handling.

Organelle biogenesis in biological systems can occur by *de novo* synthesis from (1) a pre-existing membrane source, (2) fission,[294] (3) fusion,[295] and (4) decay, such as through partitioning during cell division or autophagy.[296] For example, biogenesis of mitochondria occurs by growth and division of pre-existing organelles,[297] a process that could presumably be artificially accelerated

---

[291] Image from: https://www.ck12.org/book/ck-12-biology-concepts/r6/section/2.25/. See also: https://en.wikipedia.org/wiki/Mitochondrion.

[292] Freitas RA Jr., Nanomedicine, Volume I: Basic Capabilities, Landes Bioscience, Georgetown, TX, 1999, Table 8.17, "Approximate Quantification of the Components of a Typical 20-μm Human Tissue Cell"; http://www.nanomedicine.com/NMI/Tables/8.17.jpg.

[293] Anderson S, Bankier AT, Barrell BG, de Bruijn MHL, Coulson AR, Drouin J, Eperon IC, Nierlich DP, Roe BA, Sanger F, Schreier PH, Smith AJH, Staden R, Young IG. Sequence and organization of the human mitochondrial genome. Nature. 1981 Apr 9;290(5806):457-465; https://pubmed.ncbi.nlm.nih.gov/7219534/. See also: https://en.wikipedia.org/wiki/Mitochondrial_DNA.

[294] Lowe M, Barr FA. Inheritance and biogenesis of organelles in the secretory pathway. Nat Rev Mol Cell Biol. 2007 Jun;8(6):429-39; https://www.ncbi.nlm.nih.gov/pubmed/17505521/.

[295] Denesvre C, Malhotra V. Membrane fusion in organelle biogenesis. Curr Opin Cell Biol. 1996 Aug;8(4):519-23; https://www.ncbi.nlm.nih.gov/pubmed/8791453/.

[296] van der Vaart A, Mari M, Reggiori F. A picky eater: exploring the mechanisms of selective autophagy in human pathologies. Traffic. 2008 Mar;9(3):281-9; https://www.researchgate.net/profile/Fulvio_Reggiori/publication/5859063_A_picky_eater_exploring_the_mechanisms_of_selective_autophagy_in_human_pathologies/links/542408dc0cf238c6ea6e896e.pdf.

[297] Valero T. Mitochondrial biogenesis: pharmacological approaches. Curr Pharm Des. 2014;20(35):5507-9; https://www.ncbi.nlm.nih.gov/pubmed/24606795.

using a bioreactor setup or by other means.[298] The inventory of known proteins comprising all mammalian mitochondria (the full mitochondrial "parts list") now appears complete.[299]

Mainstream research is also pursuing the possibility of artificial mitochondria. For example, the light-driven proton pump bacteriorhodopsin and the enzyme ATP synthase have successfully been co-reconstituted into small unilamellar vesicles[300] and polymersomes.[301] The energy from the reduction of oxygen might be usable for ATP production by replacing bacteriorhodopsin with ubiquinol bo_3 oxidase in small unilamellar vesicles[302] and polymersomes[303] – their co-reconstitution having been achieved in cell-sized giant unilamellar vesicles[304] where ATP synthase has been shown to induce nonequilibrium membrane fluctuation.[305]

---

[298] Komen JC, Thorburn DR. Turn up the power - pharmacological activation of mitochondrial biogenesis in mouse models. Br J Pharmacol. 2014 Apr;171(8):1818-36; http://www.ncbi.nlm.nih.gov/pmc/articles/PMC3976607/. Thevis M, Schänzer W. Emerging drugs affecting skeletal muscle function and mitochondrial biogenesis - Potential implications for sports drug testing programs. Rapid Commun Mass Spectrom. 2016 Mar 15;30(5):635-51; http://www.ncbi.nlm.nih.gov/pubmed/26842585.

[299] Rath S, Sharma R, Gupta R, Ast T, Chan C, Durham TJ, Goodman RP, Grabarek Z, Haas ME, Hung WHW, Joshi PR, Jourdain AA, Kim SH, Kotrys AV, Lam SS, McCoy JG, Meisel JD, Miranda M, Panda A, Patgiri A, Rogers R, Sadre S, Shah H, Skinner OS, To TL, Walker MA, Wang H, Ward PS, Wengrod J, Yuan CC, Calvo SE, Mootha VK. MitoCarta3.0: an updated mitochondrial proteome now with sub-organelle localization and pathway annotations. Nucleic Acids Res. 2021 Jan 8;49(D1):D1541-D1547; https://www.ncbi.nlm.nih.gov/pmc/articles/pmid/33174596/.

[300] Pitard B, Richard P, Duñach M, Girault G, Rigaud JL. ATP synthesis by the F_0F_1 ATP synthase from thermophilic *Bacillus* PS3 reconstituted into liposomes with bacteriorhodopsin. 1. Factors defining the optimal reconstitution of ATP synthases with bacteriorhodopsin. Eur J Biochem. 1996 Feb 1;235(3):769-778; https://febs.onlinelibrary.wiley.com/doi/epdf/10.1111/j.1432-1033.1996.00769.x.

[301] Choi HJ, Montemagno CD. Artificial organelle: ATP synthesis from cellular mimetic polymersomes. Nano Lett. 2005 Dec;5(12):2538-2542; https://pubmed.ncbi.nlm.nih.gov/16351211/.

[302] Nilsson T, Lundin CR, Nordlund G, Ädelroth P, von Ballmoos C, Brzezinski P. Lipid-mediated Protein-protein Interactions Modulate Respiration-driven ATP Synthesis. Sci Rep. 2016 Apr 11;6:24113; https://www.ncbi.nlm.nih.gov/pmc/articles/PMC4827085/. von Ballmoos C, Biner O, Nilsson T, Brzezinski P. Mimicking respiratory phosphorylation using purified enzymes. Biochim Biophys Acta. 2016 Apr;1857(4):321-331; https://core.ac.uk/download/pdf/33091349.pdf.

[303] Otrin L, Marušič N, Bednarz C, *et al*. Toward Artificial Mitochondrion: Mimicking Oxidative Phosphorylation in Polymer and Hybrid Membranes. Nano Lett. 2017 Nov 8;17(11):6816-6821; https://pure.mpg.de/rest/items/item_2506715/component/file_2623632/content. Marušič N, Otrin L, Zhao Z, Lira RB, Kyrilis FL, Hamdi F, Kastritis PL, Vidaković-Koch T, Ivanov I, Sundmacher K, Dimova R. Constructing artificial respiratory chain in polymer compartments: Insights into the interplay between bo_3 oxidase and the membrane. Proc Natl Acad Sci U S A. 2020 Jun 30;117(26):15006-15017; https://www.ncbi.nlm.nih.gov/pmc/articles/PMC7334566/.

[304] Biner O, Schick T, Müller Y, von Ballmoos C. Delivery of membrane proteins into small and giant unilamellar vesicles by charge-mediated fusion. FEBS Lett. 2016 Jul;590(14):2051-2062; https://febs.onlinelibrary.wiley.com/doi/pdf/10.1002/1873-3468.12233%4010.1002/%28ISSN%291873-3468%28CAT%29FreeEditorsChoiceArticles%28VI%29FECA.

Whether a biogenesis-type approach to manufacturing organelles is feasible or advisable is a matter for future research, but the premise of this paper is that positionally-controlled processes may serve as the foundation for most or all organelle assembly operations. To this end, assembling a $d_{organelle}$ = 1 μm diameter spherical vesicular organelle using nanorobot-mediated positionally-controlled processes might proceed in 4 steps:

(A) **Build Lipid Membrane.** A mould-based semaphore-assisted deposition of organelle phospholipid membranes is initiated for two matching hemispheres (Section 3.1). A close-packed array of nanorobotic manipulator arms (image, below)[306] spaced at 100 nm intervals are employed to bond the lipid molecules onto the mould in a efficient pattern. Each nanomanipulator has H_{manip} = 100 nm of accessible horizontal space, work area of $A_{manip} = H_{manip}^2 = 10^4$ nm^2, maximum tip velocity of v_{manip} ~ 1 cm/sec), and a system volume (= mechanism + working volume) of $V_{manip} = H_{manip}^3 = 10^6$ nm^3. If nanomanipulator productivity $\mathbb{D}_{mols} \sim \psi_V V_{manip}$ = 2600 molecules/manipulator-sec, taking $\psi_V = 2.6 \times 10^{24}$ molecules/m^3-sec on the conservative assumption that nanorobotic manipulators should have at least the same volumetric productivity as ribosomes in an aqueous operating environment,[307] and given that there are $n_{lipidmols} \sim 2.5 \times 10^6$ lipid molecules/μm^2 in each layer of a plasma membrane lipid bilayer,[308] then the hemispheric mould surface under each nanomanipulator in the

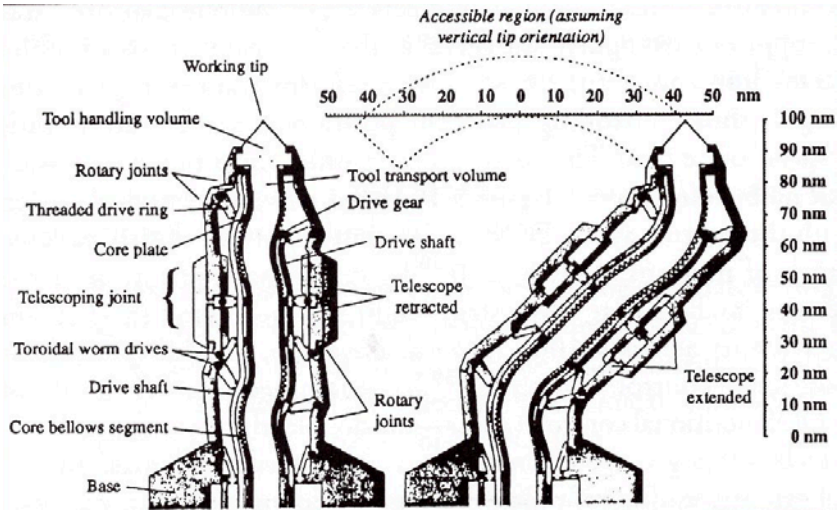

---

[305] Almendro-Vedia VG, Natale P, Mell M, Bonneau S, Monroy F, Joubert F, López-Montero I. Nonequilibrium fluctuations of lipid membranes by the rotating motor protein F_1F_0-ATP synthase. Proc Natl Acad Sci U S A. 2017 Oct 24;114(43):11291-11296; https://www.ncbi.nlm.nih.gov/pmc/articles/PMC5664490/.

[306] Freitas RA Jr. Nanomedicine, Volume I: Basic Capabilities, Landes Bioscience, Georgetown TX, 1999, Fig. 9.8; http://www.nanomedicine.com/NMI/Figures/9.8.jpg. Adapted from: Drexler KE. Nanosystems: Molecular Machinery, Manufacturing, and Computation, John Wiley & Sons, New York, 1992, Section 13.4.1, "A bounded-continuum design for a stiff manipulator"; https://www.amazon.com/dp/0471575186/.

[307] Ribosome volumetric productivity $\psi_V = 2.6 \times 10^{24}$ residues/m^3-sec when bonding amino acid molecules (each of which becomes a "residue") to proteins in an aqueous working environment (Section 2.2.3).

[308] Freitas RA Jr. Nanomedicine, Volume I: Basic Capabilities, Landes Bioscience, Georgetown, TX, 1999; Section 8.5.3.2, "Cell Membrane"; http://www.nanomedicine.com/NMI/8.5.3.2.htm.

array receives one complete lipid layer of $n_{lipidmols}\ A_{manip} \sim 25{,}000$ lipid molecules in $t_{lipidlayer} \sim n_{lipidmols}\ A_{manip} / \mathfrak{D}_{mols} \sim 9.6$ sec, dissipating $P_{manipulator} \sim 0.1$ pW/manipulator while in continuous motion. A hemispheric mould for an organelle of diameter $d_{organelle} = 1$ μm requires $n_{maniparray} \sim \pi d_{organelle}^2 / 2A_{manip} \sim 157$ nanomanipulators consuming $n_{maniparray}\ P_{manipulator} \sim 157$ pW of power, and needs $2t_{lipidlayer} \sim 19$ sec to lay down a complete hemispheric lipid bilayer of $N_{bilayerlipids} = \pi d_{organelle}^2\ n_{lipidmols}\ n_{maniparray} \sim 1.2 \times 10^9$ bilayer lipid molecules in that time.

(B) **Insert Membrane Proteins.** The same 157-arm manipulator array is next employed to embed transmembrane proteins into the lipid membrane and to attach integral and related proteins into the inward-facing surface of the membrane. The plasma membrane of a human tissue cell typically contains $n_{proteinmols} \sim 42{,}000$ protein molecules/μm^2,[309] so each manipulator in the array requires $t_{proteininsert} \sim n_{proteinmols}\ A_{manip} / \mathfrak{D}_{mols} \sim 0.16$ sec to complete all protein insertion operations within its $A_{manip} = 10^4$ nm^2 workspace. The entire array of $n_{maniparray} \sim 157$ manipulators can insert $N_{proteininsert} = (\pi/2)\ d_{organelle}^2\ n_{proteinmols}\ n_{maniparray} \sim 10^7$ protein molecules in that time.

(C) **Build Internal Structure.** The internal structure of the organelle is built in place using the manipulator array. The solid volume of the $d_{organelle} = 1$ μm diameter hemisphere under construction is $V_{hemisphere} = \pi d_{organelle}^3 / 12 = 0.262$ μm^3. Taking the most conservative assumption, the entire hemispheric volume could be filled with covalently bonded $N_{hemisphericprotein} = \rho_{protein}\ V_{hemisphere} / m_{protein} \sim 4.2 \times 10^6$ protein molecules of average mass $m_{protein} \sim 8.4 \times 10^{-23}$ kg/molecule (~50,000 dalton protein molecules)[310] and mean protein density $\rho_{protein} \sim 1350$ kg/m^3 in a filling time of $t_{proteinbuild} \sim N_{hemisphericprotein} / n_{maniparray}\ \mathfrak{D}_{mols} \sim 10$ sec using a single 157-manipulator array. Note that the internal structure of the mitochondrion has moderate complexity because of the presence of an internal highly invaginated membrane that produces numerous small compartments or cristae that may change shape in response to local pH gradients and functional state;[311] any necessary additional assembly steps should be determined in future research.

(D) **Join and Release.** The two equal hemispheres are pressed together face to face, causing them to seamlessly join because of the inherent miscibility of the lipid bilayers along the equatorial perimeter of each face. After any further post-processing is completed,[312] the finished

---

[309] Freitas RA Jr. Nanomedicine, Volume I: Basic Capabilities, Landes Bioscience, Georgetown, TX, 1999; Section 8.5.3.2, "Cell Membrane"; http://www.nanomedicine.com/NMI/8.5.3.2.htm.

[310] Freitas RA Jr. Nanomedicine, Volume I: Basic Capabilities, Landes Bioscience, Georgetown, TX, 1999; Table 3.2; http://www.nanomedicine.com/NMI/Tables/3.2.jpg.

[311] Khalifat N, Puff N, Bonneau S, Fournier JB, Angelova MI. Membrane deformation under local pH gradient: mimicking mitochondrial cristae dynamics. Biophys J. 2008 Nov 15;95(10):4924-33; https://www.ncbi.nlm.nih.gov/pmc/articles/PMC2576396/.

[312] For example, it may be deemed desirable to decorate the exterior surfaces of organelle membranes with protein (Section 2.2.3) or carbohydrate (Section 2.2.4) moieties, to manually link cytosolic filament networks that are otherwise incapable of properly self-sealing, or to insert sorting rotor* probes through the outer membrane into the sealed interior of the organelle to extract or insert particular molecules of interest (Section 4.2). A list of all essential post-processing steps should be compiled, and the nanorobotic means for accomplishing all post-processing steps elucidated, in future research.

vesicular organelle can be released from the moulds by switching the semaphores from hydrophilic to hydrophobic.

The total manufacturing requirement for all five vesicular organelles is $R_{VesicularOrgs} = R_{VesiMill} + R_{DropMill} + R_{LysoMill} + R_{PeroxMill} + R_{MitoMill} = 0.177$ kg/hr to sustain the overall cell production rate of $R_{CellMill} \sim 1$ kg/hr. The 157-manipulator array can lay down $m_{bilayerlipids} \sim m_{lipid}\ N_{bilayerlipids} \sim 1.4 \times 10^{-15}$ kg of bilayer lipid molecules in $2t_{lipidlayer} \sim 19$ sec, or $\psi_1 = m_{bilayerlipids} / 2t_{lipidlayer} \sim 7.4 \times 10^{-17}$ kg/array-sec; insert $m_{proteininsert} \sim m_{protein}\ N_{proteininsert} \sim 8.4 \times 10^{-16}$ kg of protein molecules in $t_{proteininsert} \sim 0.16$ sec, or $\psi_2 = m_{proteininsert} / t_{proteininsert} \sim 5.3 \times 10^{-15}$ kg/array-sec; and build out $m_{hemisphericprotein} \sim m_{protein}\ N_{hemisphericprotein} \sim 3.5 \times 10^{-16}$ kg of protein molecules in $t_{proteinbuild} \sim 10$ sec, or $\psi_3 = m_{hemisphericprotein} / t_{proteinbuild} \sim 3.5 \times 10^{-17}$ kg/array-sec, taking average lipid molecule mass as $m_{lipid} \sim 1.17 \times 10^{-24}$ kg/molecule (~700 daltons) and average protein molecule as $m_{protein} \sim 8.4 \times 10^{-23}$ kg/molecule (~50,000 daltons). Hence we require $N_{arrays} = (R_{VesicularOrgs} / \psi_1) + (R_{VesicularOrgs} / \psi_2) + (R_{VesicularOrgs} / \psi_3) \sim 2.1 \times 10^{12}$ arrays to deliver enough vesicular organelles to satisfy the required production rate of $R_{CellMill} \sim 1$ kg/hr of cells. These arrays have an estimated total volume of $V_{arrays} \sim n_{maniparray}\ V_{manip}\ N_{arrays} \sim 0.33$ cm^3.

If the solid volume of the mould structures, including all interior mechanisms, is some multiple α_{mould} of the volume of the organelles that are being manufactured, then a cubical mould enclosing a spherical organelle of diameter $d_{organelle} = 1$ μm would have a cubical edge length of $L_{cube} = (\pi\ \alpha_{mould} / 6)^{1/3}\ d_{organelle} = 1.26$ μm, taking $\alpha_{mould} = 3.8$.[313] Since each array services one hemispherical mould having a solid volume of $0.5\ L_{cube}^3 \sim 1$ μm^3, the total solid volume of all moulds is $V_{VesOrgMoulds} = 0.5\ L_{cube}^3\ N_{arrays} = 2.1$ cm^3. Assuming a manipulator density of $\rho_{manip} \sim 100$ kg/m^3 (i.e., $\sim 10^{-19}$ kg / 10^6 nm^3) and a mould density approximating 10% of diamond at $\rho_{mould} \sim 350$ kg/m^3, then the vesicular organelle manufacturing equipment has a volume of $V_{CellMillVO} = V_{arrays} + V_{VesOrgMoulds} \sim$ **2.4 cm^3**, a mass of $m_{CellMillVO} = \rho_{manip}\ V_{arrays} + \rho_{mould}\ V_{VesOrgMoulds} \sim$ **0.768 gm**, and a power draw of $P_{CellMillVO} = n_{maniparray}\ N_{arrays}\ P_{manip} \sim$ **33 watts** for the manipulator arrays.

It might be necessary to introduce certain solutes or ions into the cytosol in order to prevent newly introduced vesicular organelles from shrinking, swelling, or bursting due to unwanted osmotic imbalances. Preventing this activity is especially important since new organelles may be introduced with internal inventories of enzymes and at least some reactive chemicals. This issue and its resolution are the proper subject of future research.

---

[*] Drexler KE. Nanosystems: Molecular Machinery, Manufacturing, and Computation, John Wiley & Sons, New York, 1992, Section 13.2.1(a) "Modulated receptors for selective transport: Basic concepts"; https://www.amazon.com/dp/0471575186/. Freitas RA Jr. Nanomedicine, Volume I: Basic Capabilities, Landes Bioscience, Georgetown, TX, 1999; Section 3.4.2, "Sorting Rotors"; http://www.nanomedicine.com/NMI/3.4.2.htm.

[313] By simple geometry, a cube of edge L with a hemispheric hole on one face of maximum radius R = L/2 has a cubical volume (including the hemispheric hole) equal to $L^3 / [(1/2)(4/3)\ \pi\ R^3] = 12 / \pi = 3.8$ times the volume of the hemispheric hole.

3.4 Membraneous Organelles

Two essential organelles found in human cells – the (1) Golgi apparatus and (2) endoplasmic reticulum – are essentially collections of membrane sheets arranged to form compartments through which a variety of packaged biochemicals can progressively pass and be processed.

These organelles could be laboriously assembled fragment by fragment via positionally-controlled nanorobotic pick-and-place operations. However, the preliminary assessment is that under the correct conditions both membraneous organelles should largely self-assemble in place from simpler vesicular components. These components can be manufactured by the previously-described vesicular organelle subsystem of the cell mill (Section 3.3), then be deployed by nanorobotic means to the correct intracellular positions for self-assembly. This supposition should be examined and critically re-assessed in future research.

(1) The **Golgi apparatus**[314] is "part of the endomembrane system in the cytoplasm [that] packages proteins into membrane-bound vesicles inside the cell before the vesicles are sent to their destination. The Golgi is of particular importance in processing proteins for secretion, containing a set of glycosylation enzymes that attach various sugar monomers to proteins as the proteins move through the apparatus."

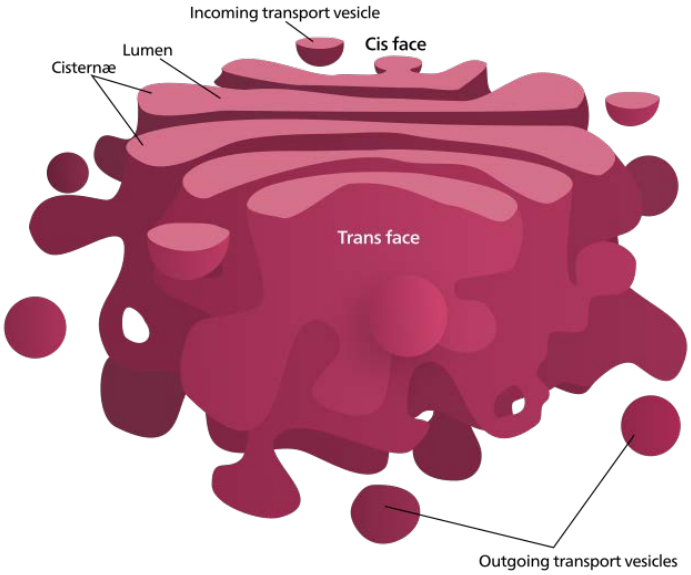

Mammalian cells typically contain 40-100 stacks of cisternae located near the cell nucleus close to the centrosome (Section 3.2(5)), with each stack consisting of 4-8 cisternae or membrane-bounded compartments linked together via microtubule[315] (Section 4.1(4)) connections. Each cistern has a "*cis*" entry face that receives protein-containing vesicles migrating from the endoplasmic reticulum and a "*trans*" exit face from which vesicles containing proteins that have been chemically modified during their slow passage through the Golgi are released and slowly migrate to lysosomes, secretory vessels, or to the cell surface.

---

[314] https://en.wikipedia.org/wiki/Golgi_apparatus.
[315] https://en.wikipedia.org/wiki/Microtubule#Intracellular_organization.

There is some confidence in the self-assembly approach because the Golgi body is known to disintegrate prior to cell mitosis and then reassemble with remarkable precision after cytokinesis,[316] so deployment of manufactured Golgi material in the correct intracellular position after extraction of the original material should result in self-assembly of a fully functional Golgi stack.[317] In the most widely-accepted cisternal progression/maturation model of the self-assembling Golgi apparatus,[318] coat protein II (COPII; image, left)[319]-coated vesicles fuse to form the first *cis*-cisterna of the Golgi stack, which progresses to become mature *trans*-Golgi network (TGN) cisternae as coat protein I (COPI; image, right)[320]-coated vesicles continually recycle Golgi-specific proteins from older to younger cisternae (retrograde transport). Individual stacks have different assortments of enzymes that allow progressive processing of cargo proteins as they travel from the *cis* face to the *trans* face.[321] Once matured, the TGN cisternae dissolve to become secretory vesicles. If this model is correct, then the cell mill need only manufacture the appropriate COPII- and COPI-coated vesicles (Section 3.3(1)) that are normally produced in the endoplasmic reticulum, then progressively release these vesicles in the

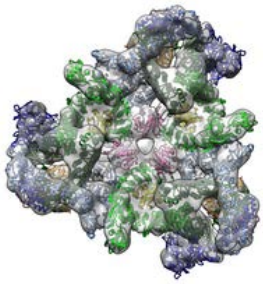

---

[316] Lowe M, Nakamura N, Warren G. Golgi division and membrane traffic. Trends Cell Biol. 1998 Jan;8(1):40-44; https://pubmed.ncbi.nlm.nih.gov/9695807/. Zaal KJM, Smith CL, Polishchuk RS, Altan N, Cole NB, Ellenberg J, Hirschberg K, Presley JF, Roberts TH, Siggia E, Phair RD, Lippincott-Schwartz J. Golgi membranes are absorbed into and reemerge from the ER during mitosis. Cell. 1999 Dec 10;99(6):589-601; https://core.ac.uk/download/pdf/82536976.pdf.

[317] Rabouille C, Misteli T, Watson R, Warren G. Reassembly of Golgi stacks from mitotic Golgi fragments in a cell-free system. J Cell Biol. 1995 May;129(3):605-18; http://citeseerx.ist.psu.edu/viewdoc/download?doi=10.1.1.273.3233&rep=rep1&type=pdf. Puri S, Linstedt AD. Capacity of the golgi apparatus for biogenesis from the endoplasmic reticulum. Mol Biol Cell. 2003 Dec;14(12):5011-5018; https://www.ncbi.nlm.nih.gov/pmc/articles/PMC284802/. Kühnle J, Shillcock J, Mouritsen OG, Weiss M. A modeling approach to the self-assembly of the Golgi apparatus. Biophys J. 2010 Jun 16;98(12):2839-2847; https://www.ncbi.nlm.nih.gov/pmc/articles/PMC2884245/. Tachikawa M, Mochizuki A. Golgi apparatus self-organizes into the characteristic shape via postmitotic reassembly dynamics. Proc Natl Acad Sci U S A. 2017 May 16;114(20):5177-5182; https://www.ncbi.nlm.nih.gov/pmc/articles/PMC5441826/.

[318] Glick BS, Luini A. Models for Golgi traffic: a critical assessment. Cold Spring Harb Perspect Biol. 2011 Nov 1;3(11):a005215; https://www.ncbi.nlm.nih.gov/pmc/articles/pmid/21875986/.

[319] https://en.wikipedia.org/wiki/COPII.
[320] https://en.wikipedia.org/wiki/COPI.

[321] Day KJ, Staehelin LA, Glick BS. A three-stage model of Golgi structure and function. Histochem Cell Biol. 2013 Sep;140(3):239-249; https://www.ncbi.nlm.nih.gov/pmc/articles/pmid/23881164/. Alberts B., *et al*. Molecular Biology of the Cell, 6th Edition, W.W. Norton & Company, 2014; https://www.amazon.com/Molecular-Biology-Sixth-Bruce-Alberts/dp/0815344325/.

desired perinuclear location near the centrosome inside the manufactured cell, along with sufficient microtubular components (Section 4.1(4)), and the Golgi apparatus should spontaneously assemble as a viable intracellular organelle.

As an experimental example of this, Golgi stacks have been reassembled from isolated Golgi components (including random assortments of vesicles "▲", tubules ">", and cisternal remnants "→"; image, below left) to create a large reassembled Golgi stack (image, below right; scale bar = 0.5 μm).[322]

A fully-assembled Golgi complex is several microns wide with a typical volume of $V_{Golgi} \sim 4.5 \times 10^{-16}$ m^3 and mass $m_{Golgi} = 4.9 \times 10^{-13}$ kg,[323] representing $f_{Golgi} \sim V_{Golgi} / V_{cell} \sim 5.6$ % of the volume of a "typical" $V_{cell} \sim 8000$ μm^3 tissue cell, so a cell mill manufacturing $R_{CellMill} \sim 1$ kg/hr of cells must assemble $R_{GolgiMill} \sim f_{Golgi}\ R_{CellMill} \sim 0.056$ kg/hr of Golgi vesicles to sustain the overall cell production rate.

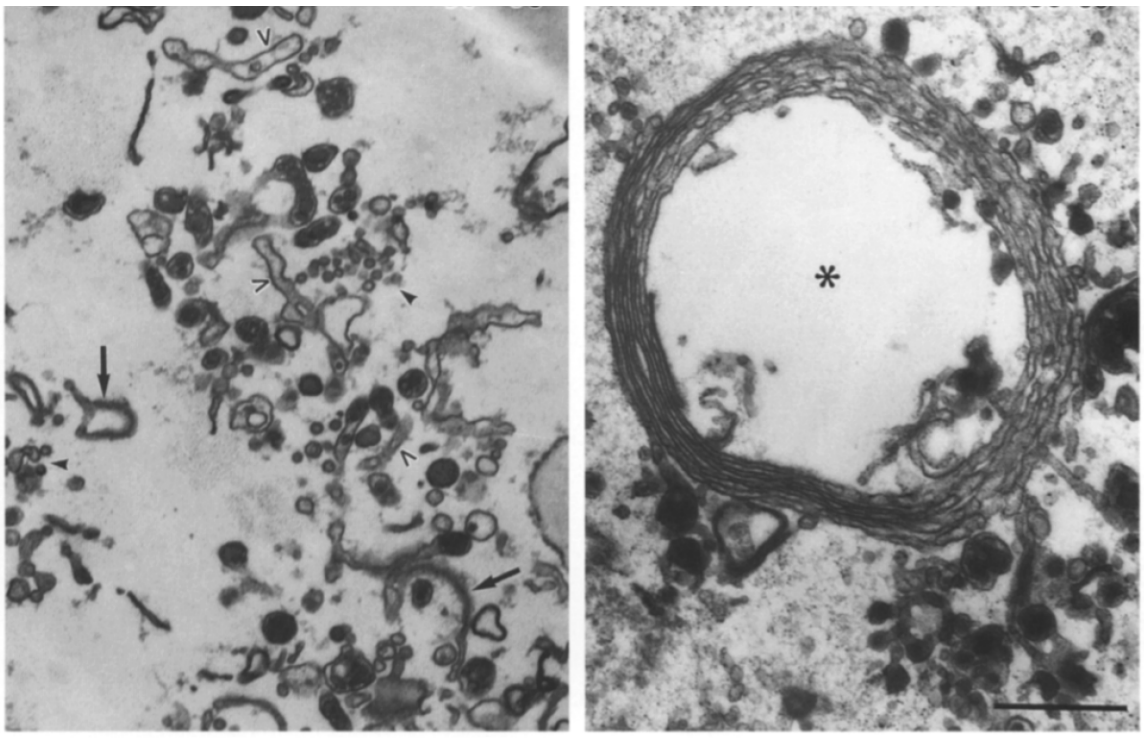

[322] Rabouille C, Misteli T, Watson R, Warren G. Reassembly of Golgi stacks from mitotic Golgi fragments in a cell-free system. J Cell Biol. 1995 May;129(3):605-18; http://citeseerx.ist.psu.edu/viewdoc/download?doi=10.1.1.273.3233&rep=rep1&type=pdf.

[323] Freitas RA Jr., Nanomedicine, Volume I: Basic Capabilities, Landes Bioscience, Georgetown, TX, 1999, Table 8.17, "Approximate Quantification of the Components of a Typical 20-μm Human Tissue Cell"; http://www.nanomedicine.com/NMI/Tables/8.17.jpg.

(2) The **endoplasmic reticulum**[324] is "a type of organelle made up of two subunits – rough endoplasmic reticulum (RER)[325] and smooth endoplasmic reticulum (SER)[326] – [that] forms an interconnected network of flattened, membrane-enclosed sacs known as cisternae (in the RER), and tubular structures in the SER, [whose] membranes are continuous with the outer nuclear membrane. The two types of ER share many of the same proteins and engage in certain common activities such as the synthesis of certain lipids and cholesterol. Different types of cells contain different ratios of the two types of ER depending on the activities of the cell. The outer (cytosolic) face of the rough endoplasmic reticulum is studded with ribosomes that are the sites of protein synthesis. The smooth endoplasmic reticulum lacks ribosomes and functions in lipid synthesis (but not metabolism), the production of steroid hormones, and detoxification."

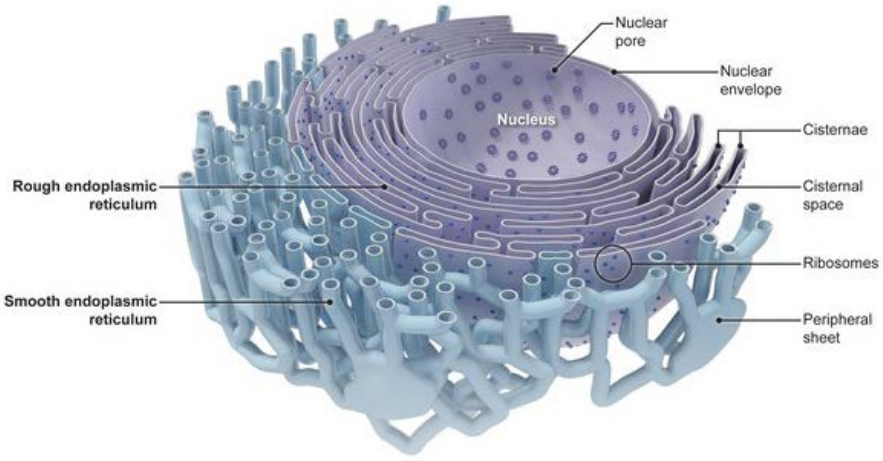

Self-assembly of endoplasmic reticulum from manufactured material also appears likely,[327] though coordination with nucleus manufacture (Section 3.5) is essential and the viability and specific methodology of ER self-assembly processes must be tested and experimentally confirmed by future research. Synthetic cells with multicompartment vesicles, nested vesicles, or "vesosomes" have been created (A) from spontaneous or induced endobudding of giant

---

[324] Image from: Goyal U, Blackstone C. Untangling the web: mechanisms underlying ER network formation. Biochim Biophys Acta. 2013 Nov;1833(11):2492-8; https://www.ncbi.nlm.nih.gov/pmc/articles/pmid/23602970/. See also:.https://en.wikipedia.org/wiki/Endoplasmic_reticulum.

[325] https://en.wikipedia.org/wiki/Endoplasmic_reticulum#Rough_endoplasmic_reticulum.
[326] https://en.wikipedia.org/wiki/Endoplasmic_reticulum#Smooth_endoplasmic_reticulum.

[327] Ferencz CM, Guigas G, Veres A, Neumann B, Stemmann O, Weiss M. Shaping the endoplasmic reticulum *in vitro*. Biochim Biophys Acta. 2016 Sep;1858(9):2035-2040; https://www.sciencedirect.com/science/article/pii/S0005273616302127. Ferencz CM, Guigas G, Veres A, Neumann B, Stemmann O, Weiss M. *In Vitro* Reconstitution of the Endoplasmic Reticulum. Curr Protoc Cell Biol. 2017 Sep 1;76:11.22.1-11.22.16; https://pubmed.ncbi.nlm.nih.gov/28862340/. Li Q, Han X. Self-Assembled Rough Endoplasmic Reticulum-Like Proto-Organelles. iScience. 2018 Oct 26;8:138-147; https://www.ncbi.nlm.nih.gov/pmc/articles/PMC6180236/.

unilamellar vesicles,[328] (B) from mimicking the natural process of endosymbiosis,[329] (C) by using capillary-based microfluidics devices,[330] or (D) by using self-assembly of stacked microsized bicelles.[331] Multicompartment systems have been introduced into living cells where they have successfully performed enzymatic cascade reactions.[332] Enzymes have been incorporated and operated inside polymersomes[333] and vesicles,[334] and complex enzyme cascades producing monoterpenes,[335] isobutanol[336] and polyhydroxybutyrate[337] have been operated *in vitro* using glucose as feedstock. In another study, a synthetic pathway that captures and converts or "fixes" CO_2 required an *in vitro* metabolic network of 17 reactions established with enzymes originating from nine different organisms, including three engineered enzymes.[338]

---

[328] Okumura Y, Nakaya T, Namai H, Urita K. Giant vesicles with membranous microcompartments. Langmuir. 2011 Apr 5;27(7):3279-3282; https://pubmed.ncbi.nlm.nih.gov/21395271/.

[329] Paleos CM, Pantos A. Molecular recognition and organizational and polyvalent effects in vesicles induce the formation of artificial multicompartment cells as model systems of eukaryotes. Acc Chem Res. 2014 May 20;47(5):1475-1482; https://pubmed.ncbi.nlm.nih.gov/24735049/.

[330] Deng NN, Yelleswarapu M, Zheng L, Huck WT. Microfluidic Assembly of Monodisperse Vesosomes as Artificial Cell Models. J Am Chem Soc. 2017 Jan 18;139(2):587-590; https://pubs.acs.org/doi/full/10.1021/jacs.6b10977.

[331] Li Q, Han X. Self-Assembled "Breathing" Grana-Like Cisternae Stacks. Adv Mater. 2018 Jun;30(25):e1707482; https://pubmed.ncbi.nlm.nih.gov/29707837/.

[332] Godoy-Gallardo M, Labay C, Trikalitis VD, *et al*. Multicompartment Artificial Organelles Conducting Enzymatic Cascade Reactions inside Cells. ACS Appl Mater Interfaces. 2017 May 17;9(19):15907-15921; https://pubmed.ncbi.nlm.nih.gov/28117959/.

[333] Peters RJ, Marguet M, Marais S, Fraaije MW, van Hest JC, Lecommandoux S. Cascade reactions in multicompartmentalized polymersomes. Angew Chem Int Ed Engl. 2014 Jan 3;53(1):146-150; https://core.ac.uk/download/pdf/19745137.pdf.

[334] Elani Y, Law RV, Ces O. Vesicle-based artificial cells as chemical microreactors with spatially segregated reaction pathways. Nat Commun. 2014 Oct 29;5:5305; https://core.ac.uk/download/pdf/76995237.pdf.

[335] Korman TP, Opgenorth PH, Bowie JU. A synthetic biochemistry platform for cell free production of monoterpenes from glucose. Nat Commun. 2017 May 24;8:15526; https://www.ncbi.nlm.nih.gov/pmc/articles/PMC5458089/.

[336] Opgenorth PH, Korman TP, Iancu L, Bowie JU. A molecular rheostat maintains ATP levels to drive a synthetic biochemistry system. Nat Chem Biol. 2017 Sep;13(9):938-942; https://pubmed.ncbi.nlm.nih.gov/28671683/.

[337] Opgenorth PH, Korman TP, Bowie JU. A synthetic biochemistry module for production of bio-based chemicals from glucose. Nat Chem Biol. 2016 Jun;12(6):393-395; https://pubmed.ncbi.nlm.nih.gov/27065234/.

[338] Schwander T, Schada von Borzyskowski L, Burgener S, Cortina NS, Erb TJ. A synthetic pathway for the fixation of carbon dioxide *in vitro*. Science. 2016 Nov 18;354(6314):900-904; https://www.ncbi.nlm.nih.gov/pmc/articles/PMC5892708/.

A fully-assembled endoplasmic reticulum partly surrounds the nucleus and may have a typical volume of V_{ER} ~ 1.54 x 10^{-15} m^3 (including ~1120 μm^3 for rough ER and ~420 μm^3 for smooth ER)[339] and mass m_{ER} ~ 1.7 x 10^{-12} kg, representing f_{ER} ~ V_{ER} / V_{cell} ~ 19.3 % of the volume of a "typical" V_{cell} ~ 8000 μm^3 tissue cell, so a cell mill manufacturing $R_{CellMill}$ ~ 1 kg/hr of cells must assemble R_{ERMill} ~ f_{ER} $R_{CellMill}$ ~ 0.193 kg/hr of endoplasmic reticulum vesicles (plus any necessary supplementary ribosomes) to sustain the overall cell production rate.

The vesicles from which the Golgi and ER organelles may be self-assembled can be manufactured using the same specialty cell mill employed in the manufacture of vesicular organelles (Section 3.3). The total manufacturing requirement for both membraneous organelles is $R_{MembraneousOrgs}$ = $R_{GolgiMill}$ + R_{ERMill} = 0.249 kg/hr to sustain the overall cell production rate of $R_{CellMill}$ ~ 1 kg/hr, which implies that the membraneous organelle manufacturing equipment has a volume of $V_{CellMillMO}$ = ($R_{MembraneousOrgs}$ / $R_{VesicularOrgs}$) $V_{CellMillVO}$ ~ **4.4 cm^3**, a mass of $m_{CellMillMO}$ = ($R_{MembraneousOrgs}$ / $R_{VesicularOrgs}$) $m_{CellMillVO}$ ~ **10.4 gm**, and a power draw of $P_{CellMillMO}$ = ($R_{MembraneousOrgs}$ / $R_{VesicularOrgs}$) $P_{CellMillVO}$ ~ **46 watts** for the manipulator arrays.

3.5 Cell Nucleus

One of the largest organelles in the human cell is the cell nucleus,[340] a vesicular organelle: "The main structures making up the nucleus are the nuclear envelope,[341] a double membrane that encloses the entire organelle and isolates its contents from the cellular cytoplasm (image, right); and the nuclear matrix (which includes the nuclear lamina[342]), a network within the nucleus that adds mechanical support (image, below), much like the cytoskeleton supports the cell as a whole. The nuclear lamina (composed mostly of lamin proteins)[343] forms an organized meshwork on the internal face of the envelope, while less organized support is provided on the cytosolic face of the envelope.[344] Both systems provide structural support for the nuclear envelope and anchoring sites for chromosomes and

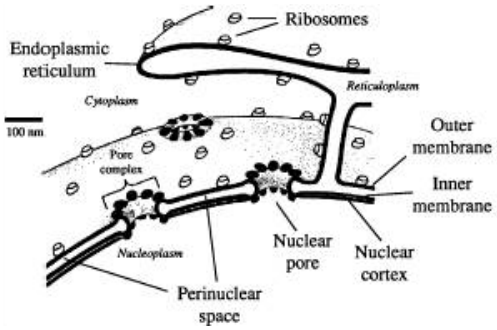

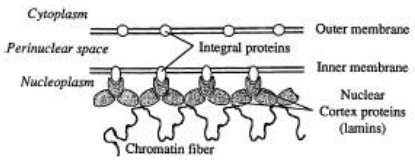

[339] Freitas RA Jr., Nanomedicine, Volume I: Basic Capabilities, Landes Bioscience, Georgetown, TX, 1999, Table 8.17, "Approximate Quantification of the Components of a Typical 20-μm Human Tissue Cell"; http://www.nanomedicine.com/NMI/Tables/8.17.jpg.

[340] https://en.wikipedia.org/wiki/Cell_nucleus.
[341] https://en.wikipedia.org/wiki/Nuclear_envelope.
[342] https://en.wikipedia.org/wiki/Nuclear_lamina.
[343] https://en.wikipedia.org/wiki/Lamin.

[344] Alberts B, Johnson A, Lewis J, Raff M, Roberts K, Walter P, eds. Chapter 4. Molecular Biology of the Cell, 4th edition, Garland Science, 2002, pp. 191-234; https://www.ncbi.nlm.nih.gov/books/NBK26842/.

nuclear pores. The contents of the nucleus are held in the nucleoplasm similar to the cytoplasm in the rest of the cell. The fluid component of this is termed the nucleosol, similar to the cytosol in the cytoplasm. Although the interior of the nucleus does not contain any membrane-bound subcompartments, its contents are not uniform, and a number of nuclear bodies exist, made up of unique proteins, RNA molecules, and particular parts of the chromosomes."

The average nucleus of a "typical" $V_{cell} \sim 8000\ \mu m^3$ tissue cell might be ~8 μm in spherical[345] diameter with a typical volume of $V_{nucleus} \sim 2.68 \times 10^{-16}\ m^3$ and mass of $m_{nucleus} = 2.9 \times 10^{-13}$ kg.[346] While a few human cells are multinucleate (e.g., skeletal muscle cells[347] and osteoclasts[348]), most cells have just one nucleus representing $f_{nucleus} \sim V_{nucleus} / V_{cell} \sim 3.4\%$ of cell volume, so a cell mill manufacturing $R_{CellMill} \sim 1$ kg/hr of cells must assemble $R_{NuclMill} \sim f_{nucleus}\ R_{CellMill} \sim 0.034$ kg/hr of cell nucleus mass to sustain the overall cell production rate.

A 9-step nanorobotically-assisted positional assembly of a cell nucleus might proceed as follows:

(1) **Build outer membrane.** Manufacture a concave hemispherical lipid bilayer and insert the appropriate membrane proteins to create the outer membrane, in the same manner as previously described (Section 3.3(A)-(B)) using a concave mould.

(2) **Build inner membrane.** Manufacture a convex hemispherical lipid bilayer and insert the appropriate membrane proteins to create the inner membrane, in the same manner as previously described (Section 3.3(A)-(B)) but using a convex mould, and including all integral proteins that will create the perinuclear space when the two membranes are joined.

(3) **Combine inner and outer membranes.** Press the convex hemispherical membrane onto the concave hemispherical membrane, bonding the two membranes via the integral proteins and forming the perinuclear space.

(4) **Install nuclear pores.** Insert nuclear pore complexes[349] through both membranes in an appropriate number density, which may range from 3-4 pores/μm^2 in some white cells up to 50 pores/μm^2 in oocytes,[350] though a "typical" 20 μm tissue cell may have ~3000 pores in the ~200

---

[345] The nucleus of polymorphonuclear leukocytes is not spherical and normally has three lobes; https://en.wikipedia.org/wiki/Granulocyte.

[346] Freitas RA Jr., Nanomedicine, Volume I: Basic Capabilities, Landes Bioscience, Georgetown, TX, 1999, Table 8.17, "Approximate Quantification of the Components of a Typical 20-μm Human Tissue Cell"; http://www.nanomedicine.com/NMI/Tables/8.17.jpg.

[347] https://en.wikipedia.org/wiki/Skeletal_muscle.
[348] https://en.wikipedia.org/wiki/Osteoclast#Structure.
[349] https://en.wikipedia.org/wiki/Nuclear_pore.

[350] Becker WM, Deamer DW. The World of the Cell, Second Edition, Benjamin/Cummings Publishing Company, Redwood City CA, 1991; https://www.amazon.com/dp/0805308709/.

μm^2 nuclear surface at a mean density of ~15 pores/μm^2.[351] The human nuclear pore complex is a 1.84 x 10^{-19} kg (110 MDa) truncated conical structure ~100 nm wide (image, right)[352] comprised of ~456 individual protein molecules of 34 different types,[353] and can be assembled in the same manner as the macromolecular organelles (Section 3.2), initially omitting the cytoplasmic filaments (Section 4.1(4)) which may be added later, prior to release of the finished nucleus.

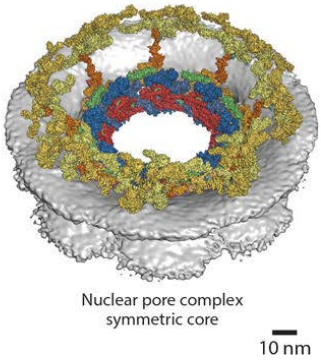

(5) **Install nuclear cortex.** To the integral proteins previously installed in the inner membrane,[354] attach on the nucleosolic face a 30-100 nm thick fibrillar network composed of lamins and nuclear lamin-associated membrane proteins[355] that can be manufactured in the same manner as previously described (Section 2.2.3).

(6) **Install chromosomes.** Attach chromatin molecules (Section 3.2(6)) to the nuclear cortex using nanorobotic manipulators analogous to those previously described for rapid chromosome sequencing (Section 2.2.1.2). (Chromatin molecules have been directly manipulated inside cells using optical and magnetic tweezers,[356] long before the advent of nanorobotics.)

(7) **Establish the nucleolus.** Future research should verify the presumption that when the newly manufactured cell is metabolically activated (Section 4.2), the previously-installed chromatin will spontaneously self-arrange to form the nucleolus,[357] the

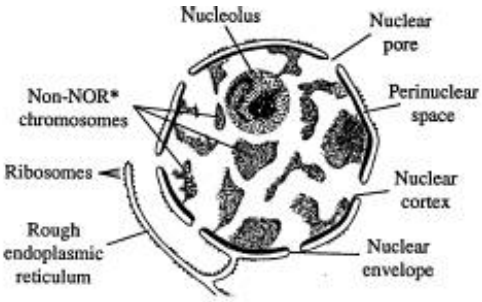

---

[351] Pokrywka N, Goldfarb D, Zillmann M, DeSilva A. The Transport of Macromolecules Across the Nuclear Envelope. In: Bittar EE, Bittar N, eds., Cellular Organelles, JAI Press, Greenwich CT, 1995, pp. 19-54; https://www.amazon.com/dp/044454657X/.

[352] Lin DH, Hoelz A. The Structure of the Nuclear Pore Complex (An Update). Annu Rev Biochem. 2019 Jun 20;88:725-783; https://www.ncbi.nlm.nih.gov/pmc/articles/pmid/30883195/.

[353] Lin DH, Stuwe T, Schilbach S, *et al*. Architecture of the symmetric core of the nuclear pore. Science. 2016 Apr 15;352(6283):aaf1015; https://www.ncbi.nlm.nih.gov/pmc/articles/pmid/27081075/.

[354] https://en.wikipedia.org/wiki/Inner_nuclear_membrane_protein.
[355] https://en.wikipedia.org/wiki/Nuclear_lamina#Structure_and_composition.

[356] Kanger JS, Subramaniam V, van Driel R. Intracellular manipulation of chromatin using magnetic nanoparticles. Chromosome Res. 2008;16(3):511-22; https://www.researchgate.net/profile/Vinod_Subramaniam/publication/5392507_Intracellular_manipulation_of_chromatin_using_magnetic_nanoparticles/links/00b7d52e03fa9b3e22000000.pdf. Hong J, Purwar P, Cha M, Lee J. Spatial control of chromosomal location in a live cell with functionalized magnetic particles. Nanoscale. 2015 Dec 7;7(45):19110-7; http://www.ncbi.nlm.nih.gov/pubmed/26524004.

[357] https://en.wikipedia.org/wiki/Nucleolus.

primary site of ribosome biogenesis[358] in the cell. The nucleolus is composed of proteins, DNA, and RNA and forms around specific chromosomal regions called nucleolar organizing regions (NOR).[359] Human NORs are located on the short arms of the acrocentric chromosomes 13, 14, 15, 21 and 22, in the genes RNR1, RNR2, RNR3, RNR4, and RNR5, respectively, that code for ribosomal RNA.[360] Activating the nucleolus may require the prepositioning of RNA polymerase I,[361] RNA polymerase III,[362] and small nucleolar RNAs[363] in the fibrillar center (FC), the protein fibrillarin[364] in the dense fibrillar component (DFC), and the protein nucleophosmin[365] in the granular component (GC) of the nucleolus. The nucleolus additionally enables "nucleolar detention" of a number of post-translational regulatory proteins[366] which future research may determine must also be initially provided.

(8) **Emplace nuclear bodies.** Besides the nucleolus, the cell nucleus normally contains a number of small nuclear bodies including 1-5 compact structures 0.1-2 μm in size called Cajal bodies,[367] ~5 μm polymorphic interphase karyosomal association (PIKA) domains,[368] PSE-binding transcription factor (PTF) domains,[369] 25-50 nuclear speckles 20-25 nm in size,[370] 10-30

---

[358] https://en.wikipedia.org/wiki/Ribosome_biogenesis#Eukaryotes.
[359] https://en.wikipedia.org/wiki/Nucleolus_organizer_region.

[360] McStay B. Nucleolar organizer regions: genomic 'dark matter' requiring illumination. Genes Dev. 2016 Jul 15;30(14):1598-1610; https://www.ncbi.nlm.nih.gov/pmc/articles/pmid/27474438/.

[361] https://en.wikipedia.org/wiki/RNA_polymerase_I.
[362] https://en.wikipedia.org/wiki/RNA_polymerase_III.
[363] https://en.wikipedia.org/wiki/Small_nucleolar_RNA.
[364] https://en.wikipedia.org/wiki/Fibrillarin.
[365] https://en.wikipedia.org/wiki/NPM1.

[366] Audas TE, Jacob MD, Lee S. Immobilization of proteins in the nucleolus by ribosomal intergenic spacer noncoding RNA. Mol Cell. 2012 Jan 27;45(2):147-157; https://www.cell.com/molecular-cell/pdf/S1097-2765(11)00954-3.pdf.

[367] https://en.wikipedia.org/wiki/Cajal_body.

[368] Saunders WS, Cooke CA, Earnshaw WC. Compartmentalization within the nucleus: discovery of a novel subnuclear region. J Cell Biol. 1991 Nov;115(4):919-931; https://www.ncbi.nlm.nih.gov/pmc/articles/pmid/1955462/.

[369] Pombo A, Cuello P, Schul W, Yoon JB, Roeder RG, Cook PR, Murphy S. Regional and temporal specialization in the nucleus: a transcriptionally-active nuclear domain rich in PTF, Oct1 and PIKA antigens associates with specific chromosomes early in the cell cycle. EMBO J. 1998 Mar 16;17(6):1768-78; https://www.ncbi.nlm.nih.gov/pmc/articles/pmid/9501098/.

[370] Lamond AI, Spector DL. Nuclear speckles: a model for nuclear organelles. Nat Rev Mol Cell Biol. 2003 Aug;4(8):605-612; http://spectorlab.labsites.cshl.edu/wp-content/uploads/sites/14/2014/06/LamondSpector2003.pdf. See also: https://www.uniprot.org/locations/SL-0186 and https://en.wikipedia.org/wiki/Cell_nucleus#Splicing_speckles.

paraspeckles 0.2-1 μm in size,[371] and perichromatin fibrils.[372] These proteins can be manufactured in the same manner as previously described (Section 2.2.3) and installed in reasonable locations using a nanorobotic manipulator arm, if future research confirms that their installation in the nucleus of some or all cell types is essential for full cell viability and functionality.

(9) **Join and Release.** The two equal hemispheres representing opposite halves of the nucleus are pressed together face to face, causing them to seamlessly join because of the inherent miscibility of the lipid bilayers at the equatorial perimeter of each face (Section 3.3(D)). After any further post-processing is completed,[373] the finished cell nucleus can be released from the moulds by switching the presentation semaphores embedded in the mould surfaces from hydrophilic to hydrophobic.

The total manufacturing requirement for building a cell nucleus as a vesicular organelle is $R_{NuclMill} \sim 0.034$ kg/hr to sustain the overall cell production rate of $R_{CellMill} \sim 1$ kg/hr. Taking the same productivity metrics of $\psi_1 \sim 7.4 \times 10^{-17}$ kg/array-sec, $\psi_2 \sim 5.3 \times 10^{-15}$ kg/array-sec, and $\psi_3 \sim 3.5 \times 10^{-17}$ kg/array-sec as estimated for the other vesicular organelles (Section 3.3), we require $N_{arraysCN} = (R_{CellMill} / \psi_1) + (R_{CellMill} / \psi_2) + (R_{CellMill} / \psi_3) \sim 4 \times 10^{11}$ arrays to deliver enough cell nucleus mass to satisfy the required production rate of $R_{CellMill} \sim 1$ kg/hr of cells. These arrays have an estimated total volume of $V_{arraysCN} \sim n_{maniparray} V_{manip} N_{arraysCN} \sim 0.063$ cm^3, taking $n_{maniparray} = 157$ manipulators/array and $V_{manip} = 10^6$ nm^3/manipulator as before.

If the solid volume of the mould structures, including all interior mechanisms, is the same multiple $\alpha_{mouldCN} \sim 3.8$ of the volume of the organelle that is being manufactured as before (Section 3.3), then a cubical mould enclosing a spherical cell nucleus of diameter $d_{organelleCN} = 8$ μm would have a cubical edge length of $L_{cubeCN} = (\pi \alpha_{mouldCN} / 6)^{1/3} d_{organelleCN} \sim 10$ μm. Since each array services one hemispherical mould having a solid volume of $0.5 L_{cubeCN}^3 \sim 500$ μm^3, and since two separate moulds are required (i.e., one concave and one convex), the total solid volume of all moulds is $V_{NuclMoulds} = L_{cubeCN}^3 N_{arraysCN} \sim 400$ cm^3. Assuming a manipulator density of $\rho_{manip} \sim 100$ kg/m^3 (i.e., $\sim 10^{-19}$ kg / 10^6 nm^3) and a mould density approximating 10% of diamond at $\rho_{mould} \sim 350$ kg/m^3, then the cell nucleus manufacturing equipment has a volume of $V_{CellMillCN} = V_{arraysCN} + V_{NuclMoulds} \sim$ **400 cm^3**, a mass of $m_{CellMillCN} = \rho_{manip} V_{arraysCN} + \rho_{mould} V_{NuclMoulds} \sim$ **140 gm**, and a power draw of $P_{CellMillCN} = n_{maniparray} N_{arraysCN} P_{manip} \sim$ **6 watts** for the manipulator arrays.

---

[371] https://en.wikipedia.org/wiki/Paraspeckle.

[372] Matera AG, Terns RM, Terns MP. Non-coding RNAs: lessons from the small nuclear and small nucleolar RNAs. Nat Rev Mol Cell Biol. 2007 Mar;8(3):209-220; https://pubmed.ncbi.nlm.nih.gov/17318225/.

[373] An example might include the attachment of cytoplasmic filaments on the cytosolic face of the nuclear pore complex. A list of all essential post-processing steps should be compiled, and the nanorobotic means for accomplishing all post-processing steps elucidated, in future research.

4. Cell Assembly Module

The foundational concept of a cell mill is the hypothesis that the components of a cell are essentially modular, hence can be manufactured separately and later assembled into a complete working biological cell.[374] This "modularity" hypothesis seems plausible and has received at least some experimental support, but should be tested further in future research that attempts to reassemble living cells from even larger numbers of component parts than have been achieved to date (see below). Fully bottom-up methods of cell assembly from basic parts *in vitro* have been discussed for more than a decade by practitioners of the emerging field of synthetic biology[375] (though mostly in the context of creating a viable "minimal cell" for research purposes),[376] but all of these methods seem to rely upon the conventional principles of self-assembly which have inherent limitations that will no longer apply if the principles of positionally-controlled assembly are employed, as described below.

The exemplar cell mill would be a cytomanufacturing system crudely analogous to 3D printing[377] but with full vertical integration. As long ago as 1970, an *Amoeba proteus* single-cell organism was physically reassembled from its major subcellular components – nucleus, cytoplasm, and cell

---

[374] Jeon KW, Lorch IJ, Danielli JF. Reassembly of living cells from dissociated components. Science. 1970 Mar 20;167(3925):1626-7; http://science.sciencemag.org/content/sci/167/3925/1626.full.pdf.

[375] Deamer D. A giant step towards artificial life? Trends Biotechnol. 2005 Jul;23(7):336-8; https://citeseerx.ist.psu.edu/document?repid=rep1&type=pdf&doi=adf5e4e794ecf5c7498921cc977fc03d9792a923.

[376] Forster AC, Church GM: Towards synthesis of a minimal cell. Mol Syst Biol 2006, 2:45; https://www.embopress.org/doi/pdf/10.1038/msb4100090. Liu AP, Fletcher DA. Biology under construction: *in vitro* reconstitution of cellular function. Nat Rev Mol Cell Biol. 2009 Sep;10(9):644-650; https://www.ncbi.nlm.nih.gov/pmc/articles/pmid/19672276/. Jewett MC, Forster AC: Update on designing and building minimal cells. Curr Opin Biotechnol 2010, 21:697-703; https://www.ncbi.nlm.nih.gov/pmc/articles/PMC2952674/. Caschera F, Noireaux V. Integration of biological parts toward the synthesis of a minimal cell. Curr Opin Chem Biol. 2014 Oct;22:85-91; http://www.noireauxlab.org/html%20pages/docs%20website/publications/Caschera%20and%20Noireaux%20-%202014%20COCB.pdf. Göpfrich K, Platzman I, Spatz JP. Mastering Complexity: Towards Bottom-up Construction of Multifunctional Eukaryotic Synthetic Cells. Trends Biotechnol. 2018 Sep;36(9):938-951; https://www.ncbi.nlm.nih.gov/pmc/articles/PMC6100601/. Schwille P, *et al*. MaxSynBio: Avenues Towards Creating Cells from the Bottom Up. Angew Chem Int Ed Engl. 2018;57(41):13382-13392; http://www.mpikg.mpg.de/rl/P/archive/445onl.pdf. Ganzinger KA, Schwille P. More from less - bottom-up reconstitution of cell biology. J Cell Sci. 2019 Feb 4;132(4):jcs227488; https://jcs.biologists.org/content/joces/132/4/jcs227488.full.pdf. Liu AP. The rise of bottom-up synthetic biology and cell-free biology. Phys Biol. 2019 May 7;16(4):040201; https://www.ncbi.nlm.nih.gov/pmc/articles/pmid/31018188/.

[377] Mandrycky C, Wang Z, Kim K, Kim DH. 3D bioprinting for engineering complex tissues. Biotechnol Adv. 2016 Jul-Aug;34(4):422-434; https://www.ncbi.nlm.nih.gov/pmc/articles/PMC4879088/. Lam EHY, Yu F, Zhu S, Wang Z. 3D Bioprinting for Next-Generation Personalized Medicine. Int J Mol Sci. 2023 Mar 28;24(7):6357; https://www.ncbi.nlm.nih.gov/pmc/articles/PMC10094501/.

membrane – taken from three different cells,[378] demonstrating the physical capability of manually assembling living cells from more primitive parts using micropipette-level technology. A viable 5-component cell reassembly was demonstrated four years later by Morowitz,[379] who reported that "cell fractions from four different animals can be injected into the eviscerated ghost of a fifth amoeba, and a living functioning organism results." Mammalian cells have also been assembled from separate nuclear and cytoplasmic parts,[380] and intracellular organelles have been individually manipulated both directly[381] and nanosurgically,[382] a key capability that will be needed to assemble whole cells.

Early cell mills might make limited use of more traditional biotechnologies such as cloning, stem cells, tissue engineering, animal cell reactors,[383] cell-like bioreactors,[384] transdifferentiation[385] and

---

[378] Jeon KW, Lorch IJ, Danielli JF. Reassembly of living cells from dissociated components. Science. 1970 Mar 20;167(3925):1626-7; http://science.sciencemag.org/content/sci/167/3925/1626.full.pdf.

[379] Morowitz HJ. Manufacturing a living organism. Hospital Practice 1974 Nov; 9(11):210-215; https://www.tandfonline.com/doi/abs/10.1080/21548331.1974.11706459.

[380] Veomett G, Prescott DM, Shay J, Porter KR. Reconstruction of mammalian cells from nuclear and cytoplasmic components separated by treatment with cytochalasin B. Proc Natl Acad Sci U S A. 1974 May;71(5):1999-2002; http://www.ncbi.nlm.nih.gov/pmc/articles/PMC388372/pdf/pnas00058-0421.pdf. Veomett G, Prescott DM. Reconstruction of cultured mammalian cells from nuclear and cytoplasmic parts. Methods Cell Biol 1976;13:7-14; http://www.ncbi.nlm.nih.gov/pubmed/1263853.

[381] Weber G, Greulich KO. Manipulation of cells, organelles, and genomes by laser microbeam and optical trap. Int Rev Cytol. 1992;133:1-41; http://www.ncbi.nlm.nih.gov/pubmed/1577585. Felgner H, Grolig F, Müller O, Schliwa M. *In vivo* manipulation of internal cell organelles. Methods Cell Biol. 1998;55:195-203; http://www.ncbi.nlm.nih.gov/pubmed/9352518. Bayoudh S, Mehta M, Rubinsztein-Dunlop H, Heckenberg NR, Critchley C. Micromanipulation of chloroplasts using optical tweezers. J Microsc. 2001 Aug;203(Pt 2):214-22; http://onlinelibrary.wiley.com/doi/10.1046/j.1365-2818.2001.00843.x/full. Sacconi L, Tolić-Nørrelykke IM, Stringari C, Antolini R, Pavone FS. Optical micromanipulations inside yeast cells. Appl Opt. 2005 Apr 10;44(11):2001-7; http://www.researchgate.net/profile/Francesco_Pavone/publication/7902546_Optical_micromanipulations_inside_yeast_cells/links/0c960520f4d61165f0000000.pdf. Maghelli N, Tolić-Nørrelykke IM. Optical trapping and laser ablation of microtubules in fission yeast. Methods Cell Biol. 2010;97:173-83; https://publications.mpi-cbg.de/Maghelli_2010_5020.pdf.

[382] Freitas RA Jr. "Chapter 23. Comprehensive Nanorobotic Control of Human Morbidity and Aging," in Gregory M. Fahy, Michael D. West, L. Stephen Coles, and Steven B. Harris, eds, The Future of Aging: Pathways to Human Life Extension, Springer, New York, 2010, pp. 685-805; Section 6.4.2, "Cell nanosurgery"; http://www.nanomedicine.com/Papers/Aging.pdf.

[383] Bliem R, Konopitzky K, Katinger H. Industrial animal cell reactor systems: aspects of selection and evaluation. Adv Biochem Eng Biotechnol 1991; 44:1-26; http://www.ncbi.nlm.nih.gov/pubmed/1781316. Nelson KL, Geyer S. Bioreactor and process design for large-scale mammalian cell culture manufacturing. Bioprocess Technol 1991; 13:112-143; http://www.ncbi.nlm.nih.gov/pubmed/1367130.

[384] Noireaux V, Libchaber A. A vesicle bioreactor as a step toward an artificial cell assembly. Proc Natl Acad Sci U S A. 2004 Dec 21;101(51):17669-74; http://www.ncbi.nlm.nih.gov/pmc/articles/PMC539773/.

nuclear reprogramming.[386] Artificial lipid vesicles have been prepared containing polymerase enzymes that can synthesize RNA from externally added substrates, and the entire translation apparatus, including ribosomes, has been captured in vesicles.[387] Relatively primitive methods have been demonstrated for the isolation and manipulation of individual organelles,[388] and whole cells can be inspected, sorted,[389] and transported by optical tweezers,[390] microgrippers,[391] or other conventional means[392] to a collection area for export and further use.

Full nanorobotic assembly of biological cells will require one or more micromanipulators that can reach across at least ~20 μm distances spanning the width of the "typical" tissue cell under construction, performing molecular and organelle pick-and-place operations while physically accessing the supply of premanufactured organelles and other needed cell building materials. For scaling purposes, if the size of the previously-described nanomanipulator (Section 3.3(A)) was increased 100-fold in all three dimensions from 100 nm to x_{micro} = 10 μm in length and from 30 nm to 3 μm in cylindrical diameter, the resulting micromanipulator would have a 10^6-fold larger

---

[385] Collas P, Håkelien AM. Teaching cells new tricks. Trends Biotechnol 2003 Aug; 21:354-361; http://www.ncbi.nlm.nih.gov/pubmed/12902172.

[386] Tada T. Nuclear reprogramming: an overview. Methods Mol Biol 2006; 348:227-236; http://www.ncbi.nlm.nih.gov/pubmed/16988383.

[387] Deamer D. A giant step towards artificial life? Trends Biotechnol. 2005 Jul;23(7):336-8; http://www.pai.utexas.edu/faculty/isaxena/BIO320/A%20giant%20step%20towards%20artificial%20life%20-%202005.pdf.

[388] Olson KJ, Ahmadzadeh H, Arriaga EA. Within the cell: analytical techniques for subcellular analysis. Anal Bioanal Chem. 2005 Jun;382(4):906-17; http://www.ncbi.nlm.nih.gov/pubmed/15928950. Satori CP, Kostal V, Arriaga EA. Review on recent advances in the analysis of isolated organelles. Anal Chim Acta. 2012 Nov 13;753:8-18; http://www.ncbi.nlm.nih.gov/pmc/articles/PMC3484375/.

[389] Grover SC, Skirtach AG, Gauthier RC, Grover CP. Automated single-cell sorting system based on optical trapping. J Biomed Opt. 2001 Jan;6(1):14-22; http://www.ncbi.nlm.nih.gov/pubmed/11178576.

[390] Zhang H, Liu KK. Optical tweezers for single cells. J R Soc Interface. 2008 Jul 6;5(24):671-90; http://www.ncbi.nlm.nih.gov/pmc/articles/PMC2408388/.

[391] Kim K, Liu X, Zhang Y, Sun Y. Nanonewton force-controlled manipulation of biological cells using a monolithic MEMS microgripper with two-axis force feedback. J Micromech Microeng 2008 Apr 1;18(5):055013; http://amnl.mie.utoronto.ca/data/J35.pdf. Leong TG, Randall CL, Benson BR, Bassik N, Stern GM, Gracias DH. Tetherless thermobiochemically actuated microgrippers. Proc Natl Acad Sci U S A. 2009 Jan 20;106(3):703-8; http://www.ncbi.nlm.nih.gov/pmc/articles/PMC2630075/. Yin C, Wei F, Zhan Z, Zheng J, Yao L, Yang W, Li M. Untethered microgripper-the dexterous hand at microscale. Biomed Microdevices. 2019 Aug 15;21(4):82; https://pubmed.ncbi.nlm.nih.gov/31418070/.

[392] Gach PC, Wang Y, Phillips C, Sims CE, Allbritton NL. Isolation and manipulation of living adherent cells by micromolded magnetic rafts. Biomicrofluidics. 2011 Sep;5(3):32002-3200212; http://www.ncbi.nlm.nih.gov/pmc/articles/PMC3194786/. Liu D, et al. All-Purpose Magnetic Micromanipulation System With Two Modes: Chopstick-Like Two-Finger Microhand and Hydrodynamic Tweezer. IEEE/ASME Trans Mechatronics 2022 Jun;27(3):1582-1593; https://ieeexplore.ieee.org/abstract/document/9460810.

work volume of $V_{micromanip}$ = 1000 μm^3, along with a central transport channel ~1 μm in diameter which is wide enough to accommodate most but not all organelles. Maximum tip velocity would remain the same at v_{manip} ~ 1 cm/sec (Section 3.3(A)). An arrangement of n_{micro} = 8 such manipulators arranged as two opposed sets of 2 x 2 manipulators would provide access to a 20 μm x 20 μm area from each side, roughly fulfilling the requirement of full access to a 20 μm x 20 μm x 20 μm tissue cell space.[393] Power density scales inversely linearly with size,[394] so the ~10^8 W/m^3 power density of the nanomanipulator (Section 3.3(A)) reduces to ~10^6 W/m^3 for the micromanipulator, giving a power dissipation estimate of $P_{micromanip}$ ~ 1000 pW. (Note that since strength scales as the square of the linear dimension,[395] the posited micromanipulator should be able to apply 10^6 times more force than the original nanomanipulator device if necessary.)

A description of one possible cell assembly process in Section 4.1 is followed by a discussion of cell metabolic control during fabrication, storage, and installation in Section 4.2, cell mill system scaling in Section 4.3, the computational requirements for operating a cell mill in Section 4.4, and finally a comparison of the cell-manufacturing productivity of cell mills as compared to representative biological systems in Section 4.5.

4.1 Cell Assembly Process

Presuming access to a sufficient inventory of premanufactured generic and personalized biomolecules (Section 2), macromolecular organelles (Section 3.2), vesicular organelles (Section 3.3) including the nucleus (Section 3.5), and membraneous organelles (Section 3.4), the following is a general description of how the final assembly of a tissue cell might proceed:

(1) **Build plasma membrane.** Build a lipid bilayer plasma membrane on the inside surfaces of two 20 μm hemispheric moulds in the manner previously described (Section 3.3(A)).

(2) **Insert membrane proteins.** Insert integral proteins into the plasma membrane, including cytoskeletal components on the cytosolic wall, in an appropriate surface number density in the manner previously described (Section 3.3(B)).

---

[393] A few cells may require a somewhat larger assembly space and somewhat longer manipulators. For example, the ovum is the largest compact cell in the human body with a diameter of ~100 μm.[*] Longer cells could be transported as segments capped with temporary sealed interfaces that can be removed at the time of final *in situ* assembly or installation.

[*] Alberts B, Johnson A, Lewis J, Raff M, Roberts K, Walter P, eds. Molecular Biology of the Cell, 4th edition, Garland Science, New York, 2002; https://www.ncbi.nlm.nih.gov/books/NBK26842/.

[394] Drexler KE. Nanosystems: Molecular Machinery, Manufacturing, and Computation, John Wiley & Sons, New York, 1992, Table 2.1; https://www.amazon.com/dp/0471575186/.

[395] Drexler KE. Nanosystems: Molecular Machinery, Manufacturing, and Computation, John Wiley & Sons, New York, 1992, Section 2.3.2 and Table 2.1; https://www.amazon.com/dp/0471575186/.

Table 5. Number of organelles to be installed in a representative 8000 μm^3 tissue cell

Organelle	Approx. # per Cell	Section Reference	Organelle	Approx. # per Cell	Section Reference
Proteasomes	10^7	3.2(1)	Lysosomes	300	3.3(3)
Ribosomes	10^7	3.2(2)	Peroxisomes	300	3.3(4)
Glycosomes	10^5	3.2(3)	Mitochondria	1000	3.3(5)
Vaults	3000	3.2(4)	Golgi apparatus	1	3.4(1)
Centrioles	2	3.2(5)	Endo. reticulum	1	3.4(2)
Golgi vesicles	200,000	3.3(1)	Nucleus	1	3.5
Secretory vesicles	50,000	3.3(2)			
Lipid droplets	100	3.3(2)	***Total***	***20,354,705***	

(3) **Assemble cell corpus.** Micromanipulators are employed to emplace organelles in appropriate locations and numbers (**Table 5**) in the growing corpus of the cell, in each of the two hemispheres. Placement of the manufactured nucleus (Section 3.5) will be assigned to one of the two hemispheres, which will also determine the location of the attached membraneous endoplasmic reticulum (Section 3.4(2)). Supportive cytoskeletal elements (Section 4.1(4)) may be employed during assembly to provide positional and structural fixity of the organelles, and organelle installation should be closely coordinated with cytoskeletal emplacement (see Section 4.1(4)). Determination of the optimum assembly sequence for all components in each hemisphere is a suitable topic for future research.

Table 6. Approximate quantification of cytoskeletal components[396]

Cytoskeletal Fiber Component	Fiber Thickness (nm)	Total Volume per Cell (μm^3)	Total Surface Area per Cell (μm^2)	Total Length per Cell (m)
Microfilaments	5-7	360	200,000	10
Superfine filaments	2-4	45	40,000	5
Intermediate filaments	8-12	100	30,000	1
Microtubules	25	370	10,000	0.6
Thick filaments	15	< 9	2,000	0.04
TOTALS		***884***	***282,000***	***17***

[396] Freitas RA Jr., Nanomedicine, Volume I: Basic Capabilities, Landes Bioscience, Georgetown, TX, 1999, Table 8.17, "Approximate Quantification of the Components of a Typical 20-μm Human Tissue Cell"; http://www.nanomedicine.com/NMI/Tables/8.17.jpg; and Section 8.5.3.11, "Cytoskeleton", http://www.nanomedicine.com/NMI/8.5.3.11.htm

(4) **Build out cytoskeleton.** Complete the installation of all remaining essential cytoskeletal features, which may include ~17 meters of cytoskeletal fibers and filaments inside a "typical" tissue cell representing ~11% of total cell volume (**Table 6**). (That's about 8 times the ~2-meter length[397] of all DNA strands in the nucleus if fully stretched out.) Cytoskeleton elements have been directly manipulated inside cells using conventional optical and magnetic tweezers,[398] but the availability of much stronger micromanipulators within the Cell Assembly Module that can reach into the growing cytoplasm and precisely position cytoskeletal components will provide much faster and more efficient assembly operations. The dynamic nature of some cytoskeletal components[399] under physiological conditions may necessitate special procedures for cytoskeleton build-out that should be investigated in future research, but the molecules in each case can be fabricated in Protein Mills (Section 2.2.3).

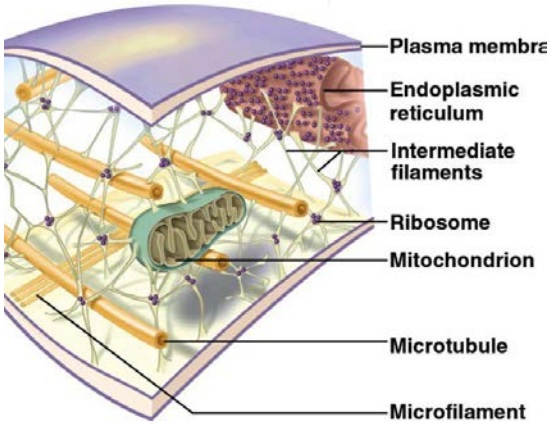

Cytoskeletal emplacement should be closely coordinated with organelle installation (see Section 4.1(3)). For example, α- and β-spectrin[400] filaments joined to actin[401] polymer **microfilaments**[402] should first be installed on the cytosolic surface of the cell plasma membrane before the rest of the cytoplasm is laid down (Section 4.1(2)), possibly with some assistance from self-assembly.[403] Actin microfilaments are 5-7 nm in diameter and may run out to several microns in length. They represent ~59% of the total cytoskeletal length and 43% of total cytoskeletal volume (**Table 6**)

---

[397] McGraw-Hill Encyclopedia of Science and Technology, McGraw-Hill, NY, 2012. Ashworth H. How long is your DNA? Science Focus, 2020; https://www.sciencefocus.com/the-human-body/how-long-is-your-dna/.

[398] Felgner H, Frank R, Schliwa M. Flexural rigidity of microtubules measured with the use of optical tweezers. J Cell Sci. 1996 Feb;109 (Pt 2):509-16; http://jcs.biologists.org/content/joces/109/2/509.full.pdf. de Vries AH, Krenn BE, van Driel R, Kanger JS. Micro magnetic tweezers for nanomanipulation inside live cells. Biophys J. 2005 Mar;88(3):2137-44; http://www.ncbi.nlm.nih.gov/pmc/articles/PMC1305265/.

[399] e.g., https://en.wikipedia.org/wiki/Microtubule#Microtubule_dynamics.
[400] https://en.wikipedia.org/wiki/Spectrin.
[401] https://en.wikipedia.org/wiki/Actin.
[402] https://en.wikipedia.org/wiki/Microfilament.

[403] Liu AP, Richmond DL, Maibaum L, Pronk S, Geissler PL, Fletcher DA. Membrane-induced bundling of actin filaments. Nat Phys. 2008 Aug 31;4:789-793; https://www.ncbi.nlm.nih.gov/pmc/articles/PMC2739388/. Carvalho K, Tsai FC, Lees E, Voituriez R, Koenderink GH, Sykes C. Cell-sized liposomes reveal how actomyosin cortical tension drives shape change. Proc Natl Acad Sci U S A. 2013 Oct 8;110(41):16456-61; https://www.ncbi.nlm.nih.gov/pmc/articles/PMC3799374/. Miyazaki M, Chiba M, Eguchi H, Ohki T, Ishiwata S. Cell-sized spherical confinement induces the spontaneous formation of contractile actomyosin rings *in vitro*. Nat Cell Biol. 2015 Apr;17(4):480-489; https://pubmed.ncbi.nlm.nih.gov/25799060/.

and are capable of self-assembly and disassembly in response to molecular cues via polymerization and depolymerization at a speed of 0.1-1 μm/sec.[404]

Microfilaments should be initially be installed sparingly, serving as large-scale tensile elements to maintain overall cellular structural integrity and creating a 3D tensegrity[405] structure in concert with much larger and more rigid **microtubules**[406] which should be laid down in a sparse framework at the same time to serve as compressive elements. Microtubules are 25 nm diameter cylinders up to 25 μm in length, representing 42% of total cytoskeleton volume but only ~4% of total cytoskeletal fiber length (**Table 6**). They can also self-assemble with a typical polymerization speed of ~0.06 μm/sec,[407] with the speed of polymerization strongly force-dependent[408] and biochemically controlled.[409] Most microtubules in living cells have a half-life of 5-10 minutes with a few lasting for hours,[410] but uncontrolled re- or de-polymerization will not be permitted within the Cell Assembly Module during cell construction where no GTP or ATP is available to energize polymerization activity. We must also emplace appropriate numbers of kinesin[411] and dynein[412] transport motor molecules that normally convey vesicles and granules at up to ~2 μm/sec through the cell on microtubule tracks. These motor molecules will be biologically inert during fabrication, storage, and installation because the ATP that powers them will not yet have been inserted into the cytoplasm (Section 4.2).

After a coarse 3D fiber network is in place (with very large gaps), organelles can be attached to the skeletal framework via **intermediate filaments**,[413] the most stable of the cytoskeletal elements as they are not subject to constant de-/re-polymerization. Intermediate filaments represent ~11% of skeletal volume and ~6% of total skeletal fiber length (**Table 6**). Once bound organelles are secured in their proper places, microfilaments and microtubules can be biochemically induced to self-assemble into the gaps via induced polymerization, filling out the

---

[404] Maniotis AJ, Chen CS, Ingber DE. Demonstration of mechanical connections between integrins, cytoskeletal filaments, and nucleoplasm that stabilize nuclear structure. Proc Natl Acad Sci U S A. 1997 Feb 4;94(3):849-54; https://www.ncbi.nlm.nih.gov/pmc/articles/PMC19602/.

[405] https://en.wikipedia.org/wiki/Tensegrity.
[406] https://en.wikipedia.org/wiki/Microtubule.

[407] Schulze E, Kirschner M. Microtubule dynamics in interphase cells. J Cell Biol. 1986 Mar;102(3):1020-31; https://core.ac.uk/download/pdf/186861731.pdf.

[408] Janson ME, de Dood ME, Dogterom M. Dynamic instability of microtubules is regulated by force. J Cell Biol. 2003 Jun 23;161(6):1029-1034; https://www.ncbi.nlm.nih.gov/pmc/articles/pmid/12821641/.

[409] Zwetsloot AJ, Tut G, Straube A. Measuring microtubule dynamics. Essays Biochem. 2018 Dec 7;62(6):725-735; https://www.ncbi.nlm.nih.gov/pmc/articles/PMC6281472/.

[410] Infante AS, Stein MS, Zhai Y, Borisy GG, Gundersen GG. Detyrosinated (Glu) microtubules are stabilized by an ATP-sensitive plus-end cap. J Cell Sci. 2000 Nov;113 (Pt 22):3907-3919; https://jcs.biologists.org/content/joces/113/22/3907.full.pdf.

[411] https://en.wikipedia.org/wiki/Kinesin.
[412] https://en.wikipedia.org/wiki/Dynein.
[413] https://en.wikipedia.org/wiki/Intermediate_filament.

bulk of the cytoskeleton network. For example, it has been demonstrated that a minimal system consisting of giant unilamellar vesicles and externally supplied microtubules and kinesin can produce membrane networks in the presence of ATP[414] and GTP[415] without the aid of other proteins.[416] Another example is the analogous GTPase enzyme dynamin,[417] which self-assembles into spiral tubules in the absence of GTP and disassembles with the addition of GTP.[418]

(5) **Join hemispheres.** After the cell corpus and cytoskeleton are fully assembled, the two equal hemispheres representing opposite halves of the manufactured cell are pressed together face to face, causing them to seamlessly join because of the inherent miscibility of the lipid bilayers at the equatorial perimeter of each face (Section 3.3(D)). Any necessary post-processing work[419] should also be completed during this stage.

(6) **Decorate and release.** Detach one external hemispheric mould by switching the presentation semaphores embedded in the mould surface from hydrophilic to hydrophobic, then decorate the exposed external face of the plasma membrane with glycocalyx[420] and any other required external structures. The hemispheric mould is then reattached and the same process is repeated with the other external hemispheric mould. Once both hemispheres are completed, any final biochemical modifications to the cell may be made (e.g., extracting or injecting biomolecules to bring the cell to any state of activation or metabolic activity desired; Section 4.2) after which the finished cell is released from the moulds either for storage or for activation and immediate use.

---

[414] https://en.wikipedia.org/wiki/Adenosine_triphosphate.
[415] https://en.wikipedia.org/wiki/Guanosine_triphosphate.

[416] Leduc C, Campàs O, Zeldovich KB, Roux A, Jolimaitre P, Bourel-Bonnet L, Goud B, Joanny JF, Bassereau P, Prost J. Cooperative extraction of membrane nanotubes by molecular motors. Proc Natl Acad Sci U S A. 2004 Dec 7;101(49):17096-101; https://www.ncbi.nlm.nih.gov/pmc/articles/PMC535380/.

[417] https://en.wikipedia.org/wiki/Dynamin.

[418] Pucadyil TJ, Schmid SL. Real-time visualization of dynamin-catalyzed membrane fission and vesicle release. Cell. 2008 Dec 26;135(7):1263-75; https://www.ncbi.nlm.nih.gov/pmc/articles/PMC2673235/.

[419] One example of such work is bonding cytoskeletal elements across the join plane between the two hemispheres, in whatever manner may be required, using membrane-inserted manipulators or nanorobots. It may also be desirable to insert sorting rotor* probes through the plasma membrane into the cytosol to extract or insert particular molecules of interest (Section 4.2). A list of all essential post-processing steps should be compiled, and the nanorobotic means for accomplishing all post-processing steps elucidated, in future research.
* Drexler KE. Nanosystems: Molecular Machinery, Manufacturing, and Computation, John Wiley & Sons, New York, 1992, Section 13.2.1(a) "Modulated receptors for selective transport: Basic concepts"; https://www.amazon.com/dp/0471575186/. Freitas RA Jr. Nanomedicine, Volume I: Basic Capabilities, Landes Bioscience, Georgetown, TX, 1999; Section 3.4.2, "Sorting Rotors"; http://www.nanomedicine.com/NMI/3.4.2.htm.

[420] https://en.wikipedia.org/wiki/Glycocalyx.

4.2 Cytometabolic Activity Management

All biological cells that are fabricated in a cell mill will initially be produced in a metabolically inactive state, aka. "comprehensive metabolic arrest".[421] This allows finished cells to be stored indefinitely in advance of need, without degradation or any requirement for continuous nutrient supply or waste management services. When fabricated cells are eventually removed from storage for immediate use, they will be injected with suitable biochemicals that are sufficient to initiate normal cell metabolism, bringing the cell to any state of activation or metabolic activity desired.

Chemical substances that can initiate, activate, assist or sustain biochemical activity are called "activating molecules". An initial enumeration of likely metabolically activating molecules was compiled as part of an analysis of metabolic inactivation previously published in 2022,[422] and most importantly includes molecular oxygen,[423] glucose and ATP,[424] and between 100-10,000 cell metabolite molecular species having cytosolic concentrations of 10^{-1}-10^{-7} molecules/nm^3.[425] (The exact list of relevant metabolites must be determined by future research.) Once these "activating molecules" are released into the cell, biochemical activity will immediately begin; but until these key molecules are injected, biochemical activity remains suspended.

4.3 Cell Mill System Scaling

The required cell mass production rate of $R_{CellMill} \sim 1$ kg/hr of cells equates to a manufacturing rate of $N_{CellMill} = R_{CellMill} / m_{cell} = 1.17 \times 10^{11}$ cells/hr = 3.26×10^7 cells/sec for the Cell Assembly Module, taking cell mass $m_{cell} = \rho_{cell} V_{cell} = 8.51 \times 10^{-12}$ kg/cell, cell density $\rho_{cell} = 1064$ kg/m^3, and cell volume $V_{cell} = 8000$ μm^3.

---

[421] Freitas RA Jr. Cryostasis Revival: The Recovery of Cryonics Patients through Nanomedicine. Alcor Life Extension Foundation, Scottsdale AZ, 2022; Section 4.10, "Molecular Extraction"; https://www.alcor.org/cryostasis-revival/.

[422] Freitas RA Jr. Cryostasis Revival: The Recovery of Cryonics Patients through Nanomedicine. Alcor Life Extension Foundation, Scottsdale AZ, 2022; Section 4.10.1, "Targeted Extraction"; https://www.alcor.org/cryostasis-revival/

[423] Freitas RA Jr. Cryostasis Revival: The Recovery of Cryonics Patients through Nanomedicine. Alcor Life Extension Foundation, Scottsdale AZ, 2022; Section 4.10.1.1, "Oxygen"; https://www.alcor.org/cryostasis-revival/

[424] Freitas RA Jr. Cryostasis Revival: The Recovery of Cryonics Patients through Nanomedicine. Alcor Life Extension Foundation, Scottsdale AZ, 2022; Section 4.10.1.2, "Glucose and ATP"; https://www.alcor.org/cryostasis-revival/

[425] Freitas RA Jr. Cryostasis Revival: The Recovery of Cryonics Patients through Nanomedicine. Alcor Life Extension Foundation, Scottsdale AZ, 2022; Section 4.10.1.3, "Cell Metabolites and Leaked Blood Plasma Components"; https://www.alcor.org/cryostasis-revival/

How many micromanipulators are needed in the Cell Assembly Module? If one micromanipulator can install one organelle by traversing a single round-trip armswing of maximum length $x_{RTarmswing}$ = 20 μm, taking $n_{armorgs}$ = 1 round-trip armswing per organelle, and if there are $n_{organelles}$ = 20,354,705 organelles to be emplaced in each cell (**Table 5** in Section 4.1), then the total armswing travel distance to place all organelles in one cell is $x_{organelles} = n_{organelles}$ $n_{armorgs}$ $x_{RTarmswing}$ = 407 meters. The placement time for all organelles in one 8000 μm^3 cell using one micromanipulator is therefore $t_{organelles} = x_{organelles} / v_{manip}$ = 40,700 sec, given the maximum micromanipulator arm velocity of v_{manip} ~ 1 cm/sec. This establishes a per-cell micromanipulator work requirement of $r_{placement}$ = 40,700 micromanipulator-sec/cell, which implies that achieving the cell mass production rate of $R_{CellMill}$ ~ 1 kg/hr of cells will require the cell mill to operate, in parallel, $N_{micromanip} = r_{placement}$ $N_{CellMill}$ = 1.33 x 10^{12} micromanipulators having a total mechanical volume of $V_{CellMillMM} = N_{micromanip}$ $V_{micromanip}$ = 1330 cm^3, taking individual micromanipulator volume as $V_{micromanip}$ = 1000 μm^3. Assuming n_{micro} = 8 micromanipulators at each cell manufacturing site (Section 4), the start-to-finish manufacturing time for a cell is $\tau_{cellthroughput} \sim t_{organelles} / n_{micro}$ ~ 1.41 hours.

There are two moulds for each cell manufacturing site, so the Cell Assembly Module requires $N_{CAMmoulds} = N_{micromanip} / (n_{micro} / 2)$ = 3.33 x 10^{11} moulds. If each mould is α_{mould} = 3.8 times the volume of the cell being manufactured, then each such mould is $V_{CAMM} = \alpha_{mould}$ V_{cell} = 30,400 μm^3 in volume, taking V_{cell} = 8000 μm^3, and the total volume of all cell moulds is $V_{CAMmoulds} = V_{CAMM}$ $N_{CAMmoulds}$ = 10,100 cm^3.

The total volume of all micromanipulators and moulds in the Cell Assembly Module is $V_{MM} = V_{CellMillMM} + V_{CAMmoulds}$ = 11,430 cm^3. Taking micromanipulator density as ρ_{manip} ~ 0.1 gm/cm^3 and mould density as ρ_{mould} ~ 0.35 gm/cm^3, the total mass of all micromanipulators and moulds in the Cell Assembly Module is $M_{MM} = \rho_{manip}$ $V_{CellMillMM} + \rho_{mould}$ $V_{CAMmoulds}$ = 3668 gm. Power consumption for all Cell Assembly Module micromanipulators is $P_{MM} \sim N_{micromanip}$ $P_{micromanip}$ ~ 1330 watts, taking $P_{micromanip}$ ~ 1000 pW for each micromanipulator.

If we add the volume, mass and power requirements for the preceding Molecular Synthesis Module (Section 2) and the Cytocomponent Assembly Module (Section 3), and if we add another ~82,000 cm^3 for support structures having a similar density as the micromanipulators, then the total volume of the cell mill is ~0.1 m^3 – a cubical box ~46 cm (~18 inches) on a side – with a total mass of ~12.5 kg and a total power draw of ~5 kW, as summarized in **Table 7** below.

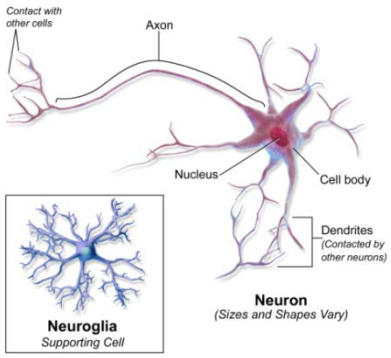

Some biological cells, most notably muscle and neuron-related cells,[426] will not be neatly spherical or cubical in shape as assumed throughout the present analysis but will possess long processes that extend well beyond the central cell body (images, right). Special procedures, jigs, and manipulators for assembling these and other nonstandard cell shapes are readily conceived but lie beyond the scope of this paper and therefore must be left for future research.

[426] There are several hundred neuron types and subtypes in the entire human nervous system, as described at the NeuroMorpho database (http://neuromorpho.org/) and the "Neuroscience Lexicon" at http://neurolex.org/wiki/Category:Neuron.

Table 7. Summary of exemplar cell mill volume, mass, and power requirements				
Nanorobotic Subsystem	**Section Reference**	**Volume** (cm^3)	**Mass** (gm)	**Power** (W)
Generic Synthesis Unit	2.1.2	36.5	73	3400
Nano Sequencer	2.2.1.2	0.0001	0.0002	0.92×10^{-6}
DNA Mill	2.2.2	50	1	1.3
Protein Mill	2.2.3	3000	60	78
Carbohydrate Mill	2.2.4	3000	60	78
Macromolecular Organelle Mill	3.2	170	3	4
Vesicular Organelle Mill	3.3	2.4	0.768	33
Membraneous Organelle Mill	3.4	4.4	10.4	46
Cell Nucleus Mill	3.5	400	140	6
Subtotals		6663	348	3546
+ Cell Assembly Unit	4	11,430	3668	1330
Active system subtotal		18,093	4016	4876
+ Unspecified support structures (e.g., storage, refrigeration, housings, nano-computers, data/power distribution)	4.3	~81,907	~8484	~124
Totals for Cell Mill		***100,000*** ($0.1\ m^3$)	***12,500*** (12.5 kg)	***5000*** (5 kW)

To summarize: Starting from simple organic molecule feedstock, a nanorobotic cell mill of volume $V_{CellMill} \sim 0.1\ m^3$, mass $M_{CellMill} \sim 12.5$ kg, and power consumption $P_{CellMill} = 5$ kW produces $R_{CellMill} \sim 1000$ gm/hr of viable biological cells that are autologous to a specified human body. Relevant productivity metrics for the cell mill are therefore: $\psi_{V\text{-}CellMill} = R_{CellMill} / V_{CellMill} \sim$ **2.78 gm/m^3-sec**, $\psi_{m\text{-}CellMill} = R_{CellMill} / M_{CellMill} \sim$ **0.0222 gm/kg-sec**, and $\psi_{P\text{-}CellMill} = R_{CellMill} / P_{CellMill} \sim$ **0.0556 gm/kW-sec**.

4.4 Cell Mill Computational Requirements

The computational requirements for operating a cell mill appear to be surprising modest. A preliminary analysis of the four main subsystems gives the following results:

(1) **Generic Synthesis Unit** (Section 2.1.2). The Generic Synthesis Unit or GSU includes $N_{FS} = 36.5$ trillion Fabrication Subunits, each consisting of ~100 million atoms and ~0.001 μm^3 in volume, operating at ~0.1 MHz producing ~10^5 molecules/sec. According to

classical descriptions of high-density nanocomputing,[427] a 3D array of diamondoid register rods can achieve a storage density of $i_{nano} = 10^7$ bits/μm^3 with a $t_{nano} = 10^{10}$ bit/sec data access speed, and a specific processing power of $U_{nano} \sim 10^{30}$ bit/sec-m^3.[428] If we assume that each Fabrication Subunit needs $i_{FS} \sim 10^7$ bits/Subunit-sec data processing capacity and $Z_{FS} \sim 10^6$ bits/Subunit of working memory to operate,[429] then the total required nanocomputer (CPU) volume is $V_{GSU\text{-}CPU} = N_{FS}\ i_{FS} / U_{nano}$ = **0.365 mm^3** and the required volume of nanocomputer memory is $V_{GSU\text{-}Mem} = N_{FS}\ Z_{FS} / i_{nano}$ = **3.65 cm^3**. Assuming a modest set of reusable molecular tools, the instructions for synthesizing ~100,000 different molecules if we require ~1000 synthesis steps per molecule and ~1000 bits to describe each step demand $Z_{process} \sim 10^{11}$ bits, which occupy a negligible $V_{process} = Z_{process} / i_{nano}$ = **0.00001 mm^3** (~10,000 μm^3) of the 3.65 cm^3 GSU memory. (This must be stored in accessible network caches outside of the Fabrication Subunits, whose internal volume is only ~0.001 μm^3.) The energy usage in mature nanocomputer CPUs should be comparable to the experimentally-confirmed[430] classical Landauer limit[431] for non-reversible computational energy dissipation of $E_{Landauer300K} \sim k_B T \ln(2) = 2.9 \times 10^{-21}$ J/bit, assuming T = 300 K operation and taking Boltzmann's constant $k_B = 1.38 \times 10^{-23}$ J/K, hence $P_{GSU\text{-}CPU} = N_{FS}\ i_{FS}\ E_{Landauer300K}$ ~ **1.1 watts**.

(2) **Personalized Synthesis Unit** (Section 2.2). The data requirements for manufacturing personalized molecules should be roughly similar to the requirements for generic molecules, hence $V_{PSU\text{-}CPU}$ ~ **0.365 mm^3**, $V_{PSU\text{-}Mem}$ ~ **3.65 cm^3**, and $P_{PSU\text{-}CPU}$ ~ **1.1 watts**. An additional requirement is that genome sequencing must be performed once for each patient, with the results translated into personalized DNA, protein, and carbohydrate molecule synthesis formulations

---

[427] Drexler KE. Nanosystems: Molecular Machinery, Manufacturing, and Computation, John Wiley & Sons, New York, 1992, Chapter 12 "Nanomechanical Computational Systems"; https://www.amazon.com/dp/0471575186/. Freitas RA Jr. Nanomedicine, Volume I: Basic Capabilities, Landes Bioscience, Georgetown TX, 1999, Section 10.2.1, "Nanomechanical Computers"; http://www.nanomedicine.com/NMI/10.2.1.htm.

[428] Assuming 1 GHz operation of a (400 nm)^3 CPU,[*] and using 64-bit words: (64 bits/operation) (10^9 operations/sec) / (400 nm)^3 = 1 x 10^{30} bits/sec-m^3.
[*] Drexler KE. Nanosystems: Molecular Machinery, Manufacturing, and Computation, John Wiley & Sons, New York, 1992, Chapter 12 "Nanomechanical Computational Systems"; https://www.amazon.com/dp/0471575186/.

[429] This is roughly comparable to the estimated ~10^7 bit/sec data processing capacity and the 5 x 10^6 bit onboard mass memory requirement for the microbivore,[*] a complex medical nanorobotic system that is ~10,000 times larger in size than the proposed Fabrication Subunit.
[*] Freitas RA Jr. Microbivores: Artificial Mechanical Phagocytes using Digest and Discharge Protocol. J. Evol. Technol. 2005 Apr;14:55-106; http://www.jetpress.org/volume14/freitas.pdf.

[430] Bérut A, Arakelyan A, Petrosyan A, Ciliberto S, Dillenschneider R, Lutz E. Experimental verification of Landauer's principle linking information and thermodynamics. Nature. 2012 Mar 7;483(7388):187-189; https://www.nature.com/articles/nature10872.

[431] Landauer R. Irreversibility and heat generation in the computing process. IBM J Res Devel. 1961;5:183-191; http://fab.cba.mit.edu/classes/MAS.862/notes/computation/Landauer-1961.pdf. Bennett C, Landauer R. The fundamental physical limits of computation. Sci Am. 1985 Jul;253(1):48-57; http://web.eecs.umich.edu/~taustin/EECS598-HIC/public/Physical-Limits.pdf.

(which will have a similar information content per unit mass as the generic molecules). According to one summary,[432] the "size" of the human genome may be regarded as either (A) ~0.125 GB (gigabytes) to store just the 0.1% of the genome that differs among individuals, (B) ~0.7 GB to store all 3 billion bases as 2-bit words, or (C) ~200 GB of raw data that is generated by modern-day gene sequencing machines, which produce lots of "short reads" with many overlaps and repeats. Assuming $Z_{genome} \sim 100 \times 10^9$ bits/genome to include all relevant epigenetic information (e.g., methylation patterns), the required additional volume of nanocomputer memory is only $V_{PSU\text{-}genome} = Z_{genome} / i_{nano} \sim$ **0.00001 mm^3** (~10,000 μm^3).

(3) **Cytocomponent Assembly Module** (Section 3). The Cytocomponent Assembly Module or CCAM must manufacture, from prefabricated molecular components supplied by the Molecular Synthesis Module, 6 types of macromolecular organelles at the rate of 0.0111 kg/hr, 5 vesicular organelles at 0.177 kg/hr, Golgi and ER organelles at 0.249 kg/hr, and cell nuclei at 0.034 kg/hr, a total production rate of $R_{CCAM} \sim 0.471$ kg/hr. Assuming memory and data processing intensity is similar to the Molecular Synthesis Module – atomic precision is not required, but there are offsetting complex interface issues between joined components – then $V_{CCAM\text{-}CPU} \sim (R_{CCAM} / R_{CellMill}) V_{GSU\text{-}CPU} \sim$ **0.172 mm^3**, $V_{CCAM\text{-}Mem} \sim (R_{CCAM} / R_{CellMill}) V_{GSU\text{-}Mem} \sim$ **1.72 cm^3**, and $P_{CCAM\text{-}CPU} \sim (R_{CCAM} / R_{CellMill}) P_{GSU\text{-}CPU} \sim$ **0.5 watts**.

(4) **Cell Assembly Module** (Section 4.3). Analogously to the CCAM, the Cell Assembly Module or CAM must manufacture $R_{CAM} = R_{CellMill} \sim 1$ kg/hr of finished cells, using prefabricated biocomponents supplied by the GSU, PSU, and CCAM, hence $V_{CAM\text{-}CPU} \sim V_{GSU\text{-}CPU} \sim$ **0.365 mm^3**, $V_{CAM\text{-}Mem} \sim V_{GSU\text{-}Mem} \sim$ **3.65 cm^3**, and $P_{CAM\text{-}CPU} \sim P_{GSU\text{-}CPU} \sim$ **1.1 watts**. Assuming all cell assembly information for ~20 million organelles of ~500 different cell types can be encoded in ~10^6 bits per organelle, there is an additional nanocomputer memory requirement of $Z_{celldata} = (20 \times 10^6$ organelles/cell) (500 cytotypes) (10^6 bits/organelle) ~ 10^{16} bits, adding $V_{CAM\text{-}celldata} = Z_{celldata} / i_{nano} \sim$ **1 mm^3** of additional nanocomputer memory volume.

Hence the computational requirements for the cell mill will include $V_{GSU\text{-}Mem} + V_{process} + V_{PSU\text{-}Mem} + V_{PSU\text{-}genome} + V_{CCAM\text{-}Mem} + V_{CAM\text{-}Mem} + V_{CAM\text{-}celldata} =$ **12.7 cm^3 of nanocomputer memory** and $V_{GSU\text{-}CPU} + V_{PSU\text{-}CPU} + V_{CCAM\text{-}CPU} + V_{CAM\text{-}CPU} =$ **0.0013 cm^3 of nanocomputer CPUs** consuming $P_{GSU\text{-}CPU} + P_{PSU\text{-}CPU} + P_{CCAM\text{-}CPU} + P_{CAM\text{-}CPU} =$ **3.8 watts of power** during cell mill operation.

4.5 Cell Mills Compared to Biology

Table 8 provides a crude comparison of the productivity of a nanorobotic cell mill to the productivity of a few living systems. From this data, the cell mill appears to be ~10 times more energy-efficient, ~100 times more volume-efficient, and ~1000 times more mass-efficient than eukaryotic macroscale plants and animals at the task of fabricating cell-rich biological materials, including cells. *E. coli* may be ~10 times more mass-efficient and ~100 times more volume- and energy-efficient than the cell mill, in part because the bacterium's less-complex cell contains no nucleus or other membrane-bound organelles, only one chromosome comprising a single circular strand of DNA, and no biostructural provisions for participating in differentiated multicellular

---

[432] https://medium.com/precision-medicine/how-big-is-the-human-genome-e90caa3409b0.

aggregates (e.g., tissues, organs, plants, or animals), thus enabling much faster replication of an isolated cell. Highly specialized red bone marrow produces more complex white cells in addition to red cells and platelets, hence ranks closer in its productivity metrics to the cell mill.

Table 8. Productivity in gm/sec per unit feature (volume, mass, and power) of proposed cell mill and representative biological manufacturing systems

Manufacturing System	ψ_V	ψ_m	ψ_P
E. coli bacterium[433]	830 gm/m^3-sec	0.83 gm/kg-sec	2.6 gm/kW-sec
Red bone marrow[434]	3.5 gm/m^3-sec	0.0034 gm/kg-sec	0.16 gm/kW-sec
Cell Mill	2.8 gm/m^3-sec	0.022 gm/kg-sec	0.056 gm/kW-sec
Mature bamboo plant[435]	0.020 gm/m^3-sec	0.000034 gm/kg-sec	0.0016 gm/kW-sec
Angus beef cow[436]	0.014 gm/m^3-sec	0.000016 gm/kg-sec	0.0084 gm/kW-sec

[433] One of the fastest growing bacterial species, *Escherichia coli* has a mass of ~1 x 10^{-15} kg and volume ~1 x 10^{-18} m^3 (https://ecmdb.ca/e_coli_stats), a replication time of ~1200 sec,[*] and a power consumption during exponential growth of 6.4 x 10^6 ATP/sec,[†] with exergonic ATP hydrolysis releasing 7.3 kcal/mole,[‡] giving a bacterium power generation of ~0.325 pW while replicating.
[*] Gibson B, Wilson DJ, Feil E, Eyre-Walker A. The distribution of bacterial doubling times in the wild. Proc Biol Sci. 2018 Jun 13;285(1880):20180789; https://www.ncbi.nlm.nih.gov/pmc/articles/PMC6015860/.
[†] Deng Y, Beahm DR, Ionov S, Sarpeshkar R. Measuring and modeling energy and power consumption in living microbial cells with a synthetic ATP reporter. BMC Biol. 2021 May 17;19(1):101; https://www.ncbi.nlm.nih.gov/pmc/articles/PMC8130387/.
[‡] Dunn J, Grider MH. Physiology, Adenosine Triphosphate. StatPearls [Internet], 13 Feb 2023; https://www.ncbi.nlm.nih.gov/books/NBK553175/.

[434] An adult human male has ~1.17 kg of hematopoietically active red bone marrow of density ~1029 kg/m^3 (https://itis.swiss/virtual-population/tissue-properties/database/density/), producing ~490 billion cells/day[*] including ~238 billion/day red cells of volume ~94 μm^3/cell at ~1110 kg/m^3, ~164 billion/day white cells of volume ~1800 μm^3/cell at ~1080 kg/m^3, and ~88 billion/day platelets of volume ~8.9 μm^3/cell at ~1030 kg/m^3. Marrow power draw is speculatively estimated as ~25 W, assuming the metabolic intensity of active red bone marrow to be 200-300 kcal/kg-day.
[*] Hindorf C, Glatting G, Chiesa C, Lindén O, Flux G. EANM Dosimetry Committee guidelines for bone marrow and whole-body dosimetry. Eur J Nucl Med Mol Imaging. 2010 Jun;37(6):1238-50; https://eanm.org/publications/guidelines/EJNMMI_Bone_Marrow_Dosimetry_06_2010.pdf.

[435] Bamboo is the fastest growing plant on Earth. Assuming a mature bamboo plant with 30 culms of which 3 culms are growing at ~90 cm/day (~1 kg/day), with an average culm diameter of 10 cm, wall thickness 1 cm, height of 20 m, density 600 kg/m^3, and dry biomass energy content of ~18 MJ/kg, implying a mature plant mass of ~1018 kg and volume ~1.70 m^3 with a chemical energy draw of ~208 W/kg. Liese W, Köhl M, eds. Bamboo: The Plant and its Uses. Springer, 2015; https://www.amazon.com/dp/3319141325/ref.

[436] An Angus cow (beef cattle) typically weighs ~500 kg (https://cosleyzoo.org/black-angus-cow/), has meat with a density of ~852 kg/m^3 (https://institut-agro-rennes-angers.hal.science/hal-02286677) hence a whole-animal volume of ~0.587 m^3, takes ~2 years to grow to maturity, and has a 64-100 MJ/day metabolizable energy requirement for pregnant cows (https://www.feedinglivestock.vic.gov.au/beef-resources/useful-tables-beef/), giving an estimated power generation of ~950 W/cow.

5. Tissue Mills

As noted in the Introduction (Section 1), the ability to quickly manufacture viable autologous human cells would enable the rapid replacement of damaged tissues and organs, and would also permit whole-body rejuvenation[437] or repair thus enabling survival after even the most extreme injuries or medical circumstances.[438]

Freitas first proposed the tissue mill and organ mill concepts in 1999.[439] Specifically, a complete set of human tissues and organs can be achieved by printing these biological structures from their constituent cells as the primary building blocks, in combination with a variety of biological fibers, meshes, mineralized structures, and other binding and connective materials. A generic architectural file, altered as desired to fit the relevant specific human individual, will include descriptions of all cellular and noncellular components, after which all identified individual cells can be manufactured in the Cell Assembly Module of the cell mill (Section 4) and the noncellular materials can be manufactured in the Molecular Synthesis Module of the cell mill (Section 2).

The most convenient liquid assembly environment is pure water. Because water can leach out of cells in a watery bath due to a concentration imbalance of ions and many soluble small molecules via osmosis[440] during a long assembly process, and the need to maintain metabolic stasis during assembly, the architectural file must delete all metabolites from the initial description and any water-soluble molecules must be temporarily withheld or offset using a proper mix of dissolved solutes sufficient to create osmotically-inactive cells. (Missing molecules can later be restored to cells during the metabolic activation phase prior to use; Section 4.2.)

For the present analysis, we will assume that cell printing occurs in an aqueous environment at ~273 K (0 °C) and ~1 atm ambient pressure, and that all cells are manufactured without any water-leachable soluble molecules, metabolites, or ions (all of which are restored to the cell later; Section 4.2). The architectural file is converted to a cell print file that details each cell that needs to be built, where each cell should be positioned and oriented, and the interfaces between each cell and other cells or biomaterials. The cell print file also provides the cell mill with molecular descriptions for each cell to be fabricated, which the cell mill can reproduce to the fullest limits of

---

[437] Freitas RA Jr. Chapter 23. Comprehensive Nanorobotic Control of Human Morbidity and Aging. In: Fahy GM, West MD, Coles LS, Harris SB, eds, The Future of Aging: Pathways to Human Life Extension, Springer, New York, 2010; http://www.nanomedicine.com/Papers/Aging.pdf.

[438] Freitas RA Jr. Cryostasis Revival: The Recovery of Cryonics Patients through Nanomedicine. Alcor Life Extension Foundation, Scottsdale AZ, 2022; Appendix D, "Cell Mills"; https://www.alcor.org/cryostasis-revival/.

[439] Freitas RA Jr. Nanomedicine, Volume I: Basic Capabilities, Landes Bioscience, Georgetown, TX, 1999, p. 32; Table 1.4, "Medical Challenges of Increasing Difficulty and Possible Approaches"; http://www.nanomedicine.com/NMI/Tables/1.4.jpg.

[440] https://en.wikipedia.org/wiki/Osmosis.

manufacturing fidelity of which it is capable. Future research may examine the computational details of the architectural file for a tissue or organ and the process by which that file can be converted into a cell print file appropriate to each of the specific print techniques described below.

At least two alternative techniques for performing a fluidic 3D cell print of replacement human tissues have been identified: planar tissue printing (Section 5.1) and scaffolded tissue printing (Section 5.2). Future research should investigate the details of these and other possible fluidic 3D cell printing techniques,[441] then perform a trade study to determine which method may produce the most desirable results with the greatest efficiency and lowest cost. Future research must also define the appropriate size and shape of fragments of noncovalently bonded ionic solids such as hydroxyapatite[442] that may be fabricated in a cell mill, and the bonding methods appropriate for joining these fragments into extended proteinaceous matrices as found in human teeth (e.g., enamel,[443] dentin,[444] and cementum[445]) and bones.[446]

It is of interest that 3D printing of models of human brains to 30 μm (i.e., ~cellular) resolution using photopolymers of specific colors and transparencies was achieved in 2018,[447] translating CT and MRI scans of the brains of living patients into UV-hardened rubberlike plastic models.

5.1 Planar Tissue Printing

In the seemingly simplest approach, called "planar tissue printing",[448] cell-mill-manufactured cells (Section 4) and accompanying noncellular biomaterials (Section 2) are laid down layer by

---

[441] A tissue mill might employ the concept of convergent assembly (organ assembly by printing small multicellular blocks that are progressively combined into larger and larger blocks) that could complete the work in much less time. For example, convergent assembly might allow 60 tissue mills operating in parallel to combine their output to achieve a 60-fold higher production rate of ~1 kg/min. This and related approaches involve operational complexities that should be further examined in future research but are outside the scope of this paper. Freitas RA Jr., Merkle RC. Kinematic Self-Replicating Machines. Landes Bioscience, Georgetown, TX, 2004; Section 5.7, "Massively Parallel Molecular Manufacturing"; http://www.MolecularAssembler.com/KSRM/5.7.htm. Freitas RA Jr. Cryostasis Revival: The Recovery of Cryonics Patients through Nanomedicine. Alcor Life Extension Foundation, Scottsdale AZ, 2022; Section 5.4, "High Speed Molecular Reconstruction"; https://www.alcor.org/cryostasis-revival/.

[442] https://en.wikipedia.org/wiki/Hydroxyapatite.
[443] https://en.wikipedia.org/wiki/Human_tooth#Enamel.
[444] https://en.wikipedia.org/wiki/Human_tooth#Dentin.
[445] https://en.wikipedia.org/wiki/Human_tooth#Cementum.
[446] https://en.wikipedia.org/wiki/Bone#Composition.

[447] Hosny A, Keating SJ, Dilley JD, Ripley B, Kelil T, Pieper S, Kolb D, Bader C, Pobloth AM, Griffin M, Nezafat R, Duda G, Chiocca EA, Stone JR, Michaelson JS, Dean MN, Oxman N, Weaver JC. From Improved Diagnostics to Presurgical Planning: High-Resolution Functionally Graded Multimaterial 3D Printing of Biomedical Tomographic Data Sets. 3D Printing and Additive Manuf. 2018 Jun;5(2):103-113; https://www.liebertpub.com/doi/10.1089/3dp.2017.0140.

layer, plane upon plane, building up large blocks of cell-infused living tissue in the manner of present-day 3D printing[449] and organ printing[450] systems, but using robotic manipulators capable of achieving more precise positioning – the details of which should be set forth in future research.

For crude scaling purposes, we can imagine a flat Tissue Assembly Mechanism inside the tissue mill, coated with large millimanipulators 100 times larger in every dimension than the micromanipulators described in Section 4. Millimanipulators are D_{milli} = 2 R_{milli} = 300 μm in cylindrical diameter and L_{milli} = 1000 μm (1 mm) in length, with a central transport channel ~100 μm in diameter, large enough to convey even the largest human cell[451] through the device. Scaling relationships suggest that the millimanipulator has a 1 mm x 1 mm lateral motion range, an operating volume of $V_{millimanip}$ = 1 mm^3, an arm velocity of v_{manip} ~ 1 cm/sec, and a ~10^4 W/m^3 power density, giving a power dissipation estimate of $P_{millimanipVac}$ ~ 1,000,000 pW (1 μW) for the millimanipulator (compared to ~1000 pW for the micromanipulator and ~1 pW for the nanomanipulator) if operated in a vacuum. The activities of the manipulator-covered frontal face of the Tissue Assembly Mechanism would be supported by a network of transfer tubes, fluid pipes, electrical power and control lines, and other essential infrastructure behind the frontal face and extending to the backside of the Tissue Assembly Mechanism, as needed to support 3D cell printing operations. During tissue assembly, cells and non-cell materials are passed through the Tissue Assembly Mechanism within which the millimanipulators are embedded and are installed on a flat assembly stage below the Mechanism. Once fabricated, the finished tissue or organ can be separated from the stage and removed from the tissue mill for use elsewhere.

Assuming a human body tissue or organ to be manufactured by planar 3D cell printing can fit inside a cubical print chamber that is ~30 cm on each side, then a Tissue Assembly Mechanism of these dimensions with area A_{TAP} = 30 cm x 30 cm = 0.09 m^2 with adjacent millimanipulators spaced $x_{millispace}$ = L_{milli} = 1 mm apart has $n_{millimanip}$ = A_{TAP} / $x_{millispace}^2$ = 90,000 millimanipulators mounted on its surface. A millimanipulator traversing f_{milli} ~ 2% (~20 μm) of the maximum L_{milli} = 1 mm lateral motion range of the millimanipulator to install adjacent V_{cell} ~ 8000 μm^3 (~20 μm wide) cells could install $n_{millicells}$ = v_{manip} / f_{milli} L_{milli} ~ **500 cells/manipulator-sec**,[452] or $m_{millicells}$ =

---

[448] Freitas RA Jr. Cryostasis Revival: The Recovery of Cryonics Patients through Nanomedicine. Alcor Life Extension Foundation, Scottsdale AZ, 2022; Section 5.2.3.3.1, "Planar Tissue Printing"; https://www.alcor.org/cryostasis-revival/.

[449] https://en.wikipedia.org/wiki/3D_printing.
[450] https://en.wikipedia.org/wiki/Organ_printing.

[451] The ovum is the largest compact cell in the human body with a diameter of ~100 μm.* Longer cells could be transported as segments capped with temporary sealed interfaces that can be removed at the time of final *in situ* assembly or installation.
* Alberts B, Johnson A, Lewis J, Raff M, Roberts K, Walter P, eds. Molecular Biology of the Cell, 4th edition, Garland Science, New York, 2002; https://www.ncbi.nlm.nih.gov/books/NBK26842/.

[452] By comparison, conventional present-day 3D bioprinter bioinks may contain ~5-40 million cells/cm^3 with a print head extruding bioink at ~0.001 cm^3/sec, giving cell print rates of **5000-40,000 cells/sec**. Of course, placing cells with high precision and with attention to intercellular interfaces would take more time, lowering the practical print rate. Gillispie GJ, Han A, Uzun-Per M, Fisher J, Mikos AG, Niazi MKK, Yoo JJ, Lee SJ, Atala A. The Influence of Printing Parameters and Cell Density on Bioink Printing Outcomes.

$n_{millicells}\ m_{cell} \sim 4.26 \times 10^{-9}$ kg/manipulator-sec, taking cell mass as $m_{cell} = \rho_{cell}\ V_{cell} = 8.51 \times 10^{-12}$ kg/cell (Section 4.3).

The total nonaqueous cell volume in a 70 kg human body is $V_{bodycells} \sim 28{,}000$ cm^3 and $V_{noncellular} \sim 13{,}000$ cm^3 of noncellular biomaterials,[453] so achieving an $R_{TissueMill} \sim 1$ kg/hr production rate for tissues and organs that matches the $R_{CellMill} = 1$ kg/hour production rate of the cell mill, and taking the aforementioned whole-body cell and non-cell volumes as representative for tissues and organs, then the millimanipulators must install $R_{bodycells} \sim R_{CellMill}\ V_{bodycells} / (V_{bodycells} + V_{noncellular}) = 0.68$ kg/hour of cells and $R_{noncellular} \sim R_{CellMill}\ V_{noncellular} / (V_{bodycells} + V_{noncellular}) = 0.32$ kg/hour of noncellular biomaterials, both of which are produced by the cell mill. If we assume that noncellular material takes a similar amount of time to install as cells per unit volume because this material isn't as neatly packaged, then the tissue mill requires $N_{millimanipulators} = R_{TissueMill} / m_{millicells} = 65{,}200$ millimanipulators, leaving a spare capacity of $1 - (N_{millimanipulators} / n_{millimanip}) \sim 28\%$.

If the print job was taking place in vacuum, the power requirement to drive all manipulator motions would be an extremely small $P_{cellinstallVac} = n_{millimanip}\ P_{millimanipVac} \sim 0.09$ watts. Since the millimanipulators are instead moving in liquid water having an absolute viscosity of $\eta = 1.787 \times 10^{-3}$ Pa-sec at T ~ 273 K, they will also experience viscous drag. The drag power for a cylindrical robot arm translating normal to its central axis[454] is $P_{millimanipDrag} = 8\pi\ \eta\ L_{milli}\ v_{manip}^2 / [1 + \ln(L_{milli}^2 / R_{milli}^2)] = 940$ pW/manipulator, hence additional drag power needed to drive all 90,000 millimanipulators on the Tissue Assembly Mechanism is a negligible additional $P_{cellinstallDrag} = n_{millimanip}\ P_{millimanipDrag} \sim 0.00008$ watts.

Even if the aforementioned processes can serve as the foundation for fabricating most of the tissues and organs in the human body, there are some specific cases involving overlong cells that will require special handling in addition to the Tissue Assembly Mechanism. The most important example is neural tissue, whose axons can range from 500 μm to 1 meter in length. The axon of the longest motor neuron[455] in the human body is a few microns in diameter and runs from the base of the spine to the feet, a distance of up to 1 meter.[456] Muscle tissue is another special case. A typical muscle cell is cylindrical, 10-50 μm in diameter but up to 1-40 mm in length.[457]

Tissue Eng Part A. 2020 Dec;26(23-24):1349-1358; https://www.ncbi.nlm.nih.gov/pmc/articles/PMC7780841/.

[453] Freitas RA Jr. Cryostasis Revival: The Recovery of Cryonics Patients through Nanomedicine. Alcor Life Extension Foundation, Scottsdale AZ, 2022; Section 5.1, "Extract Nonstructural Bulk Materials"; https://www.alcor.org/cryostasis-revival/.

[454] Freitas RA Jr. Nanomedicine, Volume I: Basic Capabilities, Landes Bioscience, Georgetown TX, 1999; Eqn. 9.75 in Section 9.4.2.4, "Force and Power Requirements"; http://www.nanomedicine.com/NMI/9.4.2.4.htm#p6.

[455] https://biologydictionary.net/motor-neuron/.

[456] Fletcher DA, Theriot JA. An introduction to cell motility for the physical scientist. Phys Biol. 2004 Feb 12;1(1):T1-10; http://rpdata.caltech.edu/courses/aph161/Handouts/Fletcher2004.pdf.

[457] Lodish H, Berk A, Zipursky SL, *et al*. Molecular Cell Biology, 4th edition, W.H. Freeman, NY, 2000; https://www.ncbi.nlm.nih.gov/books/NBK21670/.

Both of these cell types are too large to be transported inside the 100 μm central channel of the millimanipulator because they are much longer than the L_{milli} = 1 mm central channel length, and they cannot be deterministically emplaced in a tissue workpiece because their great length and 3D positioning requirements into varying tissue depths may greatly exceed the ~1 mm^3 operating volume of a single millimanipulator or the reach of a plane of millimanipulators with a ~1 mm maximum vertical reach. Transport and emplacement of such cells may require the intervention of a small fleet of coordinated mobile shepherd nanorobots[458] that can push and pull the overlong cells into arbitrary depths and patterns inside a growing printed tissue mass. For instance, a fleet of 100,000 shepherd nanorobots might grasp and guide the installation of a sinuous 1 meter motor axon, with the robots spaced every 10 μm along the length of the axon. Future research should enumerate the types and likely numbers of overlong cells, describe and parameterize the process of their emplacement using shepherd nanorobots, and estimate the size, number, time and power consumption of the nanorobots required to complete the 3D cell print of all tissue and organ types in concert with other Tissue Assembly Mechanism systems and operations.

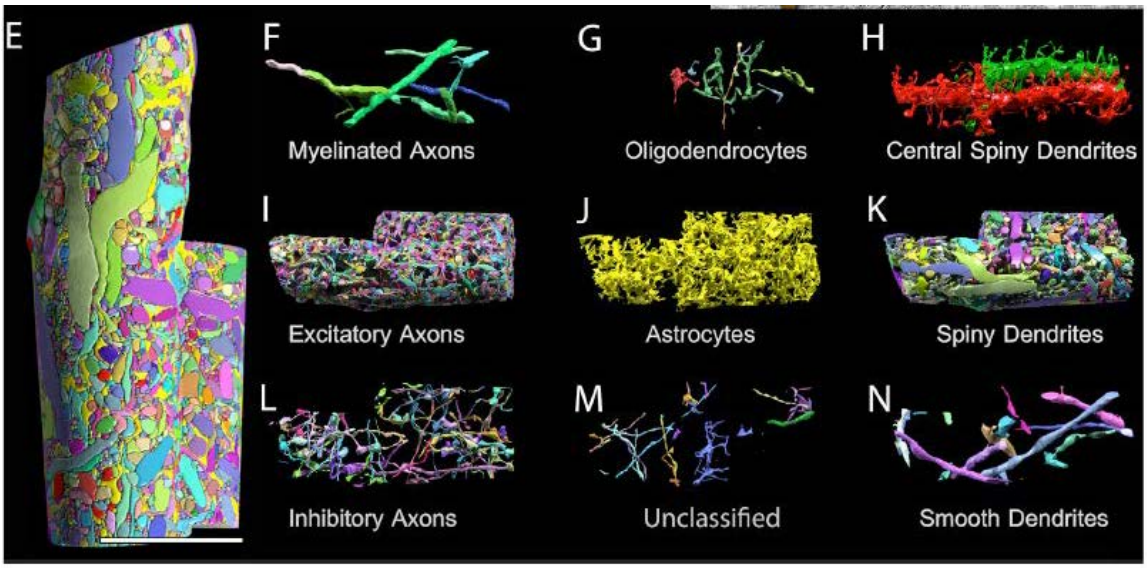

The neuropil of the brain is perhaps the tissue that is the most extremely densely packed with cells and axonal processes, as illustrated (image, above; scale bar = 7 μm)[459] in a multiscale

---

[458] Freitas RA Jr. The Alzheimer Protocols: A Nanorobotic Cure for Alzheimer's Disease and Related Neurodegenerative Conditions. IMM Report No. 48, June 2016, 433 pp; Section 5.3.2.3, "Cell Insertion and Emplacement," pp. 327-332; http://www.imm.org/Reports/rep048.pdf.

[459] Kasthuri N, Hayworth KJ, Berger DR, Schalek RL, Conchello JA, Knowles-Barley S, Lee D, Vázquez-Reina A, Kaynig V, Jones TR, Roberts M, Morgan JL, Tapia JC, Seung HS, Roncal WG, Vogelstein JT, Burns R, Sussman DL, Priebe CE, Pfister H, Lichtman JW. Saturated Reconstruction of a Volume of Neocortex. Cell. 2015 Jul 30;162(3):648-61; http://seunglab.org/wp-content/uploads/2015/09/saturatedreconstruction.pdf.

reconstruction of generic cortical neuronal somata of mouse brain. As such, it may be ideally suited to positional assembly by shepherd nanorobots as described above. Elsewhere in the body where cells are packed less densely or less intricately, large volumes of extracellular matrix (ECM)[460] may occupy much of the spaces between cells. ECM is filled with lengthy intertwined fibers of various types that vary widely according to tissue type.[461] For example, collagens representing ~25% of total mammalian protein mass[462] may exist as strands ~300 nm long and ~1.5 nm wide, spaced 4-12 μm apart in the ECM. Cartilage consisting of ~10 μm strands that are ~500-600 nm in diameter may be spaced 10-30 μm apart in the ECM.[463] Rather than attempting to positionally assemble this multitude of fibers one by one during the planar tissue print, we may be able to rely upon the cell mill to assemble specified chunks of ECM containing prefabricated fiber networks that can be deployed as building blocks by the aforementioned millimanipulators during the print job. Future research should further examine the challenge of nanoscale and microscale fiber network assembly during planar tissue printing, and devise multiple technical strategies that can be compared in an engineering trade study to select the best alternative.

5.2 Scaffolded Tissue Printing

An alternative method for 3D cell printing of human tissues or organs may be termed the "print on scaffold" approach,[464] wherein a whole-organ scaffolding is first laid down, after which nanorobots install whole cells and other biological materials onto the scaffolding to build out the rest of the tissues and structures comprising the organ. The scaffolding is removed after fabrication is complete, leaving the finished tissue or organ ready for use.

While many different types of scaffolding[465] are readily envisioned, the vasculoid concept has so far received the most conceptual attention in this context. Originally designed as a whole-body

---

[460] https://en.wikipedia.org/wiki/Extracellular_matrix.

[461] Freitas RA Jr. Cryostasis Revival: The Recovery of Cryonics Patients through Nanomedicine. Alcor Life Extension Foundation, Scottsdale AZ, 2022; Section 4.12.3.3, "ECM Reconditioning"; https://www.alcor.org/cryostasis-revival/.

[462] Stryer L. Biochemistry, 4th Edition, W.H. Freeman and Company, New York, 1995; https://www.amazon.com/dp/0716720094/.

[463] Loewy AG, Siekevitz P, Menninger JR, Gallant JAN. Cell Structure and Function: An Integrated Approach, Third Edition, Saunders College Publishing, Philadelphia PA, 1991; https://www.amazon.com/dp/0030474396/.

[464] Freitas RA Jr. Cryostasis Revival: The Recovery of Cryonics Patients through Nanomedicine. Alcor Life Extension Foundation, Scottsdale AZ, 2022; Section 5.2.3.3.2, "Scaffolded Tissue Printing"; https://www.alcor.org/cryostasis-revival/.

[465] Alternative scaffolding concepts include (1) chains of neighboring nanorobots joined via external manipulator arms into a 3D network, or (2) a network of retractile manipulators composed of metamorphic surfaces* interpenetrating the entire volume of the organ to be fabricated. * Freitas RA Jr. Nanomedicine,

vascular replacement appliance,[466] the vasculoid is a single, complex, multisegmented nanotechnological medical robotic system. It can be visualized as a set of micron-size robots shaped as rectangular "basic plates" that can be joined at the edges to form a 3D network of hollow tubes similar to capillaries and larger blood vessels (image, right) in size and extent. Each rectangular robot (image, below) has multiple external ciliary manipulators that permit rapid reconfiguration of the tubular network, among other functions.

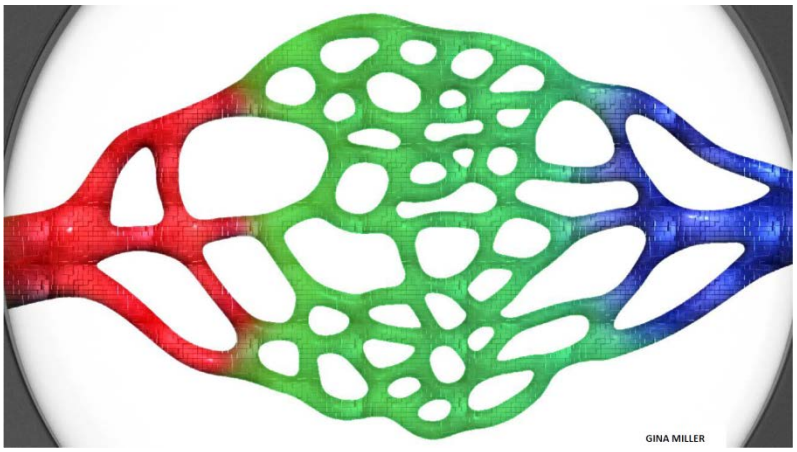

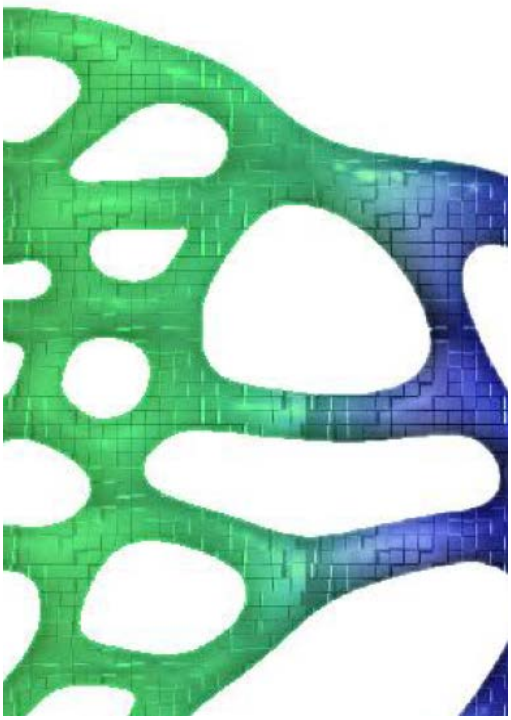

To initiate the printing process, a x_{TM} ~ 30 cm cubical water-filled print chamber is injected with pre-connected vasculoid basic plates which are unfurled into a free-hanging complete vascular network as dictated by the required microvasculature of the tissue or organ being fabricated. The vasculoid is manufactured as a folded, pre-assembled custom appliance that unpacks as a continuously-everting concentric tube, a process called progressive fractal eversion that may be visualized as turning a glove inside out. Eversion may be powered by compressed gas, ciliary action between opposed plates, or by other appropriate means, and advances at ~1 cm/sec. After a few tens of seconds, the vasculoid occupies a small excluded volume within the print chamber, forming a watertight fractal network of hollow diamondoid tubes representing the future vasculature and outlining the shape of the organ to be manufactured, with the tissue-facing underside of each basic plate exposed to the pure water environment but still devoid of all biological material.

Volume I: Basic Capabilities, Landes Bioscience, Georgetown, TX, 1999; Section 5.3, "Metamorphic Surfaces"; http://www.nanomedicine.com/NMI/8.5.1.htm.

[466] Freitas RA Jr., Phoenix CJ. Vasculoid: A personal nanomedical appliance to replace human blood. J Evol Technol. 2002 Apr;11:1-139; http://www.jetpress.org/volume11/vasculoid.pdf.

Next, shepherd nanorobots[467] install patient-personalized cells and other biomaterials fabricated in the cell mill, starting with vascular endothelial cells which are emplaced as the first coating of biological material upon all water-exposed exterior vasculoid surfaces. Fibers and other connective materials are then laid down, building up the extracellular matrix[468] as additional cells are emplaced, all according to the personalized generic tissue architecture specified for the particular organ under construction. Buildout begins by filling in the deepest tissues first and progressing outward in a roughly cylindrical radial direction, leaving ingress and egress pathways available for mobile installation nanorobots until each tissue block under construction has been completely filled with cells and other essential biomaterials. Each overlong cell such as a muscle cell or a neuron with an extended axon can be carried into place and held in proper position by shepherd nanorobots as more normal cells and other biomaterials are installed around it. If any bony skeleton is required, calciferous or other mineralized biomaterials are positionally deposited to establish the necessary exact structure.

One major benefit of scaffolded tissue printing is the possibility of massively parallel assembly operations,[469] with nanorobots delivering and installing cells all throughout the vascular framework simultaneously. As a crude scaling analysis of basic cell emplacement operations, we assume that shepherd nanorobots must install cells at the rate of $R_{TissueMill}$ ~1 kg/hr or $S_{TissueMill} \sim R_{TissueMill} / m_{cell} = 3.26 \times 10^7$ cells/sec.

We will assume that each shepherd nanorobot has a diameter of $D_{shep} = 2R_{shep} = 20$ μm and volume $V_{shep} \sim 8000$ μm^3, about the same size and volume as the biological cell that it must drag from the cell mill to an installation site somewhere in the tissue print chamber, then return emptyhanded to the cell mill to receive its next load, a total round-trip transport distance of $x_{celltransportS} \sim 2(V_{CellMill}^{1/3}/2 + x_{TM}/2) \sim 0.76$ meter at a transport speed of $v_{shep} \sim 1$ cm/sec, giving a transport time of $\tau_{transport} = x_{celltransportS} / v_{shep} \sim 76$ sec. Spherical nanorobots with $R_{shep} = 10$ μm moving in 273 K (0 °C) water having absolute viscosity $\eta = 1.787 \times 10^{-3}$ Pa-sec require a drag

---

[467] Freitas RA Jr. The Alzheimer Protocols: A Nanorobotic Cure for Alzheimer's Disease and Related Neurodegenerative Conditions. IMM Report No. 48, June 2016, 433 pp; Section 5.3.2.3, "Cell Insertion and Emplacement," pp. 327-332; http://www.imm.org/Reports/rep048.pdf.

[468] Freitas RA Jr. Cryostasis Revival: The Recovery of Cryonics Patients through Nanomedicine. Alcor Life Extension Foundation, Scottsdale AZ, 2022; Section 4.12.3.3, "ECM Reconditioning"; https://www.alcor.org/cryostasis-revival/.

[469] A loosely analogous process has been pursued in conventional organ bioengineering. As described in one study:[*] "We decellularized rat, porcine and human kidneys by detergent perfusion, yielding acellular scaffolds with vascular, cortical and medullary architecture, a collecting system and ureters. To regenerate functional tissue, we seeded rat kidney scaffolds with epithelial and endothelial cells and perfused these cell-seeded constructs in a whole-organ bioreactor. The resulting grafts produced rudimentary urine *in vitro* when perfused through their intrinsic vascular bed. When transplanted in an orthotopic position in rat, the grafts were perfused by the recipient's circulation and produced urine through the ureteral conduit *in vivo*."

[*] Song JJ, Guyette JP, Gilpin SE, Gonzalez G, Vacanti JP, Ott HC. Regeneration and experimental orthotopic transplantation of a bioengineered kidney. Nat Med. 2013 May;19(5):646-51; https://www.ncbi.nlm.nih.gov/pmc/articles/PMC3650107/.

power[470] of $P_{ShepDrag} = 6\pi\ \eta\ R_{shep}\ v_{shep}^2 = 34$ pW/nanorobot, which must be doubled to $P_{ShepDrag2} = 68$ pW/nanorobot because the robot is towing cargo of nearly equal size and viscous drag through the water. To avoid traffic congestion in the print chamber, we arbitrarily specify that the entire shepherd nanorobot population should not exceed $f_{shep} = 0.1\%$ of total print chamber volume of $x_{TM}^3 \sim 0.027\ m^3$, hence total nanorobot volume is $V_{allshep} = f_{shep}\ x_{TM}^3 = 2.7 \times 10^{-5}\ m^3$, the maximum number of shepherds is $N_{shep} = V_{allshep} / V_{shep} = 3.38 \times 10^9$ nanorobots, and the nanorobot population requires a continuous power of $P_{allshep} = N_{shep}\ P_{shep} = 3.4$ watts if we generously allow P_{shep} ($>> P_{ShepDrag2}$) = 1000 pW/nanorobot. This population of shepherd nanorobots can install cells at the rate of $R_{ShepInstall} = N_{shep} / (\tau_{transport} + \tau_{emplace}) \sim 3.93 \times 10^7$ cells/sec, assuming that each nanorobot transports and installs one cell at a time and requires $\tau_{emplace} \sim 10$ sec to emplace each cell on the workpiece, and leaving a spare capacity of $1 - (S_{TissueMill} / R_{ShepInstall}) \sim 17\%$.

With the scaffolded fabrication process complete, the vasculoid is retracted from the vasculature and the completed tissue or organ is ready for removal from the tissue mill, and subsequent use.

---

[470] Freitas RA Jr. Nanomedicine, Volume I: Basic Capabilities, Landes Bioscience, Georgetown TX, 1999, Eqn. 9.74 in Section 9.4.2.4, "Force and Power Requirements"; http://www.nanomedicine.com/NMI/9.4.2.4.htm#p3.

6. Conclusions

This paper presents a conceptual technical design and scaling study for a cell mill that can manufacture all biological components of a living cell, including viable finished biological cells, using a collection of nanorobotic subsystems employing the techniques of atomically precise molecular manufacturing.

The cell mill is conceived as a desktop appliance approximately 0.1 m^3 (100 liters) in volume – e.g., a cubical box of approximate dimensions 46 cm x 46 cm x 46 cm – with a mass of 12.5 kg drawing 5 kW of power in active operation (**Table 7**). The cell mill produces finished autologous human biological cells of all types at a rate of ~1 kg/hour with an estimated start-to-finish manufacturing time of ~1.4 hours from order placement to finished product. The feedstock chemical inputs may include a few simple molecules such as CH_4, NH_3, and H_2O containing the four most common elements of life (i.e., CHON), plus small amounts of specialty chemicals incorporating a few other elements such as sulfur (S) and phosphorus (P), and possibly trace amounts of calcium (Ca), fluorine (F), or other elements.

The conceptual design incorporates three working modules: (1) a Molecular Synthesis Module (Section 2) that synthesizes all necessary biomolecules from the simplest organic compounds to long-chain proteins and DNA; (2) a Cytocomponent Assembly Module (Section 3) that assembles the synthesized biomolecules into organelles, cytoskeleton fibers, and other cytological component structures; and (3) a Cell Assembly Module (Section 4) that assembles temporarily metabolically dormant but viable whole cells from organelles, other cytocomponents, and individual molecules as required.

A tissue mill (Section 5), when attached to a cell mill, can accept finished cells from the cell mill and use them to print or fabricate viable autologous human tissues and whole organs at the same ~1 kg/hour production rate as the cell mill.